

5-3-2008

Oxidation of lipids in a supercriticalluid medium

Darrell Lynn Sparks

Follow this and additional works at: <https://scholarsjunction.msstate.edu/td>

Recommended Citation

Sparks, Darrell Lynn, "Oxidation of lipids in a supercriticalluid medium" (2008). *Theses and Dissertations*. 3428.

<https://scholarsjunction.msstate.edu/td/3428>

This Dissertation - Open Access is brought to you for free and open access by the Theses and Dissertations at Scholars Junction. It has been accepted for inclusion in Theses and Dissertations by an authorized administrator of Scholars Junction. For more information, please contact scholcomm@msstate.libanswers.com.

OXIDATION OF LIPIDS IN A SUPERCRITICAL-FLUID MEDIUM

By

Darrell Lynn Sparks, Jr.

A Dissertation
Submitted to the Faculty of
Mississippi State University
in Partial Fulfillment of the Requirements
for the Degree of Doctor of Philosophy
in Chemical Engineering
in the Dave C. Swalm School of Chemical Engineering

Mississippi State, Mississippi

May 2008

Copyright by
Darrell Lynn Sparks, Jr.
2008

OXIDATION OF LIPIDS IN A SUPERCRITICAL-FLUID MEDIUM

By

Darrell Lynn Sparks, Jr.

Approved:

Rafael Hernandez
Assistant Professor
Dave C. Swalm School of
Chemical Engineering
(Director of Dissertation and Advisor)

W. Todd French
Assistant Professor
Dave C. Swalm School of
Chemical Engineering
(Committee Member)

L. Antonio Estévez
Professor
Department of Chemical Engineering
University of Puerto Rico at Mayagüez
(Committee Member)

Hossein Toghiani
Associate Professor
Dave C. Swalm School of
Chemical Engineering
(Committee Member)

Mark E. Zappi
Dean of Engineering
University of Louisiana
at Lafayette
(Committee Member)

Rudy E. Rogers
Professor and Director of
Graduate Studies
Dave C. Swalm School of
Chemical Engineering

W. Glenn Steele
Interim Dean of the Bagley
College of Engineering

Name: Darrell Lynn Sparks, Jr.

Date of Degree: May 2, 2008

Institution: Mississippi State University

Major Field: Chemical Engineering

Major Professor: Dr. Rafael Hernandez

Title of Study: OXIDATION OF LIPIDS IN A SUPERCRITICAL-FLUID MEDIUM

Pages in Study: 259

Candidate for Degree of Doctor of Philosophy

Efficient use of renewable feedstocks for production of chemicals and intermediates is necessary to reduce dependence upon petroleum. A large portion of these chemicals could be produced using lipids from renewable feedstocks such as vegetable oils, animal fats, and bacterial lipids. For example, many lipid sources contain unsaturated fatty acids, which can be oxidized to form a variety of products such as diacids and epoxides. These chemicals are used to formulate herbicides, detergents, plasticizers, lubricants, paints, and other useful products. One of the most common unsaturated fatty acids is oleic acid, and it can be oxidized with an ozone/oxygen mixture to produce azelaic acid and pelargonic acid. Since the ozone/oxygen mixture is a gas and oleic acid is a liquid under reaction conditions, mass transfer limitations exist. However, a reduction of the mass-transfer limitations can be achieved if the reactants coexist in a single phase. When supercritical carbon dioxide (SC-CO₂) is used as the reaction medium, it is possible for both oleic acid and the ozone/oxygen mixture to both exist in the same phase at the same time. Use of supercritical carbon dioxide also provides the

possibility of product fractionation, depending upon the solubility of the products in SC-CO₂.

The overall goal of this research was to determine if any advantages could be realized by conducting the oleic acid oxidation in a supercritical fluid medium. First, the solubility of azelaic acid and pelargonic acid in supercritical carbon dioxide was determined over a range of temperatures and pressures. Pelargonic acid was found to have a significantly higher solubility than azelaic acid, which indicated the potential for product separation with supercritical carbon dioxide. Second, the impact of the solvent medium on reaction kinetics and product formation was determined using two oxidizers: ozone and potassium permanganate. Due to experimental limitations, no reaction was observed in the case of ozone in supercritical carbon dioxide. However, oxidation of oleic acid with potassium permanganate in supercritical carbon dioxide resulted in higher oleic acid conversion and increased yields of azelaic acid and pelargonic acid compared to the oxidation without SC-CO₂.

DEDICATION

This dissertation is dedicated to my parents. Thank you for everything, Mom and Dad. Without your love and support, I would have never made it this far.

ACKNOWLEDGEMENTS

First, I would like to acknowledge those students who have worked with me in the laboratory. In particular, I would like to thank Matt Brough, Trent Jeffries, Michael Bestor, Jaricus Whitlock, Scott Crymble, Matt Thomas, Cedric Cole, Keith Barlow, Nicholas Meyer, Greg Meyer, John Slay, and Jason McEwen. I would also like to acknowledge my fellow graduate students in the Dave C. Swalm School of Chemical Engineering. I would like to thank Tracy Benson, Brian Copeland, and Matt Thomas for being great officemates. In particular, I would like to thank Stephen Dufreche, a great teacher and a true friend. Thank you for helping me with all of my technology-related issues, answering my copious questions, and tolerating my idiosyncrasies.

I would also like to acknowledge individuals that provided me with much guidance and advice: Dr. Earl G. Alley and William E. Holmes. Without your help, I would probably still be using serological pipettes. Also, thank you for the opportunity to teach you about internal standard calibration curves and *science nouveau*.

I would like to thank my committee members for the ways they have contributed to my development into a researcher, teacher, and mentor. Foremost, I would like to thank my advisor, Dr. Rafael Hernandez. You took a chance on me when you hired me as your first graduate student. I can honestly say that I have never regretted being your graduate student. Whenever I was thinking about going to graduate school and what professor I should work for, Levell Hairston, a friend of mind and one of your

undergraduate workers at the time, gave me the following advice: “Dr. Hernandez is going to be a great researcher, and he will make you great as well.” Thank you for pushing me to accomplish all that I can. You have shown me patience beyond belief. I must also thank Dr. L. Antonio Estévez for providing me with so much guidance, particularly with the solubility experiments. It has been an honor to work with you. I would also like to thank Dr. H (Hossein Toghiani) for emphasizing the importance of knowing “the whole show.” Dr. H, if anybody knows the whole show, it is you, and there is no question about it. Next, I would like to thank Dr. Zappi for showing me how to present my research to others. Dr. Zappi, you are truly a master presenter. Finally, I would like to thank Dr. Todd French (a.k.a. Superstar, El Guapo) for always keeping me laughing and teaching me a very important lesson. That lesson is that research is much more enjoyable whenever you are excited about its potential impact. It sounds like a very obvious idea, but I have seen too many graduate students who merely view their research as a means to a degree as opposed to a means of making a difference in the world.

I would like to acknowledge the rest of the faculty of the Dave C. Swalm School of Chemical Engineering. Thank you for giving me the opportunity to teach Mass Transfer Operations. In general, I think I learned more from that experience than the students. I would like to thank Dr. Charles Sparrow for taking the time to meet with me whenever I visited Mississippi State University as a high school student. If it were not for you, I probably would not have attended Mississippi State University. I would also like to thank Dr. R (Rebecca K. Toghiani) for several things. First, thank you for teaching Analysis and Simulation the semester that I took it. In all my years as a student in the Dave C. Swalm School of Chemical Engineering, I cannot recall another time

when you taught that class, but it has proven to be the most useful course I have taken in college. Second, thank you for encouraging me to go to graduate school. At that stage of my life, I really was not sure if I was cut out for graduate school, but your support made me believe that I could handle it. Finally, thank you for showing me how to get a graduate elective out of the way while still an undergraduate student. I would also like to thank Dr. Irvin Atley Jefcoat for teaching me so many of the engineering fundamentals. I must also acknowledge the staff of the Dave. C. Swalm School of Chemical Engineering: Sherre Denson, Ellen Weeks, Sandra Shumaker, and Mike Hillhouse.

Finally, I would like to thank those that supported this effort financially. As far as personal support, I would like to thank the Bagley College of Engineering for providing me with a Barrier Fellowship and the American Oil Chemists' Society for awarding me the Ralph H. Potts Memorial Fellowship. In terms of research support, I would like to acknowledge AgraPure, the United States Department of Energy Office of Energy Efficiency and Renewable Energy, and the National Science Foundation.

TABLE OF CONTENTS

DEDICATION	ii
ACKNOWLEDGEMENTS	iii
LIST OF TABLES	x
LIST OF FIGURES	xiii
CHAPTER	
I. INTRODUCTION	1
The Use of Lipids for Chemical Production	3
Lipid Structure	3
Current Uses of Lipids	4
Supercritical Fluids in Lipid Processing	9
Introduction to Supercritical Fluids	9
Current Status of Supercritical Fluids	10
II. RESEARCH HYPOTHESIS	29
Research Goal	30
Primary Objective 1: Evaluate the Solubility of Target Reaction Products in Supercritical Carbon Dioxide	30
Primary Objective 2: Impact of Supercritical Carbon Dioxide on Reaction Kinetics and Product Formation	31
III. LITERATURE REVIEW	33
Traditional Methods for Oxidizing Oleic Acid	33
Reaction of Oleic Acid with Gas Oxidants	33
Reaction of Oleic Acid with Liquid Oxidants	40
Reaction of Oleic Acid with Solid Oxidants	46
Use of Supercritical Carbon Dioxide as a Reaction Medium	52
Rationale	52
Oxidation of Organic Compounds in Supercritical Carbon Dioxide	55
Solubility of Lipids in Supercritical Carbon Dioxide	60

	Experimental Techniques.....	60
	Behavior of Lipids in Supercritical Carbon Dioxide	63
IV.	METHODS AND MATERIALS.....	74
	Introduction.....	74
	Oxidizer Generation.....	74
	Ozone Generation	74
	Potassium Permanganate	76
	Solubility in Supercritical Carbon Dioxide.....	77
	Oxidation in Supercritical Carbon Dioxide	80
	Analytical Methods.....	81
	Conversion of Reaction Products to Methyl Ester Derivatives	81
	Analysis of Fatty Acid Methyl Esters with Gas Chromatography	82
	Determination of KMnO_4 Concentration with UV/VIS Spectroscopy	90
V.	SOLUBILITY MODELING THEORY	108
	Introduction.....	108
	Semi-Empirical Methods	108
	Dimensionless Forms of the Models.....	113
	Equation of State Approach.....	115
VI.	EVALUATION OF DENSITY-BASED MODELS FOR THE SOLUBILITY OF SOLIDS IN SUPERCRITICAL CARBON DIOXIDE AND THE FORMULATION OF A NEW MODEL	119
	Introduction.....	119
	Methodology	120
	Modeling Results	121
	New Density-Based Model.....	126
	Conclusions.....	128
VII.	SOLUBILITY OF AZELAIC ACID IN SUPERCRITICAL CARBON DIOXIDE.....	145
	Introduction.....	145
	Experimental Methods	145
	Materials	145
	Procedure	146
	Results and Discussion	148
	Semi-Empirical Methods	148
	Equation-of-State (EoS) Methods.....	151
	Conclusions.....	153

VIII.	SOLUBILITY OF NONANOIC (PELARGONIC) ACID IN SUPERCRITICAL CARBON DIOXIDE	158
	Introduction.....	158
	Experimental Methods.....	160
	Materials	160
	Procedure	160
	Results and Discussion	162
	Solubility Results	162
	Modeling.....	163
	Apparatus Validation	166
	Conclusions.....	167
IX.	OXIDATION OF OLEIC ACID WITH OZONE	173
	Introduction.....	173
	Experimental Methods.....	174
	Materials	174
	Procedure	175
	Traditional Oxidation.....	175
	Oxidation in Supercritical Carbon Dioxide	177
	Analysis of Reaction Products	178
	Results and Discussion	178
	Conclusions.....	180
X.	OXIDATION OF OLEIC ACID WITH POTASSIUM PERMANGANATE	184
	Introduction.....	184
	Experimental Methods.....	186
	Materials	186
	Procedure	186
	Oxidation in the Absence of Supercritical Carbon Dioxide	186
	Oxidation in Supercritical Carbon Dioxide	187
	Analysis of Reaction Products	188
	Solubility of Potassium Permanganate in Supercritical Carbon Dioxide.....	189
	Results and Discussion	191
	Conclusions.....	194
XI.	ENGINEERING SIGNIFICANCE AND FUTURE WORK	201
XII.	CONCLUSIONS.....	206
	REFERENCES	210

APPENDIX

A.	COMPLETE SOLUBILITY REFERENCE DATA USED IN CHAPTER VI.....	223
B.	COMPLETE SOLID SOLUBILITY MODELING RESULTS	239
C.	PHYSICAL PROPERTIES OF AZELAIC ACID AND CARBON DIOXIDE USED FOR EQUATION OF STATE CALCULATIONS...	255
D.	EXPERIMENTAL AND LITERATURE VALUES OF OLEIC ACID SOLUBILITY IN SUPERCRITICAL CARBON DIOXIDE	258

LIST OF TABLES

TABLE

1.1	Fatty acid profiles of lipid feedstocks.....	13
1.2	Typical properties of supercritical fluids [Ramsay et al., 1991].....	14
1.3	Critical points of several supercritical fluids	15
4.1	GC-FID temperature program used for analysis of oleic acid ozonolysis products.....	92
4.2	GC-MS temperature program used for analysis of products generated from oleic acid oxidation with potassium permanganate	93
6.1	Sources of solid + supercritical carbon dioxide solubility data	129
6.2	Physical properties of solid compounds and carbon dioxide.....	130
6.3	Chrastil equation modeling results.....	131
6.4	del Valle-Aguilera (Eq. 5.15) modeling results	132
6.5	Adachi-Lu (Eq. 5.16) modeling results.....	133
6.6	Eq. (6.6) modeling results.....	134
6.7	Méndez-Teja (Eq. 5.18) modeling results.....	135
6.8	Modified Méndez-Teja (Eq. 5.19) modeling results.....	136
6.9	Modified Bartle (Eq. 5.21) modeling results	137
6.10	Eq. (6.8) modeling results.....	138
6.11	Eq. (6.9) modeling results.....	139
7.1	Solubility of azelaic acid in supercritical carbon dioxide.....	154

8.1	Solubility of pelargonic acid in supercritical carbon dioxide	168
8.2	Modeling results.....	169
10.1	Rate law modeling results for oxidation of oleic acid with potassium permanganate at 12.2 MPa.....	196
A.1	Solubility of naphthalene in supercritical carbon dioxide at 308.15 K.....	224
A.2	Solubility of naphthalene in supercritical carbon dioxide at 318.15 K.....	225
A.3	Solubility of naphthalene in supercritical carbon dioxide at 328.15 K.....	226
A.4	Solubility of fluorene in supercritical carbon dioxide at 308.15 K.....	227
A.5	Solubility of fluorene in supercritical carbon dioxide at 323.15 K.....	228
A.6	Solubility of fluorene in supercritical carbon dioxide at 343.15 K.....	229
A.7	Solubility of hydroquinone in supercritical carbon dioxide at 333 K.....	230
A.8	Solubility of hydroquinone in supercritical carbon dioxide at 348 K.....	231
A.9	Solubility of hydroquinone in supercritical carbon dioxide at 363 K.....	232
A.10	Solubility of anthracene in supercritical carbon dioxide at 303.15 K.....	233
A.11	Solubility of anthracene in supercritical carbon dioxide at 323.15 K.....	234
A.12	Solubility of anthracene in supercritical carbon dioxide at 343.15 K.....	235
A.13	Solubility of cholesterol in supercritical carbon dioxide at 308.15 K	236
A.14	Solubility of cholesterol in supercritical carbon dioxide at 313.15 K	237
A.15	Solubility of cholesterol in supercritical carbon dioxide at 333.15 K	238
B.1	Chrastil equation modeling results.....	240
B.2	del Valle-Aguilera (Eq. 5.3) modeling results	241
B.3	del Valle-Aguilera (Eq. 5.15) dimensionless modeling results	242
B.4	Adachi-Lu (Eq. 5.5) modeling results.....	243

B.5	Adachi-Lu dimensionless (Eq. 5.16) modeling results	244
B.6	Modeling results for Eq. (6.5).....	245
B.7	Modeling results for Eq. (6.6).....	246
B.8	Modeling results for Eq. (6.8).....	247
B.9	Modeling results for Eq. (6.9).....	248
B.10	Méndez-Teja modeling results.....	249
B.11	Modified Méndez-Teja modeling results.....	250
B.12	Bartle modeling results	251
B.13	Modified Bartle modeling results	252
B.14	Overall modeling results for Chrastil-type equations	253
B.15	Overall modeling results for non-Chrastil-type equations.....	254
C.1	Physical properties of carbon dioxide.....	256
C.2	Physical properties of azelaic acid.....	257
D.1	Solubility of oleic acid in supercritical carbon dioxide	259

LIST OF FIGURES

FIGURE

1.1	DoE biorefinery concept [NREL, 2007]	16
1.2	Common fatty acids [Wikipedia, 2007a]	17
1.3	Sample triacylglycerol structure [Bergstra, 2007]	18
1.4	Worldwide percentage of vegetable oils used for non-food applications [Vannozzi, 2006].....	19
1.5	Biodiesel sales in the United States [NBB, 2007]	20
1.6	Transesterification reaction for the production of biodiesel [Hofman, 2003]	21
1.7	Functionality of oleic acid terminal group.....	22
1.8	Possible oxirane reaction pathways [Pages-Xatart-Pares et al., 1999]	23
1.9	Use of fatty acids for polymer production [Hill, 2000]	24
1.10	Structures of oleic acid, azelaic acid, and pelargonic acid	25
1.11	Typical pressure-temperature phase diagram with critical properties corresponding to carbon dioxide [Leitner, 2000]	26
1.12	Transition from two-phase system to supercritical fluid [Clifford et al., 2007]	27
1.13	Effect of temperature and pressure on solvent density [Rayner, 2007]	28
3.1	Changes in oleic acid concentration over time due to autoxidation: Δ , 333 K; \circ , 348 K; \square , 363 K [Takahashi et al., 2000]	65
3.2	Changes in oleyl hydroperoxide concentration over time during autoxidation of oleic acid: Δ , 333 K; \circ , 348 K; \square , 363 K [Takahashi et al., 2000].....	66

8.2	Changes in dissolved oxygen concentration for oleic acid autoxidation: (a) for complete reaction time, (b) for the first two hours of reaction time: Δ , 333 K; \circ , 348 K; \square , 363 K [Takahashi et al., 2000]	67
3.4	Proposed oleic acid ozonolysis mechanism where the asterisk denotes products that theoretically cannot be incorporated into an oligomer [Reynolds et al., 2006]	68
3.5	Oxidation of oleic acid with hydrogen peroxide with alumina-supported tungstic oxide catalyst: \blacklozenge , pelargonic acid; \blacksquare , azelaic acid, \blacktriangle , octanoic acid; \bullet , oleic acid; $*$, suberic acid [Noureddini and Kanabur, 1999]	69
3.6	Hydroxylation of an olefin followed by oxidation into carboxylated species [Mercangöz et al., 2004].....	70
3.7	Combined extraction and reaction process for removal of organic pollutants [Kruse and Schmieder, 1998].....	71
3.8	Dynamic apparatus for determining solubility in a supercritical fluid [Maxwell, 1996].....	72
3.9	Supercritical CO ₂ extraction yields based upon pressure at different temperatures where the error bars indicate mean \pm 1 SD ($n = 3$) [Sparks et al., 2006]	73
4.1	LC-1234 ozone generator equipped with a Model HC Ozone Monitor utilized for this study	94
4.2	Ozone generator calibration data	95
4.3	Potassium permanganate crystals	96
4.4	Experimental apparatus used for solubility experiments	97
4.5	Magnetic stirrer calibration curve generated using photo/contact tachometer ...	98
4.6	Experimental apparatus for oxidation reactions in SC-CO ₂	99
4.7	Major components of a gas chromatograph [Punrattanasin and Spada, 1997].	100
4.8	Agilent 6890N GC-FID used in this work.....	101
4.9	Illustration of a flame ionization detector [Scott, 2007]	102
4.10	Varian 3600 GC with Saturn 2000 Mass Spectrometer used in this study	103

4.11	Schematic of a quadrupole ion trap [Downard, 2004].....	104
4.12	LAMBDA 25 UV/VIS Spectrophotometer used for determining potassium permanganate concentration	105
4.13	UV/VIS spectrophotometer double-beam design [Hargis, 1988b].....	106
4.14	UV/VIS spectrophotometer calibration curve	107
6.1	Plot of cholesterol solubility in SC-CO ₂ at pressures between 10.09 MPa and 27.89 MPa.....	140
6.2	Variation of the association constant <i>k</i> with density.....	141
6.3	Experimental naphthalene solubility and values estimated by Eq. (5.19) for pressures between 6.08 MPa and 33.44 MPa.....	142
6.4	Experimental fluorene solubility and values estimated by Eq. (5.19) for pressures between 6.99 MPa and 48.34 MPa.....	143
6.5	Overall average error of models studied.....	144
7.1	Chrastil plot of azelaic acid solubility in SC-CO ₂ : ●, 313.15 K; ○, 333.15 K; —, Chrastil Model Prediction.....	155
7.2	Méndez-Teja plot resulting from multi-linear regression of Eq. (7.4): ■, 313.15 K; ○, 333.15 K; - - -, Model Prediction	156
7.3	Experimental and EoS-predicted solubilities of azelaic acid in SC-CO ₂ : ■, 313.15 K; ○, 333.15 K; - - -, 313.15 K EoS Prediction; —, 333.15 K EoS Prediction	157
8.1	Dependence of <i>k</i> on density: - - -, oleic acid; - — - —, triolein; - - - -, trilinolein.....	170
8.2	Plot of pelargonic acid solubility (<i>c</i> ₂ [*]) in SC-CO ₂ vs. solvent density ($\rho_{r,1}$): ●, 313.15 K; ○, 333.15 K; —, 313.15 K model prediction; ●●, 333.15 K model prediction where the inset shows an enlarged view of top log cycle and the error bars correspond to uncertainties of one standard deviation (σ) taken from triplicate runs	171
8.3	Plot of oleic acid solubility (<i>c</i> ₂ [*]) in SC-CO ₂ vs. solvent density ($\rho_{r,1}$) at 323.15 K: ■, Nilsson et al., 1991; ○, Maheshwari et al., 1992; ●, this work; □, Škerget et al., 1995 where the error bars correspond to uncertainties of one standard deviation (σ) taken from triplicate runs....	172

9.1	Reactor assembly for oleic acid ozonolysis at ambient pressure.....	181
9.2	Reactor assembly for oleic acid ozonolysis in supercritical carbon dioxide.....	182
9.3	Change of oleic acid concentration over time at a temperature of 40°C and and an ozone mass concentration of 5.06 % in oxygen (1.18 SLM)	183
10.1	Change of normalized oleic acid concentration with time for oxidation of oleic acid with potassium permanganate at 12.2 MPa.....	197
10.2	Comparison of 12-hour oleic acid oxidation reactions with potassium permanganate conducted with and without supercritical carbon dioxide.....	198
10.3	Comparison of typical chromatograms for 12-hour reactions at 318.15 K.....	199
10.4	Solubility of KMnO_4 in supercritical carbon dioxide at 12.2 MPa.....	200
11.1	Conventional oleic acid oxidation process	204
11.2	Oleic acid oxidation in supercritical carbon dioxide	205

CHAPTER I

INTRODUCTION

Currently, the United States is dependent upon foreign countries to provide an adequate supply of petroleum that meets the demands of American consumers. In fact, petroleum imported from just five countries (Canada, Mexico, Saudi Arabia, Venezuela, and Nigeria) accounts for approximately 68 % of total petroleum imports into the United States [EIA, 2007a]. The United States has a strained relationship with several of the countries, such as Venezuela, upon which it depends for petroleum. Hence, reducing the dependence upon such countries for petroleum is important to the national security of the United States. Perhaps the largest incentive from the consumer's point of view to reduce dependence upon petroleum is to avoid paying increasing prices for fuel and other petroleum-based products. As petroleum prices continue to increase, alternative sources of fuels and chemicals traditionally derived from petroleum must be identified.

Each day, the average person in the United States and other industrialized nations uses products derived from petroleum. The most obvious example is the use of petroleum for energy in such areas such as transportation and electric power. Gasoline and diesel are the most commonly used transportation fuels, and both of these fuels are derived from petroleum. In fact, over 40 % of the energy used in 2005 in the United States was provided by petroleum, and petroleum consumption is expected to continue to increase over 1 % per year up to 27 million barrels per day by 2030 [EIA, 2007b].

However, through energy conservation programs and the increased promotion and use of alternative energy resources, the share of energy derived from petroleum is expected to increase at a slower rate than other energy sources. For example, the European Union (EU) has mandated that its 25 member nations participate in the *Vision 2050* program, which calls for the phasing-out of fossil fuels and nuclear energy by 2050 [INFORSE-Europe, 2007]. The *Twenty in Ten* initiative set forth by President Bush calls for reducing gasoline usage in the United States by 20 % over the next 10 years [Bush, 2007]. To achieve this goal, the President has proposed to reduce demand of gasoline by raising fuel economy standards that automobile manufacturers must meet. President Bush has also proposed to increase the supply of renewable and alternative fuels to a target of 35 billion gallons per year by 2017. In 2005, the consumption of alternative fuels was approximately 500 million gasoline equivalent gallons [EIA, 2007c]. To produce the amount of alternative fuels necessary to significantly displace petroleum-based fuels, research is being conducted in areas such as hydrogen production and biomass utilization. For example, the Department of Energy (DoE) is promoting the concept of a biorefinery in which fuels, power, and chemicals are generated from biomass [NREL, 2007]. Figure 1.1 illustrates the biorefinery concept, which is based upon two platforms: the *sugar platform* and the *syngas platform*. The *sugar platform* focuses on biochemical conversion processes such as ethanol production from sugar fermentation. The *syngas platform* deals with thermochemical conversion processes such as gasification of biomass. One of the important facets of the biorefinery concept is that it includes production of chemicals and not just fuels and power generation. Although the majority of petroleum is destined for fuel use, petroleum products comprise about 89

% of total energy consumption for non-fuel uses in the United States [EIA, 2007b]. Non-fuel uses for petroleum include paints, lubricants, asphalt, plastics, and pharmaceuticals. To displace the need for petroleum to produce chemicals and other non-fuel materials, alternative and renewable materials must be found that are similar in structure to the molecules found in petroleum. In general, petroleum is composed of hydrocarbon chains of varying lengths. Therefore, an ideal alternative to petroleum would be a renewable material easily generated in the United States that is primarily composed of hydrocarbon-based compounds. Lipids meet these criteria.

The Use of Lipids for Chemical Production

Lipid Structure

Lipids can be defined as fatty acids, fatty acid derivatives, and substances related either biosynthetically or functionally to fatty acids and their derivatives [Christie, 2003a]. Lipids are an essential component of living organisms and can be found in plants, animals, and microorganisms. Lipids are commonly called *oils* when they are plant-based and *fats* when they are animal-based. The fatty acid chains that compose lipids generally contain even numbers of carbon atoms organized in straight chains with typical lengths of 14 to 24 carbon atoms with a carboxyl group at one end [Christie, 2003a]. However, branched-chain fatty acids and fatty acids with odd-number carbon chains can also occur. Unsaturated fatty acids are also common. Figure 1.2 shows the structures for several common fatty acids. Arachidic acid, stearic acid, and palmitic acid are fully saturated, so they have a straight-chain structure. Oleic acid and erucic acid are monounsaturated fatty acids, and as can be seen in Figure 1.2, this causes a slight bend in

the fatty acid structure. As the degree of unsaturation increases, the bending of the structure becomes more pronounced. This can be seen in going from oleic acid (1 double bond) to linoleic acid (2 double bonds) to linolenic acid (3 double bonds) and finally to arachidonic acid (4 double bonds). The primary type of lipid structure consists of fatty acids attached to an alcohol, such as glycerol or cholesterol; however, the glycerol linkage is more abundant. When one or more fatty acids are attached to a glycerol backbone, the resulting structure is referred to as an *acylglycerol*. For example, if only one fatty acid is attached to the glycerol, the molecule is called a *monoacylglycerol* or, equivalently, a *monoglyceride*. When a phosphorous molecule is attached to an acylglycerol, the resulting structure is called a *glycerophospholipid* or, equivalently, a *phospholipid*. In oils and fats, the primary acylglycerol structure is the *triacylglycerol*, or *triglyceride*. Figure 1.3 shows the structure of a triacylglycerol that would be found in canola oil. As discussed in the next section, a wide range of chemical reactions can be used to convert an acylglycerol such as the triacylglycerol in Figure 1.3 into a variety of products.

Current Uses of Lipids

In 2004, approximately 120 million tons of oils and fats were generated worldwide, with only about 25 million tons being used for industrial oleochemistry applications [Vannozzi, 2006]. It should be noted that these figures do not include lipids that are currently not commercially utilized (for example, the lipids produced at municipal wastewater treatment plants). The remaining lipids were used for human and animal (livestock, pets, etc...) food. About 80 % of the lipids were derived from plant

sources, with the remaining 20 % being derived from animals. As shown in Figure 1.4, the amount of lipids being used for non-food uses has generally been increasing over the last 20 years.

One of the reasons non-food uses for lipids have increased since approximately 1999 is the surge in the biodiesel industry during that time period. As Figure 1.5 illustrates, biodiesel sales have increased from approximately 0.5 million gallons per year in 1999 to about 250 million gallons per year in 2006. Biodiesel is comprised of mono-alkyl esters of long chain fatty acids derived from the acylglycerols of vegetable oils and animal fats. In the United States, the most common biodiesel feedstock is soybean oil, which is comprised primarily of triacylglycerols [Haas, 2005]. Biodiesel is produced from triacylglycerols (and acylglycerols in general) through a process called *transesterification*. As shown in Figure 1.6, during transesterification, triacylglycerols react with an alcohol in the presence of a catalyst to produce glycerol and fatty acid alkyl esters. The reaction occurs stepwise as the triacylglycerol is converted into a diacylglycerol which is converted into a monoacylglycerol and then into glycerol. A fatty acid alkyl ester is produced in each step. Methanol is the most common alcohol used for transesterification and results in the production of fatty acid methyl esters. The type of catalyst used depends upon the free fatty acid level of the lipid feedstock. If high free fatty acids are present, then an acid catalyst such as sulfuric acid is used; otherwise, a base catalyst such as sodium hydroxide is utilized because base-catalyzed transesterification has several advantages over acid-catalyzed transesterification, including faster reaction times [Zappi et al., 2003].

Several serious hurdles exist for the biodiesel industry, including a lack of a pipeline transportation infrastructure and the low value of the glycerol byproduct. Therefore, research is being conducted on catalytically cracking lipids to produce diesel and gasoline range organic compounds [Benson et al., 2007]. By catalytically cracking the lipids, glycerol production can be avoided and the fuel can be transported through the existing petroleum pipeline network.

Perhaps the most promising area of lipid research is in the arena of chemical production. In fact, oils and fats have been called the most important renewable raw materials for the chemical industry [Metzger and Bornscheuer, 2006]. Non-fuel, non-food uses for lipids include lubricants, metal working/cutting oils, pharmaceuticals, cosmetics, surfactants, cleaning agents, solvents, and intermediates for the synthesis of plastics and coatings [Vannozzi, 2006; Bondioli, 2003]. The plethora of applications for lipids comes from the array of chemical transformations that can be applied to fatty acids. As previously mentioned, fatty acids are often bound to glycerol in acylglycerol structures. Therefore, if it is desired to separate the fatty acids from the glycerol, a very well-known technique is to hydrolyze the acylglycerol, splitting it to produce glycerol and fatty acids. Table 1.1 shows the major fatty acids that comprise several lipid feedstocks. In Table 1.1, the notation under each trivial fatty acid name denotes the length of the carbon chain and the number of C-C double bonds present. For example, the notation of oleic acid is C18:1 which means that oleic acid has a carbon chain length of 18 carbons and has 1 C-C double bond. Soybean oil, palm oil, and canola oil are all derived directly from vegetable sources and are currently used to make oleochemicals. As the name implies, beef tallow is an animal-based lipid feedstock, and it is also used

for the production of oleochemicals, albeit to a lesser extent than the vegetable-based lipids. Tall oil is a byproduct of wood pulp manufacture in the pulp and paper industry and is used in the production of soaps, lubricants, adhesives, varnishes, and drilling fluids [Logan, 1979; Neaves, 2007]. Sewage sludge lipids are not currently utilized on a large scale for the production of fuels or chemicals. However, due to the amount sewage sludge lipids generated every day, this feedstock has much potential. One of the major advantages of sewage sludge lipids over other feedstocks such as soybean and palm oil is that sewage sludge lipids would not be marketable to the food industry, so they can be used solely for fuel and chemical production [Dufreche et al., 2007].

If one looks at the fatty acid profiles given in Table 1.1, at least one commonality can be found: all the lipid feedstocks either contain a large amount of unsaturated fatty acids or contain at least one unsaturated fatty acid in a relatively large amount. Soybean, canola, and tall oil contain primarily unsaturated fatty acids. Compared to the other feedstocks shown, beef tallow, palm oil, and sewage sludge oil contain more saturated fatty acids; however, oleic acid (an unsaturated fatty acid) comprises at least 30 % of the overall fatty acid profile in each case. Since oleic acid is common over such a wide range of lipid feedstocks, it will be the fatty acid considered in this work. The functionality of typical fatty acids comes from two places: the terminal carboxyl group and one or more C-C double bonds [Metzger and Bornscheuer, 2006]. Figure 1.7 provides examples of functional groups that can be placed on the terminal group of oleic acid. However, the most common reaction for oleic acid (and unsaturated fatty acids in general) involves reactions at the C-C double bond. In particular, oleic acid is usually oxidized to form products. For example, when oleic acid is epoxidized, the resulting oxirane structure

becomes a useful intermediate to a variety of reaction pathways (Figure 1.8). The oxidation products of oleic acid are useful in many applications such as polymer production (Figure 1.9).

The largest commercial process utilizing oleic acid as the primary reactant is the oxidation of oleic acid to produce pelargonic and azelaic acids. In fact, the major global source of azelaic acid comes from ozonolysis of oleic acid [Chemical Market Reporter, 2001]. Figure 1.10 shows the chemical structures of oleic, azelaic (diacid), and pelargonic (monoacid) acids. Clearly, the products result from the complete splitting of the C-C double bond. Many oxidizers can be used to produce azelaic acid and pelargonic acid from oleic acid, but the most widely researched have been ozone, hydrogen peroxide, and potassium permanganate. However, all three oxidizers have limitations associated with their use. Under typical oxidation conditions, oleic acid is a liquid, but ozone is a gas and potassium permanganate is a solid. Although hydrogen peroxide is a liquid, it is commonly found in an aqueous medium. Since oleic acid is an organic molecule that is relatively non-polar, it has very low solubility in water. Therefore, in each oleic acid + oxidant system, mass-transfer limitations exist. To overcome the interfacial mass-transfer limitations, the oxidation reaction could be carried out in a supercritical-fluid medium. Other possible advantages of using a supercritical fluid include facilitated separation of reaction products, increased catalyst life, and changes in selectivities and rate constants due to the effect of pressure [Brennecke, 1993].

Supercritical Fluids in Lipid Processing

Introduction to Supercritical Fluids

With ever increasing demands for sustainability and stricter environmental controls, much research has gone into the area of alternative solvents. This is due to the use of large quantities of solvents in the chemical industry, especially in specialty-chemical and pharmaceutical production. In general, four pathways to the increased use of alternative or “green” solvents have been developed [Capello et al., 2007]:

- Substitution of hazardous solvents with ones that show better environmental, health, and safety properties
- The use of solvents produced from renewable resources
- Substitution of organic solvents with solvents that are environmentally harmless
- The use of ionic liquids that exhibit very low vapor pressures

Supercritical fluids have been widely researched as alternative solvents. In particular, carbon dioxide is considered a great alternative solvent because it is non-toxic and non-flammable. Knowledge of supercritical fluids can be dated back at least to the 19th century. In 1822, Baron Charles Cagniard de LaTour first observed the disappearance of distinct gas and liquid phases of an alcohol into one phase by simply increasing temperature, thus discovering the existence of what is known as the *critical point* [Rayner and Oakes, 2005]. Hence, a supercritical fluid can be defined as any substance above its critical point (critical temperature and critical pressure) but below the pressure required for condensation into a solid [Rayner and Oakes, 2005]. Figure 1.11 shows a general pressure-temperature phase diagram along with the critical properties of carbon dioxide.

The critical point is the highest temperature and pressure at which a material is in vapor-liquid equilibrium. Figure 1.12 shows the isochoric transition of carbon dioxide to its critical point. In Figure 1.12A, two distinct phases of carbon dioxide can be observed. As temperature increases, the meniscus begins to fade (Figure 1.12B). As shown in Figure 1.12C, when the temperature increases even further, the densities of the vapor and liquid approach each other, causing the meniscus to fade even further. The liquid density decreases due to thermal expansion, and the vapor becomes denser due to increasing pressure. Once the critical point has been reached, two distinct phases are no longer seen (Figure 1.12D). A single-phase system exists that exhibits properties intermediate to a liquid and vapor. Table 1.2 shows typical properties of supercritical fluids. Typically, the density of the supercritical fluid is closer to that of a liquid. However, when compared to its liquid state, a supercritical fluid has a lower viscosity and a higher diffusivity, which results in more efficient mass transfer. Supercritical fluids are often called *tunable* solvents because slight changes in temperature and pressure can have very pronounced effects on solvent properties. Figure 1.13 illustrates the effect of pressure and temperature on carbon dioxide density. Particularly in the region of the critical point, large changes in density can be achieved with just small adjustments in temperature or pressure.

Current Status of Supercritical Fluids

Supercritical fluids are useful in a variety of applications. Worldwide, supercritical fluids have been incorporated into over 100 plants in the areas of production, environmental applications, and particle engineering [Brunner, 2004]. For example,

supercritical carbon dioxide is used to decaffeinate coffee and tea and supercritical paraffins such as propane are used in mineral oil processing [Brunner, 2004; Cygnarowicz-Provost, 1996]. Table 1.3 lists commonly used supercritical fluids along with their corresponding critical temperature and critical pressure. Compared to other fluids, carbon dioxide has a relatively low critical temperature, which provides two key advantages over most other supercritical fluids. First, the energy required to get to supercritical conditions is reduced, resulting in lower operating costs. Second, it makes carbon dioxide ideal for processing materials that are temperature sensitive, such as proteins [Sovova and Stateva, 2001].

Most of the research on supercritical fluids has dealt with mass-transfer applications such as extraction and chromatography because of the unique properties a fluid obtains in the supercritical state. Since density is directly related to the solvating power of a fluid, the ability to finely control density results in facilitated separations. One of the earliest large-scale applications of supercritical fluids is the previously mentioned decaffeination of coffee and tea beginning in the 1960s [Zosel, 1978]. Since that time, the use of supercritical carbon dioxide for extractive separations of natural products such as hops and essential oils has increased significantly [Williams and Clifford, 2000].

Supercritical fluids can also be used in chemical reactions. Supercritical water has been found to be an effective oxidizer of organics such as pyridine and supercritical propane can be used in the hydrogenation of fats and oils [Baiker, 1999]. As previously mentioned, supercritical fluids can impact reactions in a variety of ways. For example, under ambient conditions, oxidation of organics with oxygen in water proceeds very

slowly due to mass-transfer limitations. However, the reaction in supercritical water proceeds much faster because the oxygen and organics are all in the same phase [Brennecke, 1993]. Besides the inherent safety features (non-toxic, non-flammable) and low critical temperature of carbon dioxide, it is also very plentiful and inexpensive. Most carbon dioxide sold is isolated from existing processes such as production of ethanol, ammonia, and hydrogen. Compared to other commonly used supercritical fluids, particularly water, carbon dioxide has a low heat of vaporization, which can lead to lower energy costs [DeSimone, 2002]. These factors make supercritical carbon dioxide a very attractive reaction medium. For example, supercritical carbon dioxide has been heavily researched for use in the production of polymers such as polymethylmethacrylate, polystyrene, and fluoropolymers [Rayner and Oakes, 2005]. Supercritical carbon dioxide has been also utilized for oxidation of organics such as cyclohexene and phenols [Rayner and Oakes, 2005]. Carbon dioxide is well-suited for oxidation reactions because it is already completely oxidized; hence, it does not form oxidation products. Also, as in the example of supercritical water, gases such as oxygen are completely miscible with supercritical carbon dioxide, eliminating mass-transfer limitations. Depending upon the solubility of reaction products in supercritical carbon dioxide, the reaction can be coupled with extraction, reducing or even eliminating the need for typical separation processes such as distillation.

Table 1.1: Fatty acid profiles of lipid feedstocks

Fatty Acid	Soybean	Beef Tallow	Palm	Canola	Tall	Sewage Sludge ^a
Palmitic (C16)	11 %	26 %	44 %	4 %	0.5 %	30 %
Stearic (C18)	4 %	31 %	-	-	3 %	13 %
Oleic (C18:1)	23 %	31 %	40 %	60 %	47 %	32 %
Linoleic (C18:2)	53 %	2 %	10 %	26 %	37 %	10 %
Linolenic (C18:3)	8 %	-	-	10 %	11 %	-
Others	1 %	10 %	6 %	-	1.5 %	15 %

^a Dufreche et al. (2007)

Table 1.2 Typical properties of supercritical fluids [Ramsay et al., 1991]

Property	Liquid	Supercritical Fluid	Gas
Density/kg·L ⁻¹	1	0.1-1	0.001
Viscosity/cP	1	0.01-0.1	0.01
Diffusivity/cm ² ·s ⁻¹	<0.00001	0.0001-0.001	0.1

Table 1.3 Critical points of several supercritical fluids

Fluid	$T_c/^\circ\text{C}$	P_c/bar
Acetone	235.05	47.01
Carbon Dioxide	31.05	73.83
Methanol	239.45	80.97
Propane	96.65	42.48
Water	373.95	220.55

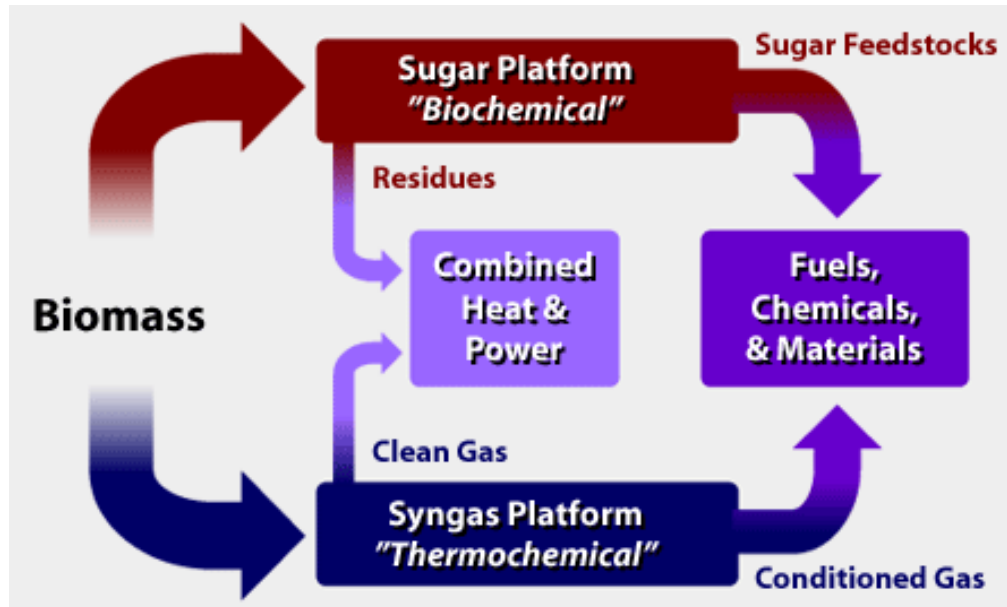


Figure 1.1: DoE biorefinery concept [NREL, 2007]

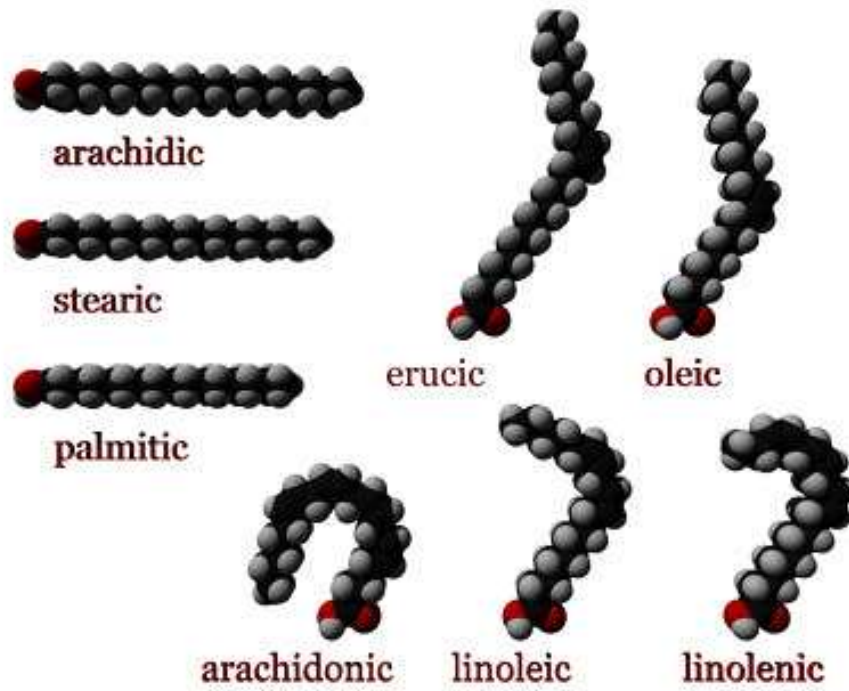


Figure 1.2: Common fatty acids [Wikipedia, 2007a]

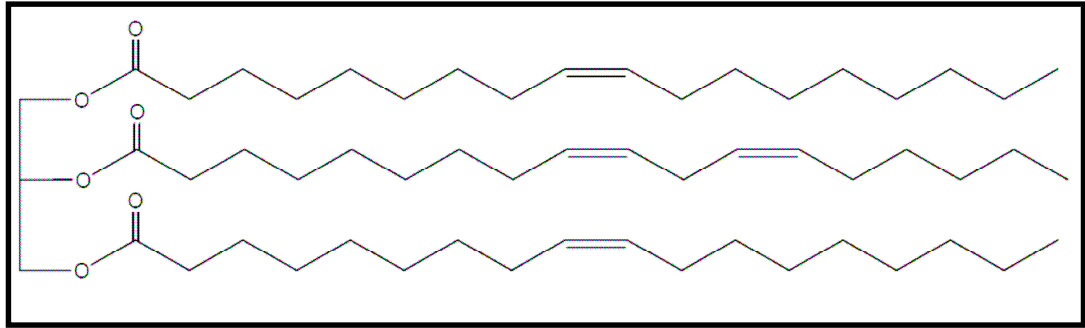


Figure 1.3: Sample triacylglycerol structure [Bergstra, 2007]

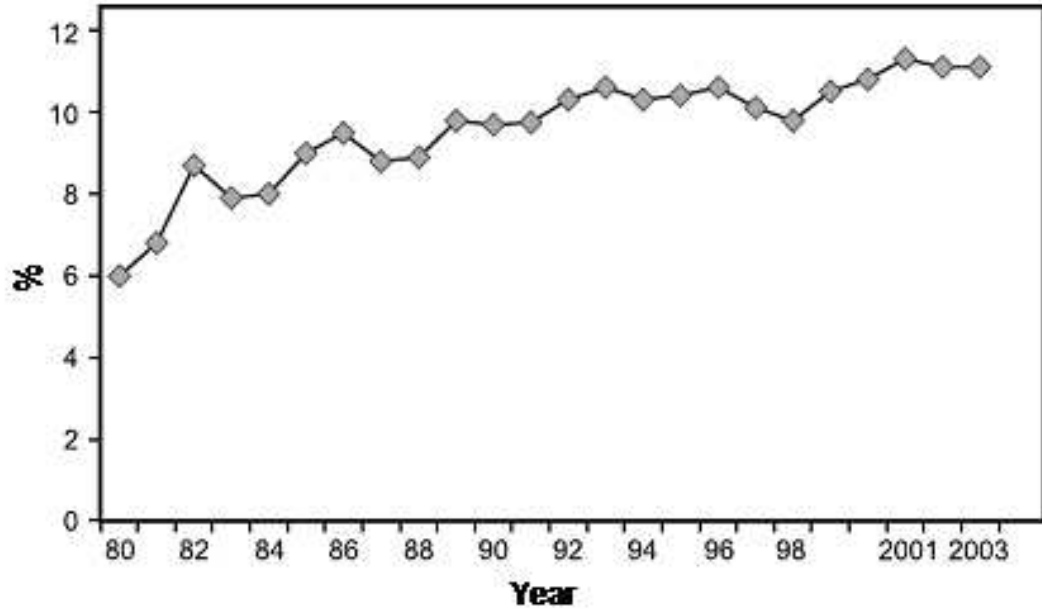


Figure 1.4: Worldwide percentage of vegetable oils used for non-food applications [Vannozzi, 2006]

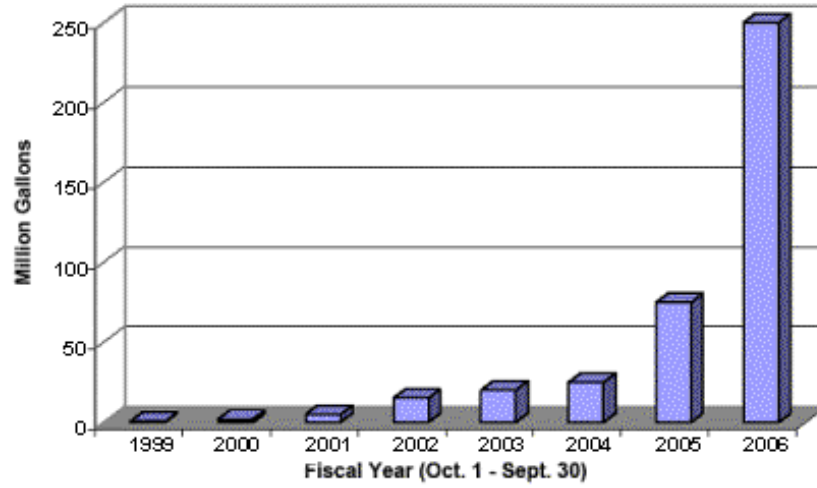


Figure 1.5: Biodiesel sales in the United States [NBB, 2007]

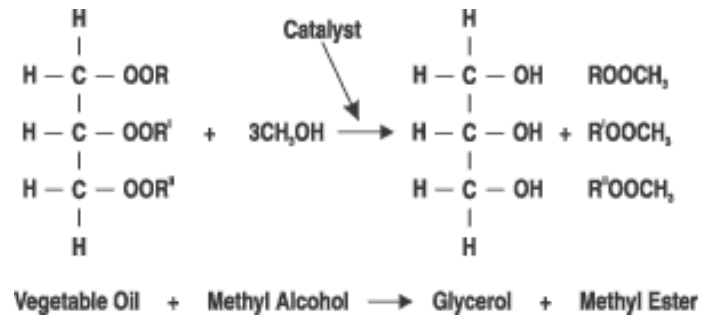


Figure 1.6: Transesterification reaction for the production of biodiesel [Hofman, 2003]

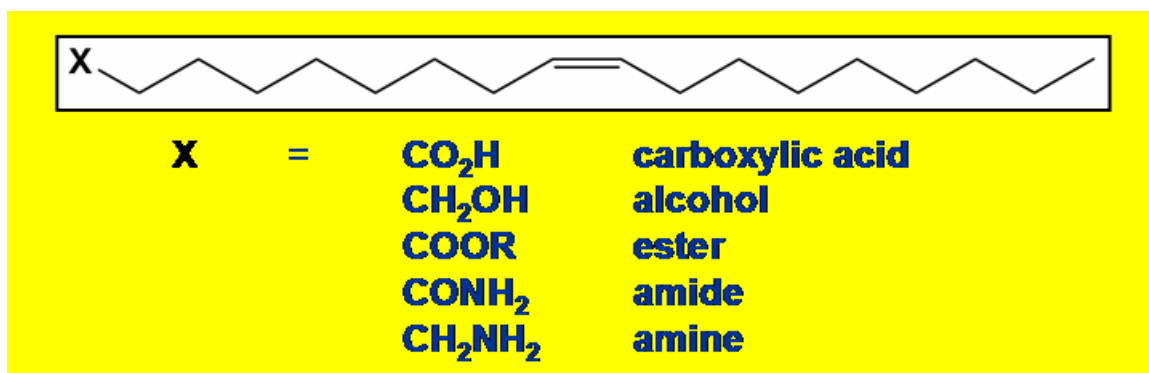


Figure 1.7: Functionality of oleic acid terminal group

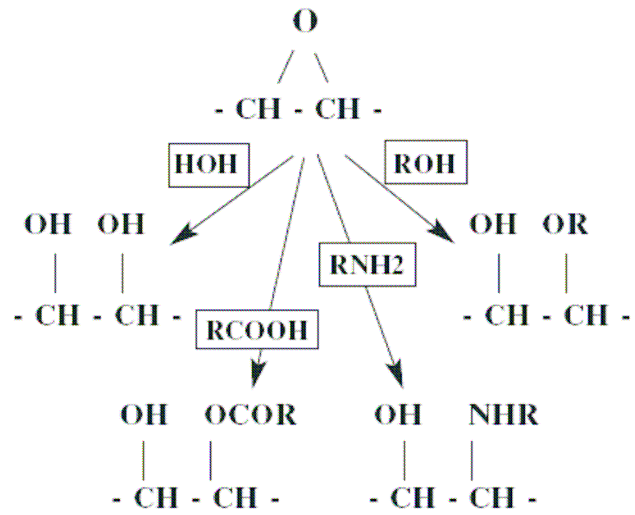


Figure 1.8: Possible oxirane reaction pathways [Pages-Xatart-Pares et al., 1999]

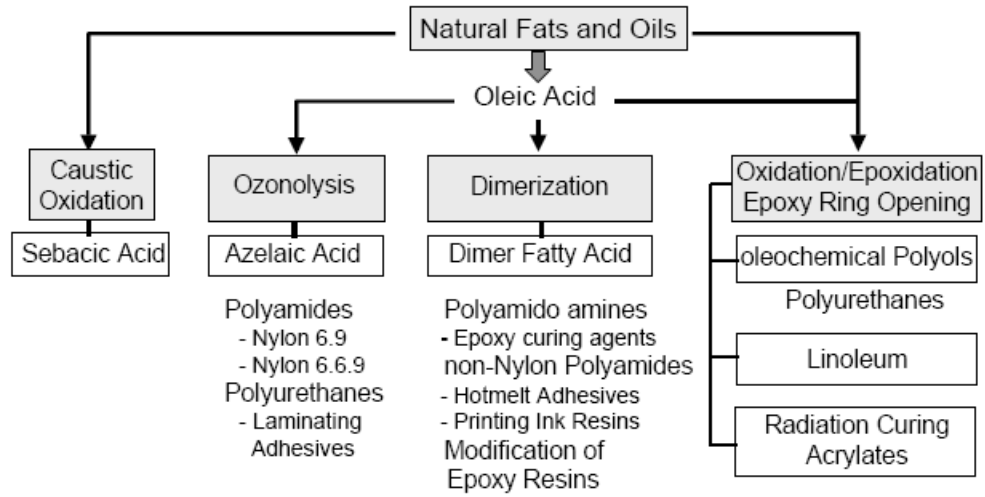


Figure 1.9: Use of fatty acids for polymer production [Hill, 2000]

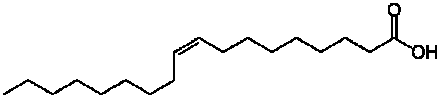
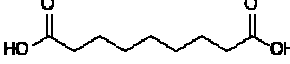
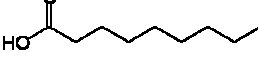
Oleic Acid	Azelaic Acid	Pelargonic Acid
		

Figure 1.10: Structures of oleic acid, azelaic acid, and pelargonic acid

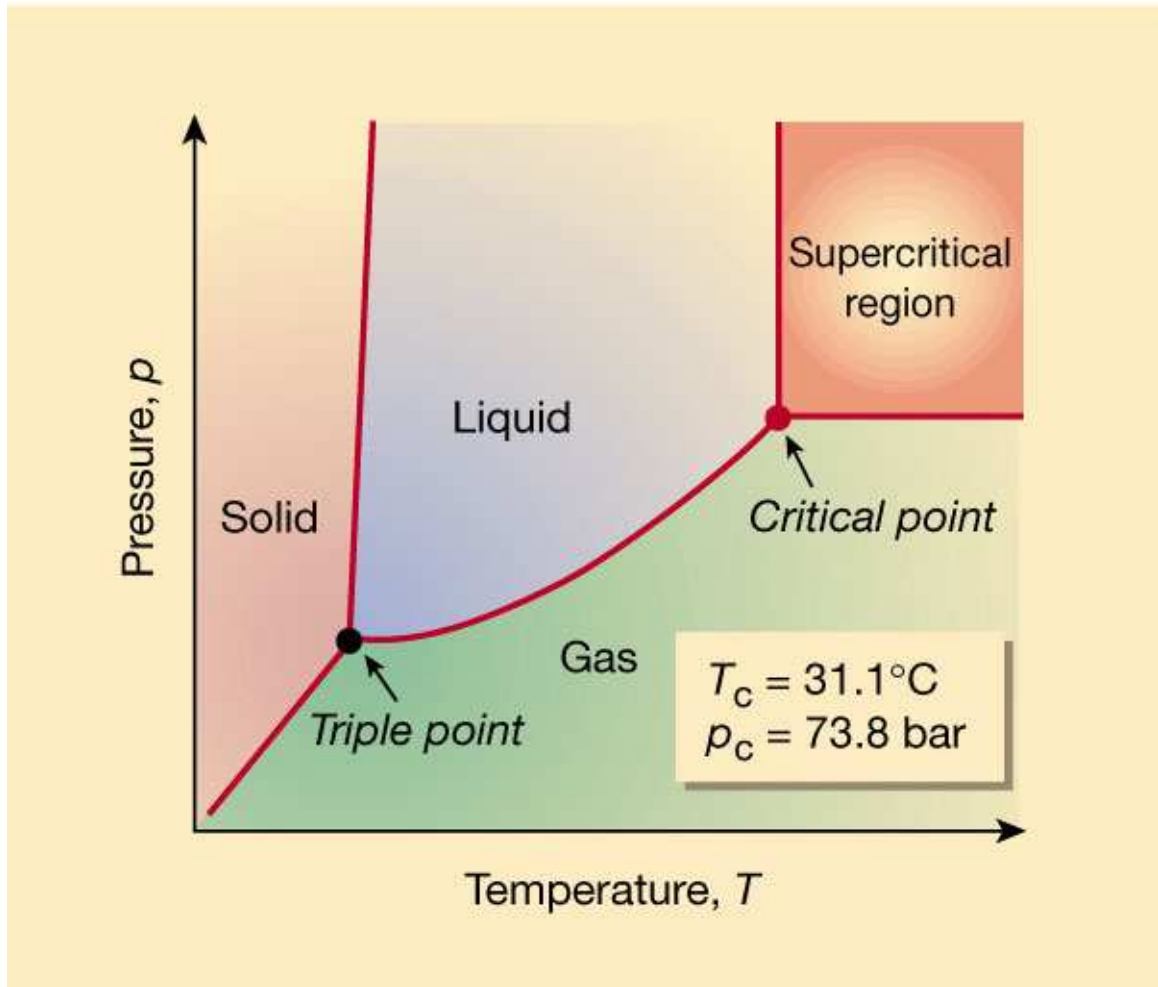


Figure 1.11: Typical pressure-temperature phase diagram with critical properties corresponding to carbon dioxide [Leitner, 2000]

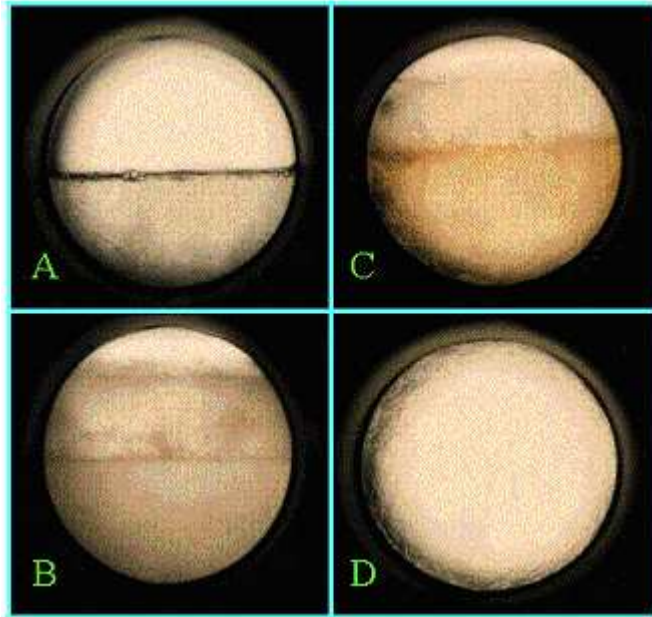


Figure 1.12: Transition from two-phase system to supercritical fluid [Clifford et al., 2007]

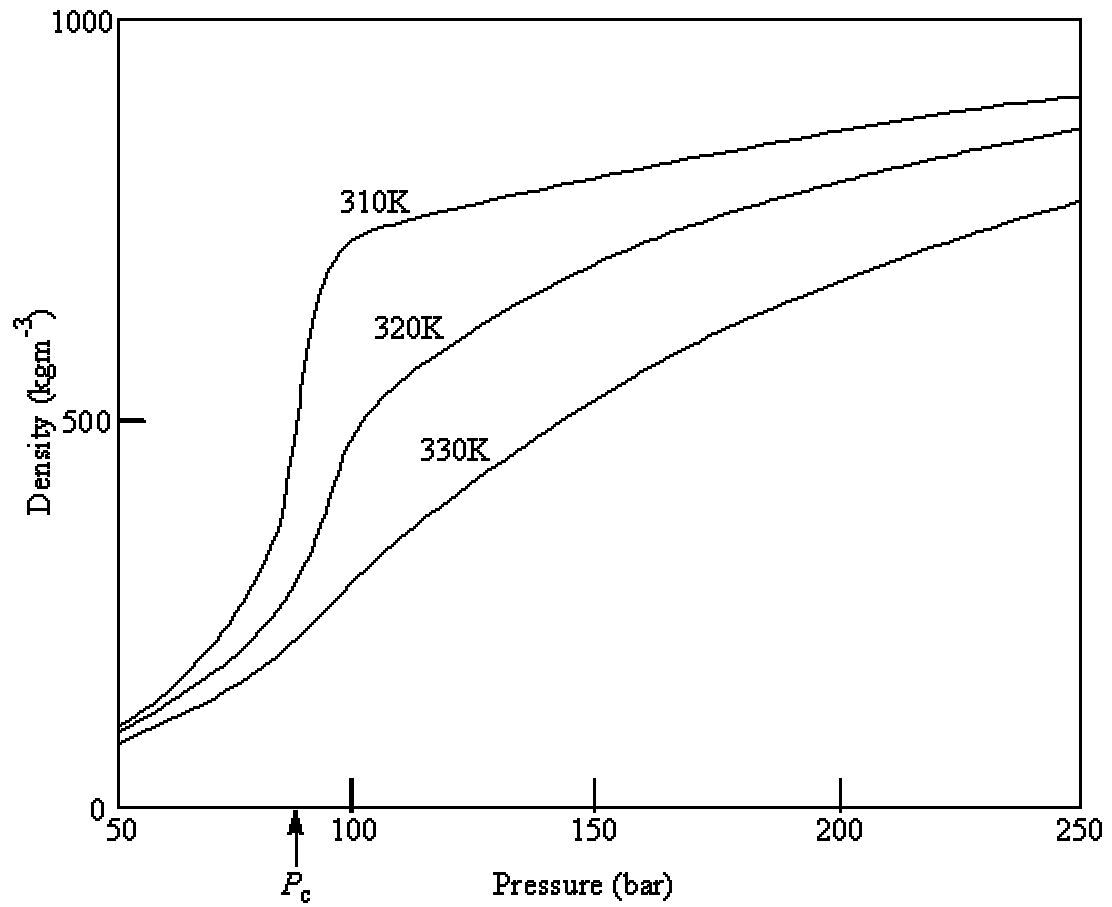


Figure 1.13: Effect of temperature and pressure on solvent density [Rayner, 2007]

CHAPTER II

RESEARCH HYPOTHESIS

The guiding hypothesis of this work was that incorporation of a supercritical fluid as a reaction medium for unsaturated fatty acid oxidation would result in enhanced reaction kinetics and facilitated product separation. Due to its relative abundance among lipid feedstocks, oleic acid served as the model fatty acid. Since it is already completely oxidized, carbon dioxide is an ideal solvent for oxidation reactions and was chosen as the supercritical fluid. Also, carbon dioxide provided the potential for coupling the oxidation reaction with product separation. As petroleum prices increase and petroleum supplies decrease, the use of lipids as renewable, alternative sources for petroleum-derived chemicals has become a major research thrust. However, a key issue is how to process the lipids in a sustainable and environmentally friendly way. By incorporating a supercritical fluid medium into oleic acid oxidation reactions, mass-transfer limitations could be reduced and reaction rates could be increased. It is envisioned that this research will offer further understanding of how a supercritical fluid affects oleic acid oxidation in terms of products formed and reaction rate and of the potential for supercritical fractionation of products. It is also desired that this research project will generate experimental solubility data for compounds in which no solubility data are currently available. This information will aid researchers in the oleochemical industry in designing unit operations that incorporate supercritical carbon dioxide.

Research Goal

The overall goal of this research was to determine if any advantages could be realized by conducting the oleic acid oxidation in a supercritical fluid medium.

Therefore, the overall goal has been divided into two primary objectives:

1. Evaluating the feasibility of separating target reaction products with supercritical carbon dioxide (SC-CO₂)
2. Determining the impact of the solvent medium on reaction kinetics and product formation during oxidation

Primary Objective 1: Evaluate the Solubility of Target Reaction Products in Supercritical Carbon Dioxide

The first primary objective required knowledge of the solubility of the target reaction products in supercritical carbon dioxide. Although the oxidation of oleic acid can result in a variety of reaction products, azelaic acid and pelargonic acid were chosen as target products for several reasons. First, these two compounds are the most valuable oxidation products produced from oleic acid. Second, both compounds have tremendous potential for future applications. Since fatty acid-supercritical fluid solubility data from literature are primarily only available for the most common fatty acids (palmitic, stearic, oleic, etc...), the data for the oxidation products will have to be generated experimentally. Both azelaic acid and pelargonic acid standards are readily available and not prohibitively expensive to use for solubility experiments. The azelaic acid and pelargonic acid solubility studies can be found in Chapter VII and Chapter VIII, respectively.

Although the solubility experiments were conducted over a range of temperatures and pressures, the experimental data were fit with several solubility models. These mathematical relationships allowed for the estimation of solubility at any point within the

range of temperatures and pressures over which the models were valid. As a result of the solubility experiments, new approaches to the use of density-based solubility models have been proposed. These approaches were validated in a study of five previously published solute-supercritical fluid systems. This study is located in Chapter VI and is preceded by a discussion of modeling theory (Chapter V).

Primary Objective 2: Impact of Supercritical Carbon Dioxide on Oxidation Reaction Kinetics and Product Formation

The second primary research objective was to perform oleic acid oxidation experiments in supercritical carbon dioxide and to determine the effect of the supercritical medium on the reactions. In particular, effects upon oleic acid conversion, reaction rate, and product formation were determined. Two oxidizers were chosen for this research: ozone and potassium permanganate. These oxidizers were chosen because their use in oxidation reactions under normal conditions results in mass-transfer-limited kinetics. Additionally, ozone was chosen because it is the same oxidizer used commercially for oleic acid oxidation reactions. The ozone and potassium permanganate oxidation studies can be found in Chapter IX and Chapter X, respectively.

As previously mentioned, knowledge of the solubility of the target reaction products in supercritical carbon dioxide is important in determining the feasibility of product fractionation. However, information on the solubility of reactants in supercritical carbon dioxide is equally important. As previously mentioned, gases such as ozone and oxygen are completely miscible with supercritical carbon dioxide. Since oleic acid-SC-CO₂ solubility data are available in the literature, this system was used to validate the experimental design used for the azelaic acid and pelargonic acid solubility studies. The

oleic acid solubility data can be found in Chapter VIII. Data on solubility of potassium permanganate in supercritical carbon dioxide was not located in the literature, so its solubility was determined experimentally, and the results are located in Chapter X.

CHAPTER III
LITERATURE REVIEW

Traditional Methods for Oxidizing Oleic Acid

Reaction of Oleic Acid with Gas Oxidants

Ozonolysis is the most well known technique for oxidizing oleic acid as a means to generate chemical products. In fact, ozonolysis of oleic acid has been performed commercially since the 1950s to produce azelaic acid and pelargonic acid. Prior to that time, chromic acid was used as the oxidant. However, this technique was fairly expensive because the spent chromic acid solutions had to be regenerated using electrolytic cells. Also, the chromic acid degraded a portion of the azelaic acid to lower dibasic acids [Kadesch, 1979].

The reference typically cited as providing the first process description of oleic acid ozonolysis is a U.S. patent by Goebel et al. (1957). This process begins by diluting technical grade oleic acid with pelargonic acid to reduce viscosity. Technical grade oleic acid typically has a purity of about 75 % and can contain other unsaturated fatty acids, such as linoleic acid, as well as saturated fatty acids like palmitic acid and stearic acid. The initial oleic ozonide is formed by continuous countercurrent contact in a vertical column between a falling solution of the oleic acid + pelargonic acid mixture and a rising stream of 2 % by weight ozone in oxygen at a temperature between 25 to 45°C. The

resulting ozonide + pelargonic acid mixture is then fed continuously into a pool of decomposed ozonide at a temperature between 75 to 120°C. This is typically done in the presence of a manganese salt while passing through a stream of oxygen. This causes aldehydes formed by the initial cleavage to be converted to acids. The aldehyde formed from the initial cleavage of oleic acid is pelargonaldehyde, which is converted to pelargonic acid. Distillation is typically used to remove the pelargonic acid, and the remaining mixture is extracted with hot water. Then the azelaic acid is removed from the aqueous extract via crystallization [Goebel et al., 1957; Kadesch, 1979].

In 2004, pelargonic acid and azelaic acid had market values of approximately \$3 per kg and \$5.50 per kg, respectively, while oleic acid had a market value of about \$0.90 per kg and ozone generation cost amounted to \$1.06/kg of ozone [Garrett and Rowland, 2004]. From a simple comparison of product value vs. reactant cost, it can be seen why this reaction has been commercialized. In fact, the potential net profit of the process is about \$0.12 per kg of oleic acid reacted [Garrett and Rowland, 2004].

Oleic acid is also a major component of edible oils used in the food industry, and its degradation can lead to rancidity in foods. As unsaturated fatty acids, such as oleic acid, break down in food and form oxidation products, the flavor of the food changes. Since oxidation products are typically lower in molecular weight compared to the starting compound, they also usually have a higher vapor pressure, which results in the food being more odiferous. Therefore, several studies have looked at the natural or autoxidation of oleic acid with oxygen; however most of these studies focus on techniques for analyzing lipid oxidation products [Frankel et al., 1977; Brimberg, 1993]. One exception is the work by Takahashi et al. (2000). In that work, the authors

performed a kinetic analysis of oleic acid autoxidation. Prior to the study by Takahashi et al., the mechanism for oleic acid was considered to consist of three steps: chain initiation, propagation, and termination as shown in Eqs. (3.1-3.4).



where LH represents the oleic acid, L[·] is the C-centered radical, LO₂[·] is the peroxy radical, and LOOH is the hydroperoxide. They collected experimental data on changes in the concentration of oleic acid (Figure 3.1), hydroperoxide (Figure 3.2), and dissolved oxygen (Figure 3.3) with time. As shown in Figure 3.1, the concentration of oleic acid slowly decreased at the beginning of the reaction, and then began to decrease at a faster rate. This behavior was particularly prevalent at 333 K over the first four data points. In general, the oxidation occurred more rapidly as temperature was increased. As shown in Figure 3.2, the hydroperoxide concentration initially increased, and then decreased. This behavior was due to the decomposition rate of hydroperoxide becoming larger than its formation rate as the reaction progressed. The maximum observed hydroperoxide concentration decreased and occurred earlier as temperature increased. Figure 3.3b shows that dissolved oxygen concentration rapidly increased initially and reached a maximum value at 20 to 30 minutes. Figure 3.3a shows that after the maximum, the dissolved oxygen concentration began to decrease, eventually reaching a low, but nonzero, value until the end of the oxidation.

Takahashi et al. (2000) found that kinetic models based solely on the mechanism shown in Eqs. (3.1-3.4) did not adequately fit the experimental results. Therefore, several modifications to the mechanisms were proposed. The hydroperoxide formed in Eq. (3.3) had been previously shown to decompose to free radicals, which, in turn, participate in the initiation reaction [Encinar, et al., 1993; Toro-Vazquez et al., 1993; Encinar et al., 1994]. Therefore, the initiation rate was proportional to the amount of hydroperoxide produced by the oxidation. Also, other studies had previously shown that oxygen reacted with hydroperoxide [Brimberg, 1993]. Hence, the following initiation reaction of hydroperoxide with oxygen was proposed:



Eq. (3.5) explains the rapid decrease in dissolved oxygen concentration observed near the beginning of the reaction. It had been previously shown that the hydroperoxide would decompose via a bimolecular reaction [Okatsu, 1983]. Therefore, an additional initiation reaction was proposed:



where $\text{LO}\cdot$ is the alkoxy radical, which had been previously found to react with oleic acid to form an alcohol [Bamfold and Tipper, 1980]. This reaction can be expressed as the following:



where LOH is the oleyl alcohol. Therefore, the alcohol was considered to be a secondary product. A previous study had shown that the alcohol product could be oxidized by oxygen to form other secondary products such as a ketone [Bamfold and Tipper, 1980].

Takahashi et al. (2000) proposed that the oxidation of the alcohol occurred consecutively

after Eq. (3.7), thus explaining the experimental observation that the dissolved oxygen concentration decreased to a constant value.

As a result of being used for food purposes, oleic acid is a key component of atmospheric organic aerosols and has been studied as a model compound for predicting aerosol oxidation products [Reynolds et al., 2006; Hung et al., 2005]. Oleic acid aerosol particles can be released into the atmosphere during food preparation such as frying. Atmospheric particles scatter radiation and act as cloud condensation nuclei (CCN), which are crucial to cloud formation. In the lower atmosphere, these particles can have a negative impact on human health, such as causing respiratory damage. Up to 50 % of atmospheric aerosol particle mass is attributable to organic compounds generated either from animals or man-made products [Reynolds et al., 2006]. These organic compounds react with oxidants such as ozone in the atmosphere to form polar oxygenated compounds. Since the vapor pressure of the oxygenated compounds is typically lower than the starting compound, a partitioning of the compounds from gas phase to condensed phase can occur. These compounds can cause increased cloud formation and are potentially hazardous to human health [Reynolds et al., 2006].

Reynolds et al. (2006) found the primary products of oleic acid aerosol ozonolysis to be pelargonaldehyde, pelargonic acid, azelaic acid, and 9-oxononanoic acid occurring in approximately equal yields. However, other higher-molecular-weight oxidation products were detected using mass spectrometry. In fact some of the products had m/z (mass-to-charge) ratios near 1000. By using mass spectrometry, the products were determined to be a mixture of linear α -acyloxyalkyl hydroperoxides, secondary ozonides, and cyclic diperoxides. It was proposed that these species were formed by reactions between

ozonolysis products and Criegee intermediates. A mechanism for oleic acid aerosol oxidation had been proposed previously by Ziemann (2005), and this mechanism is shown in Figure 3.4. The Criegee intermediates (CI 1 and CI 2) react with carboxylic acid groups to form α -acyloxyalkyl hydroperoxides (AAHP 1-5), carbonyl groups to form secondary ozonides (SOZ 1-3), and with other Criegee intermediates to generate cyclic diperoxides. Reynolds et al. proposed that these products could react with Criegee intermediates to form the larger oligomers found via mass spectrometry.

Oleic acid aerosol oxidation by ozone was also studied by Hung et al. (2005). Initially, they expected the oxidation products to be pelargonaldehyde, pelargonic acid, azelaic acid, and 9-oxononanoic acid with each being formed at 25 % carbon-normalized yield. However, their results showed that pelargonaldehyde and 9-oxononanoic acid were the major products and the minor products consisted of azelaic acid, pelargonic acid, and octanoic acid as well as high molecular weight (> 1000 amu) products. Several of the high molecular weight products were identified as α -acyloxyalkyl hydroperoxides, which were also observed by Reynolds et al.

The product distribution seen by Hung et al. did not agree with similar studies in the literature. As previously mentioned, pelargonaldehyde was found to be one of the major products in the condensed phase, but other studies had reported pelargonaldehyde as a gas-phase product [Moise and Rudich, 2002; Thornberry and Abbatt, 2004]. In fact, a study by Katrib et al. (2004) found pelargonaldehyde to be a gas-phase product only. Unfortunately, Hung et al. did not monitor gas phase products. The results for other products also differ between studies. For example, in Hung et al., the remaining product distribution included approximate yields of 14 % for 9-oxononanoic acid, 6 % for azelaic

acid, and 7 % for pelargonic acid. However Katrib et al. reported yields of 20 to 35 % for 9-oxononanoic acid and 1 to 3 % for both azelaic acid and pelargonic acid with the product distribution depending upon on the initial thickness of the oleic acid layer. As a result, Hung et al. proposed three explanations for the variation in product formation among literature studies. First, they proposed that the method of product analysis affected results. For example, analytical methods can have different selectivities for different products, resulting in discrimination. Additionally, studies do not always report the yield type. For example, in Hung et al., only condensed-phase yields were reported, but in Hearn and Smith (2004), yields were reported in terms of combined gas-phase and condensed-phase products. Also, some of the methods used in literature provide qualitative information only. Hung et al. also concluded that the physical dimension of oleic acid influenced product yields. For example, bulk reactions dominated for homogeneous aerosol particles, but surface reactions were important for nanometer-thick coatings of oleic acid on particles. Also, a volatile reaction product like pelargonaldehyde present in a 2- to 30-nm coating on a particle would quickly diffuse to the surface of the particle and evaporate. This resulted in a limitation of more condensed-phase reactions such as generation of secondary ozonides. Finally, Hung et al. suggested that molar ratio of ozone to oleic acid affected product yields. If the ratio of ozone to oleic acid was much less than unity, then the only products were those that resulted directly from the ozonolysis of oleic acid and the reaction of the Criegee intermediates with oleic acid. If the ratio of ozone to oleic acid was in excess (much greater than unity), then reactions of the Criegee intermediates with other intermediates were possible, potentially resulting in polymerization products. Some of the products formed such as

carboxylic acids would also react with ozone; however, this type of reaction would be much slower than reaction of ozone with alkenes.

Reaction of Oleic Acid with Liquid Oxidants

Oleic acid can also be reacted with liquid oxidants to yield valuable products such as azelaic acid and pelargonic acid. Most studies have utilized hydrogen peroxide as the oxidant. For example, in the work by Nouredini and Kanabur (1999), oleic acid was oxidized with hydrogen peroxide in the presence of various transition metal catalysts. As previously mentioned, the commercial oleic acid oxidation process utilizes ozone as the oxidant. However, use of ozone has several disadvantages including health and safety hazards, high capital costs, and high energy costs. Nouredini and Kanabur proposed to improve the oleic acid oxidation process by using heterogenized homogeneous catalysts with a liquid oxidant in a homogeneous reaction with oleic acid. The heterogenized homogenized catalysts combined the advantages of both homogeneous and heterogeneous catalysts. Homogenous catalysts are known to provide high selectivity, and heterogeneous catalysts are easier to recover and regenerate than traditional homogeneous catalysts.

A free-radical mechanism usually occurs in liquid-phase oxidation reactions [Nouredini and Kanabur, 1999]. Hence the reactions begin with an induction phase followed by a fast reaction period. During induction, initiation reactions result in an increase in free radical concentration until propagation becomes the dominant process. The stoichiometric equation for oleic acid oxidation with hydrogen peroxide in the presence of a catalyst is expressed as follows:



The catalysts considered by Nouredini and Kanabur included tungsten, tantalum, molybdenum, zirconium, and niobium, and the reactions were performed at a temperature of 130°C with 100 % excess hydrogen peroxide. Since oleic acid is fairly nonpolar, mass-transfer limitations existed between the oleic acid and the hydrogen peroxide, which was in an aqueous solution. Therefore, Nouredini and Kanabur added *t*-butanol to the reaction mixture to help homogenize the system. Additionally, agitation was applied at a rate of 500 RPM. The reaction products were derivatized to methyl esters prior to analysis with gas chromatography with flame ionization detection.

As expected from Eq. (3.8), the major products observed by Nouredini and Kanabur were azelaic acid and pelargonic acid. However, lower-molecular-weight mono- and dicarboxylic acids were formed during the reaction as well. These minor products included octanoic acid, succinic acid, suberic acid, heptanoic acid, hexanoic acid, sebacic acid, and pimelic acid. The formation of these short-chain fatty acids indicated that chain degradation was occurring. In general, the concentration of azelaic acid and pelargonic acid increased to a maximum value and then began to decrease. An example of this behavior can be seen in Figure 3.5. The point at which the maximum azelaic acid and pelargonic acid concentration occurred depended upon the catalyst present. In most cases, pelargonic acid appeared to be more stable than the azelaic acid.

Transition metals can potentially oxidize to their oxide form in the presence of hydrogen peroxide, and metal oxides are thought to be responsible for catalyzing fatty acid oxidation. Nouredini and Kanabur hypothesized that a transition metal that

oxidized slowly but resulted in a rate of oleic acid oxidation comparable with the direct use of metal oxides would be more economical than direct use of the metal oxide. Therefore, experiments were conducted comparing molybdenum, tungsten, tantalum, zirconium, and niobium with direct use of their metal oxides. Although tungsten and molybdenum were significantly oxidized (60 % and 100 %, respectively) by the hydrogen peroxide, the rate of oleic acid oxidation was comparable to the direct use of the oxides. However, because of the fast rate of metal oxide formation, these metals were deemed economically unfeasible. Zirconium and niobium showed resistance to oxidation with hydrogen peroxide, and the observed reaction products were similar to the products obtained without the use of any catalyst. Tantalum oxidized very slowly with hydrogen peroxide, and the rate of oleic acid oxidation was similar to the rate achieved by directly using tantalum oxide.

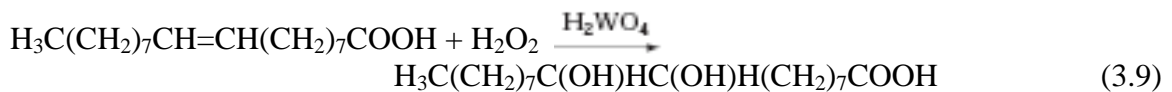
In terms of conversion, tungstic oxide on silica support resulted in an oleic conversion of 79 % after 1 hour, 96 % after 2 hours, and 98 % after 3 hours, which was the highest conversion observed among all the catalysts. When tungstic oxide was used without the silica support, the conversion of oleic acid after 1 hour was only 56 %. However, after 2 hours, the conversion of oleic acid with the unsupported catalyst was comparable to the conversion achieved with the supported tungstic oxide. Tungstic oxide on alumina support resulted in a slightly lower reaction rate compared to the silica-supported catalyst. The decrease in reaction rate was attributed to the smaller pore diameter of the alumina (135 Å) compared to silica (250 Å) and to the fact that the alumina pellets typically settled to the bottom of the reactor, creating diffusion limitations. The use of tantalum oxide supported on alumina only resulted in 77 %

conversion of oleic acid after 5 hours. Also, the yields of pelargonic acid and azelaic acid with respect to conversion of oleic acid were lower than what was achieved with the unsupported tantalum oxide and much lower than what was achieved with supported tungstic oxide. This result indicated a high rate of chain degradation and a low selectivity for the C-C double bond. The unsupported tantalum oxide resulted in an oleic acid conversion of about 96 % after 4 hours, but the final concentrations of the target products (azelaic acid and pelargonic acid) were significantly lower compared to tungstic oxide. With unsupported tantalum, the conversion of oleic acid was 96 % after 4 hours, and the final concentrations of the target products were similar to the concentrations obtained when tungstic oxide was used as the catalyst. However, the initial rate of oleic acid oxidation was relatively slow in the presence of the unsupported tantalum. Nouredini and Kanabur suspected the low initial rate was caused by the slow rate of oxidation of tantalum by hydrogen peroxide to form tantalum oxide, which catalyzes the oleic acid reaction.

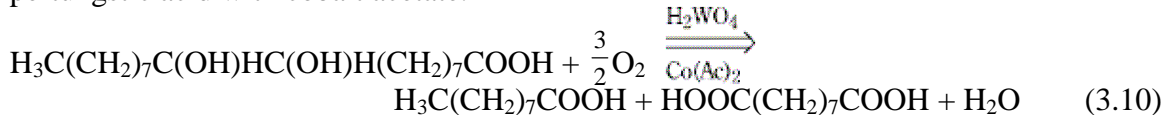
In terms of selectivity, tungstic oxide provided the highest selectivity and resulted in the lowest concentration of chain degradation products (< 5 mol %). Compared to tungstic oxide, unsupported tantalum oxide was less selective towards azelaic acid and pelargonic acid and resulted in higher concentrations of chain degradation products like octanoic acid. In all cases for the tungstic oxide- and tantalum oxide-based catalysts, the concentrations of azelaic acid and pelargonic acid were either approximately equivalent to each other or slightly more concentrated in pelargonic acid. The lone exception was unsupported tantalum, which formed more azelaic acid than pelargonic acid. The authors

suggested this was due to the lower degradation rate of azelaic acid in the presence of that particular catalyst.

Santacesaria et al. (2003) also studied oxidation of oleic acid with hydrogen peroxide. In this case, pertungstic acid (H_2WO_4) was used as a catalyst. This reaction proceeded in two steps. The first step is shown in Eq. (3.9) [Santacesaria et al., 2000]. The hydrogen peroxide reacted with oleic acid in the presence of the pertungstic acid to form dihydroxystearic acid (a diol).



The second step is shown in Eq. 3.10 [Santacesaria et al., 2000]. The diol was cleaved with molecular oxygen in the presence of catalyst formed by the reaction of the spent pertungstic acid with cobalt acetate.



One of the major disadvantages of this reaction in terms of safety was that concentrated hydrogen peroxide (60 % by weight) had to be used to stay above a previously observed threshold concentration necessary to initiate the reaction of 30 % by weight. The hydrogen peroxide also had to be stabilized with sodium stannate and sodium pyrophosphate to prevent decomposition. The maximum conversion of oleic acid to dihydroxystearic acid was only 86 % because the reaction mixture formed a “doughy” mixture, which could not be mixed efficiently. Also, product analysis after the first reaction consistently showed a small amount of epoxide, which was probably formed as a reaction intermediate.

Advanced oxidation techniques have also been studied as a means to oxidize oleic acid. Pernyeszi and D  k  ny (2001) studied the photooxidation of oleic acid in water. In this type of reaction, the photocatalyst is excited upon exposure to specific wavelengths of light, which leads to the formation of photoregenerated holes (h^+) and hydroxyl radicals (OH). In the work by Pernyeszi and D  k  ny, titanium dioxide (TiO_2) was used as the photocatalyst, resulting in the following mechanism [Ding et al., 2000]:



where a represents a species adsorbed or close to the surface of the photocatalyst and C_{inert} stands for inert species that can cause uptake of hydroxyl radicals. Ultraviolet (UV) light was used to excite the photocatalyst. Although oleic acid can be oxidized directly by UV light, the reaction is slow compared to oxidation via hydroxyl radicals.

Pernyeszi and D  k  ny began their study by first determining the maximum solubility of oleic acid in water at 25  C to be 0.02 g oleic acid per 100 mL of water (\approx 0.71 mM) by use of total organic carbon (TOC) measurements. Based upon that finding, the concentration oleic acid used for oxidation experiments was 0.06 mM. The photooxidation utilized a 0.1 % (m/v) suspension of TiO_2 (pH = 4.6) for 1.5 hours. Due to the pH of the suspension, the titanium dioxide surfaces were positively charged, so the carboxyl groups of the oleic acid readily bound to the catalyst. Since Pernyeszi and D  k  ny were focused more on destruction of organic compounds in aqueous streams than

formation of valuable oxidation products, oleic acid concentration was not directly measured; instead, TOC was monitored over time. After 1.5 hours, the TOC was reduced to less than 20 % of the initial value. A plot of TOC vs. time yielded a linear relationship, indicating that the photooxidation of oleic acid was a zero-order reaction, which was indicative of the presence of mass-transfer limitations. The rate constant was determined to be $0.0069 \text{ mmol}\cdot\text{sec}^{-1}\cdot\text{m}^{-3}$.

Reaction of Oleic Acid with Solid Oxidants

One of the most researched solid oxidants used for oleic acid oxidation is potassium permanganate. However, due to the low solubility of potassium permanganate crystals in organic compounds such as oleic acid, the potassium permanganate is usually dissolved in water, and some sort of catalyst or complexing agent is used to allow the potassium permanganate to react with the organic layer. Garti and Avni (1981) evaluated the use of emulsion technology for potassium permanganate oxidation of oleic acid. Previously, the major products of this reaction had been found to be dihydroxy, ketohydroxy, and diketo acids. The reaction of oleic acid to form a ketohydroxy product is shown in Eq. (3.16) [Coleman et al., 1956].



In the work by Coleman et al., complete oxidative cleavage of the C-C double bond was not obtained, and azelaic and pelargonic acid were not formed. The authors hypothesized that by varying the reaction environment, that azelaic acid could be formed as the major product.

All reactions were conducted at 10°C for 0.5 hour with stirring at 1,200 RPM. A constant stream of carbon dioxide was passed through the reactor to control the pH of the reaction system. The carbon dioxide reacted with the water to form carbonic acid, which neutralized the potassium hydroxide formed in Eq. (3.16). The previous study by Coleman et al. had shown that pH affected the oleic acid oxidation products formed. They found that as the pH of the system approached neutrality by addition of sulfuric acid into the system, yields of ketohydroxystearic acids increased while dihydroxystearic acid decreased. Garti and Avni began with a control experiment in which potassium permanganate was added to a two-phase mixture of water and oleic acid with no emulsifier. Based on analysis with gas chromatography, no oleic acid oxidation occurred during the control experiment. For the emulsification experiments, the following nonionic emulsifiers were considered: polyoxyethylene ethers of long-chain fatty alcohols (“Brijs”), polyoxoethylene esters of long-chain fatty acids (“Myrjs”), and long-chain carboxylic acid esters of polyoxyethylenated sorbitol, sorbitan, and isosorbides (“Tweens”). The authors studied four other variables in their study. The first variable was the emulsification preparation method. The authors considered three preparation methods:

- Mixing of oleic acid, water, and emulsifier at the same time
- Mixing of water and emulsifier, followed by dropwise addition of oleic acid
- Dropwise addition of the water + emulsifier mixture to oleic acid

The other variables were the initial concentration of oleic acid, the molar ratio of potassium permanganate to oleic acid, and amount of emulsifier used. Conversion of

oleic acid and formation of azelaic, diol-, ketol-, and diketostearic acids (but not pelargonic acid) were used to evaluate the effect of each variable.

The authors found the best preparation method to be dropwise addition of oleic acid to the water + emulsifier mixture. This method resulted in the highest conversion and highest yield of azelaic acid. Prior to the work by Garti and Avni, dropwise addition of an olefin into potassium permanganate had already become a well-established method because of the amount of heat released during the exothermic reaction [Starks, 1971]. By adding the oleic acid dropwise into the reaction, the temperature of the system could be controlled better and avoid the situation experienced by Starks (1971) in which so much heat was evolved that the reaction mixture could no longer be contained in the reactor. The mole ratio of potassium permanganate to oleic acid was varied from 1 to 6; in general, as the mole ratio increased, the conversion of oleic acid and the yield of azelaic acid increased. When the mole ratio was increased from 4 to 6, the conversion of oleic acid did not change (98 %); however, the yield of azelaic acid increased from 84 to 87 %. The initial oleic concentration was varied from a mass fraction of 5.7 % up to 14.2 %. As the oleic acid concentration increased, the conversion of oleic acid and the yield of azelaic acid both decreased, while the yields of diol-, ketol-, and diketostearic acids increased. For the study on the effect of emulsifier concentration, the concentration of Myrjs emulsifier was increased from a mass fraction of 0 % (control experiment) to 3 %. The yield of azelaic acid increased to a maximum yield of 56 % at an emulsifier mass fraction of 1 %. At emulsifier mass fractions of 2 % and 3 %, the yield of azelaic acid was only 42 % and 45 %, respectively. The maximum oleic acid conversion (85 %) also occurred at a mass fraction of 1 % emulsifier. At mass fractions of 2 % and 3 %, the

conversion of oleic acid decreased to 80 % and 56 %, respectively. The best emulsifier was found to be Myrj 59, which provided the highest conversion of oleic acid. The authors suggested that Myrj 59 was the best emulsifier because it had the best hydrophilic-lipophilic balance (HLB), a measure of the hydrophilic or lipophilic nature of a compound. The HLB of a compound is determined by Griffin's equation:

$$HLB = 20 M_h/M \quad (3.17)$$

where M_h is the formula weight of the hydrophilic portion of the compound and M is the molecular weight of the entire compound. An HLB value of 20 would correspond to a compound that is completely hydrophilic, and a value of 0 would correspond to a compound that is completely hydrophobic (lipophilic). Of the emulsifiers considered by Garti and Avin, Myrj 59 had the highest HLB with a value of 18.8.

Foglia et al. (1977) performed a study similar to Garti and Avni, except that phase-transfer catalysts were evaluated instead of emulsifiers. The phase-transfer catalysts were either quaternary ammonium halides or crown ethers and served to transfer the potassium permanganate in the aqueous phase to the organic phase where oxidation occurred. The organic compounds consisted of 1-pentadecene, *cis*-9-octadecene, and methyl oleate. The authors found that pH affected product formation. For example, oxidation of *cis*-9-octadecene in methylene chloride with aqueous potassium permanganate and a phase-transfer catalyst of tetrabutylammonium bromide (TBAB) resulted in dihydroxyoctadecane (80 % yield) at a basic pH and pelargonic acid (80 % yield) at a neutral pH. Oxidation of methyl oleate in methylene chloride with aqueous potassium permanganate and a phase-transfer catalyst of TBAB yielded pelargonic acid (67 %) and monomethyl azelate (72 %) at a neutral pH. However, at basic pH, product

yields were reduced to below 25 %. The authors speculated that this was due to saponification which caused emulsion problems during the reaction.

In the work by Garti and Avni (1981), the potassium permanganate was always used in an aqueous solution; they did not study the direct use of solid potassium permanganate. Although studies of oleic acid oxidation directly with solid potassium permanganate could not be found, similar studies have been conducted with other organic compounds. Sam and Simmons (1972) studied the oxidation of various organic molecules such as *trans*-stilbene, cyclohexene, α -pinene, and toluene in benzene with potassium permanganate. Since potassium permanganate had no detectable solubility in benzene, dicyclohexyl-18-crown-6 (crown ether) was used as a complexing agent. For their experiments, the oxidizing reagent was prepared by stirring equimolar amounts of the crown ether with potassium permanganate in benzene, allowing the concentration of potassium permanganate in benzene to be as high as 0.06 M. Then the organic compound was added to the potassium permanganate + benzene solution at 25°C. Reactions of olefins occurred within minutes, while alkylbenzenes like toluene required up to 72 hours. Very high yields of suspected oxidation products were obtained in all cases. For example, *trans*-stilbene and α -pinene were converted to benzoic acid and adipic acid in yields of 100 % and 90 %, respectively. For the oxidation of olefins with potassium permanganate without water (at least initially), the authors suggested the following overall reaction:



with the reaction being initiated by the electrocyclic addition of the permanganate ion to the olefinic π bond to form the corresponding manganate ester ion. The authors

suggested that the manganate ester was first split into corresponding aldehydes, which were then oxidized into carboxylic acids.

Although potassium permanganate is the most common solid oxidant used for oleic acid oxidation, other solid oxidants have been researched. For example, Zimmermann et al. (2005) studied oxidation of oleic acid via a catalytic ruthenium system consisting of 2.2 % RuCl_3 , 4.1 eq. NaIO_4 (oxidant) in a solvent mixture of $\text{H}_2\text{O}:\text{CH}_3\text{CN}:\text{CCl}_4$ in a ratio of 3:2:2. The goal of that study was to find a suitable solvent to replace carbon tetrachloride (CCl_4) because of environmental regulations. When CCl_4 was included as a solvent, the reaction time required for complete conversion of oleic acid was 4.5 hours and produced a 70 % yield of azelaic acid (the target product in that study). When carbon tetrachloride was removed from the solvent system, 6.5 hours were required for complete oleic acid conversion, and the azelaic acid yield dropped to 66 %. The authors concluded that the carbon tetrachloride did, in fact, play some unknown crucial role to the oxidation reaction.

Finding a suitable alternative to carbon tetrachloride was complicated by the fact that the oxidant (RuO_4) formed from the ruthenium complex was a powerful oxidizer, so solvent choice was limited. Several solvents including ethyl acetate, acetone, and cyclohexane were studied as potential replacements for carbon tetrachloride because of their resistance to oxidation. Cyclohexane resulted in a reaction time of 48 hours needed to completely oxidize the oleic acid; however, the yield of azelaic acid was 71 %. Substitution of acetone for carbon tetrachloride gave results very similar to the original solvent system. After 4.5 hours, oleic acid was completely consumed, and the yield of azelaic acid was found to be 69 %. However, the best results were obtained with ethyl

acetate. A reaction time of only 2 hours was required for complete conversion of the oleic acid, and the resulting yield of azelaic acid was 73 %. The faster reaction time achieved with ethyl acetate was attributed to the increased solubility of the oleic acid and dihydroxystearic acid (oxidation intermediate) in the H₂O:CH₃CN:AcOEt (3:2:2) solvent system. An advantage of this solvent was the ease of product separation. After evaporation of acetonitrile and ethyl acetate, the pelargonic acid phase separated from the remaining aqueous layer because pelargonic acid was insoluble in water. After pulling off the pelargonic acid from the aqueous layer, the water was cooled until the azelaic acid precipitated completely. Since azelaic acid was practically insoluble in cool water, a very low temperature was not required. Hence, the authors recommended the catalytic ruthenium system of 2.2 % RuCl₃ with 4.1 eq. NaIO₄ and a solvent system of H₂O:CH₃CN:AcOEt (3:2:2) for large-scale oxidation of oleic acid.

Use of Supercritical Carbon Dioxide as a Reaction Medium

Rationale

Initially, the idea of incorporating a supercritical fluid into a reaction may not seem like a wise decision, especially in terms of economics. Generally, use of supercritical fluids results in the need for vessels to be made to withstand higher pressures. Also, the cost of recovering the supercritical fluid must be taken into account. In the case of carbon dioxide, this would be the cost of purification and recompression. Therefore, both equipment costs and certain operating costs are incurred with the use of supercritical fluids. However, research has shown that supercritical fluids can provide several benefits that can potentially offset the costs associated with their use. For

example, incorporation of a supercritical fluid can affect reaction rate and selectivity, enhance mass and heat transfer, increase catalyst lifetime and aid in regeneration, facilitate separation, and enhance particle formation [Brennecke, 1993; Baiker, 1999].

The effect of pressure on the reaction rate constant can be explained in terms of transition-state theory in which the reactants are in thermodynamic equilibrium with a transition-state intermediary. Once formed, the intermediary, or activated complex, proceeds directly to reaction products. According to transition-state theory, the magnitude and direction of the mole fraction-based rate constant k_x is dependent upon both the sign and magnitude of the activation volume V^\ddagger as follows [Baiker, 1999]:

$$\left(\frac{\partial \ln k_x}{\partial P}\right)_{T,x} = -\frac{\Delta V^\ddagger}{RT} \quad (3.19)$$

where P is pressure, T is absolute temperature, and R is the gas constant. V^\ddagger can be expressed as follows [Brennecke, 1993]:

$$\Delta V^\ddagger = \bar{V}_{ts} - (\bar{V}_A + \bar{V}_B) \quad (3.20)$$

where \bar{V}_{ts} is the partial molar volume of the activated complex and \bar{V}_A and \bar{V}_B are the partial molar volumes of the reactants (for a bimolecular, elementary reaction). When the rate constant is related to a pressure-dependent measure of concentration, the following equation results [Baiker, 1999]:

$$\left(\frac{\partial \ln k_c}{\partial P}\right)_{T,c} = -\frac{\Delta V^\ddagger}{RT} + \left(\frac{1-n}{P}\right) \left[1 - \left(\frac{\partial \ln k_T}{\partial \ln P}\right)_{T,c}\right] \quad (3.21)$$

where n is the molecularity of the reaction and k_T is the isothermal compressibility [Baiker, 1999]. Based upon Eqs. (3.20) and (3.21), it can be seen that a negative ΔV^\ddagger

results in a rate increase with increasing pressure, while a positive ΔV^\ddagger results in a rate decrease with increasing pressure. Partial molar volumes of liquids are typically 5 to 10 $\text{cm}^3\cdot\text{mol}^{-1}$, but they can have values as high as $-15,000 \text{ cm}^3\cdot\text{mol}^{-1}$; hence, the pressure effect on reaction rate can be significant [Brennecke, 1993]. In a system in which several parallel or competing reactions occur, the pressure can also affect the individual rate constants so that the activation volumes (V^\ddagger) are not equal for each reaction. Therefore, an increase in pressure may favor one (or more) of the reactions over the others and affect product selectivity.

In the supercritical region, diffusivities are generally higher and viscosities are lower than they are in liquids. Therefore, the rate of mass transfer-limited reactions can be increased under supercritical conditions. Also, reactions that normally occur in multiphase systems that are subjected to mass-transfer limitations can be conducted in a single supercritical fluid phase, eliminating interfacial mass-transfer resistances. Also, supercritical fluids have higher thermal conductivities than in the corresponding gas phase. Therefore, heat transfer can be enhanced, especially in the case of exothermic reactions where heat removal is crucial [Baiker, 1999].

Use of supercritical fluids can also result in increase of catalyst life. Over time, catalysts can become deactivated or poisoned by organic molecules. Since the solubility of organic compounds can be much higher in supercritical fluids than in corresponding gases, the deactivation can be suppressed by switching the reaction from the gas phase to the supercritical phase. Supercritical fluids can also be used to regenerate catalysts. As previously mentioned, organic molecules that typically cause catalyst deactivation are

more soluble in supercritical fluids than in the corresponding gases. Hence, supercritical-fluid extraction can be used to remove the poisons from the catalyst.

Supercritical fluids can also facilitate the separation of compounds, particularly products. Supercritical fluids are considered *tunable* media because small changes in temperature and pressure can result in large changes in solute solubility. Hence, if the solubilities of solutes differ enough in a supercritical fluid, then they can be easily fractionated. Also, if the solubilities of products are low in a supercritical fluid compared to the reactants, then conversion can be increased in the case of an equilibrium reaction.

Supercritical fluids can also aid in controlling the particle size of materials such as catalysts. For example, two particle-forming techniques incorporating supercritical fluids are the rapid expansion of supercritical solutions (RESS) method and the supercritical antisolvent (SAS) technique [Baiker, 1999]. The basis of RESS is the rapid depressurization of a supercritical fluid phase in which the solutes are dissolved. In SAS, the solutes are dissolved in an organic liquid phase and precipitation is achieved by contacting the organic phase with a supercritical fluid having a large mutual solubility with the organic liquid and a low affinity for the solutes.

Oxidation of Organic Compounds in Supercritical Carbon Dioxide

Unfortunately, no previous studies of oleic acid oxidation in a supercritical fluid could be located. However, Mercangöz et al. (2004) studied the oxidation of soybean oil with potassium permanganate in sub/supercritical carbon dioxide. As shown in Table 1.1, soybean oil is composed primarily of unsaturated fatty acids with oleic acid accounting for about 23 % of the fatty acid profile. One of the drawbacks of typical

vegetable oils (typical meaning high in triacylglycerols) is that they cannot be directly converted to polymers; instead, they must first be converted into an alternate form. For example, through hydrolysis of the oil, the fatty acids could be isolated and then used to synthesize polymers. One of the few exceptions is castor oil, which can be polymerized in its native form due to the presence of hydroxyl groups on most of the fatty acid chains. Another approach is to add necessary functional groups to vegetable oils prior to polymerization; however, current techniques have not been commercialized due to a lack of economic feasibility. The authors stated that the major reason for this is the difficulty arising from trying to react the immiscible organic oil phase with the aqueous phase that contains the reactants necessary for functional group addition. As previously mentioned, phase-transfer catalysts and emulsifiers have been researched to deal with such problems. However, in those cases the organic compound is placed in an organic solvent, such as benzene. After functionalization of the oil, the organic solvent must be removed; however, typically a small amount of the solvent remains with the oil, which can lead to undesirable properties in polymers. Also, phase-transfer catalysts and emulsifiers are relatively expensive.

Mercangöz et al. proposed to use carbon dioxide as an alternative to phase-transfer catalysts or emulsifiers. The goal of that study was to react soybean oil with aqueous potassium permanganate in the presence of sub/supercritical carbon dioxide and monitor the consumption of soybean triglyceride double bonds (STDB) and fatty acid distribution over time. Experiments were performed at temperatures of 25 and 50°C and pressures of 7, 12, and 13 MPa. Other variables included reactor configuration, reaction time, and product-storage period. For the batch experiments, all reactants were placed in

the reactor at once and allowed to mix for 10 minutes. Then the reactor was placed in a water bath for an additional 10 minutes to allow for thermal equilibration before the carbon dioxide was pumped into the reactor. After addition of carbon dioxide and attainment of the desired pressure and temperature, mixing was initiated and the allotted reaction time for the experiment began. At the end of the designated reaction time, the mixer was turned off, and the reactor contents were given an hour to settle. Therefore, the authors did not account for at least 1.33 hours of time in which a reaction could be occurring. For the semi-batch experiments, soybean oil and potassium permanganate were placed in the reactor and mixed together. Then the reactor was pressurized with carbon dioxide, and the system was allowed to reach thermal equilibrium. Water was then added at various rates to the reactor using an HPLC pump. From that point on, the procedure was identical to the batch experiments.

Since the goal of this research was to add hydroxyl groups to the triacylglycerols, the authors were concerned about “over-oxidation” in which the diol formed from the C-C double bond would be oxidized into other species, as shown in Figure 3.6. However, though an excess amount of oxidant was used, no over-oxidation was observed. The authors found that the feed rate of water in the semi-batch experiments affected STDB consumption. For a standard 12-hour reaction at 25°C and 7 MPa, consumption for the batch experiment was 29 %. In semi-batch operation, consumption was 33 and 31% at water feed rates of 0.25 and 0.083 mL·min⁻¹. The authors had hypothesized that as the water feed rate increased, the STDB consumption would approach the result achieved in batch mode. However, the results suggested that as water feed rate was increased,

consumption improved over batch operation. Unfortunately, the authors did not explain why these results occurred.

Mercangöz et al. also performed a negative-control test in which soybean oil and aqueous potassium permanganate were mixed together in a reactor at 25°C and atmospheric pressure. The reactor was sealed from the atmosphere to prevent autoxidation of the soybean oil. The negative-control showed that the absence of dense carbon dioxide hindered the reaction. To get a better understanding of the reactant system, reactions were also conducted with methyl oleate. However, under conditions of 50°C at 12 MPa for 16 hours, no double bond consumption of the methyl oleate was observed. Based on the fact that methyl oleate was soluble in supercritical carbon dioxide but practically insoluble in water, the authors suggested that the methyl oleate result proved that the permanganate ions were not solubilized into the dense carbon dioxide phase and hence could not react with the methyl oleate.

Mercangöz et al. concluded that the high pressure promoted the dissolution of carbon dioxide in both the soybean oil and aqueous phase, resulting in them expanding to some multiple of their original volumes. Also, since the two phases were well mixed, the two immiscible phases were kept in an emulsion-like state. The authors concluded that the combined effect of these factors resulted in one, or both, of the reactants being transferred to the other phase to react in a much larger interfacial area.

Most oxidation studies incorporating supercritical carbon dioxide as a reaction medium have been focused on environmental remediation of groundwaters, soils, and sludges. Carbon dioxide is considered well-suited for this application because it is plentiful, inexpensive, nontoxic, nonflammable, and has a high solvating power for many

organic pollutants. For example, Kruse and Schmieder (1998) envisioned an integrated remediation process featuring extraction and oxidation with supercritical carbon dioxide. As can be seen Figure 3.7, supercritical carbon dioxide can be used to extract an organic pollutant, leaving a remediated matrix behind. The supercritical carbon dioxide + organic compound could then pass into a high-pressure reactor where oxidation (destruction) of the organic pollutant would occur. By depressurizing the reactor, the carbon dioxide can be separated from the reaction products and recycled. Pang et al. (1991) studied the oxidation of several model waste aromatic hydrocarbons such as toluene with air in carbon dioxide at pressures of 8 to 14 MPa and temperatures of 453 to 573 K. The degree of oxidation varied with the amount of active metal oxide catalyst on an alumina support. No reactions were observed to occur in the absence of a catalyst at temperatures below 573 K. With many of the transition metal oxide catalysts, the reaction rates were slow, and the major products formed were aldehydes and acids. However, using a 1 % Pt/Al₂O₃ catalyst resulted in almost complete oxidation of toluene at temperatures below 520 K with a consumption rate of 0.54 g of toluene reacting per 1 g of catalyst per hour.

Several drawbacks exist to using supercritical carbon dioxide as a reaction medium including the requirement for high process pressure and limitation in the availability of transition metal catalysts that display adequate solubility without modification in the supercritical fluid. Fluorocarbon “tails” can be attached to catalysts to improve their solubility; however, the user of fluorocarbon compounds is expensive and not considered environmentally friendly. To surmount these issues, Musie et al. (2001) proposed the use of carbon dioxide-expanded solvent media. In their proposed process, the conventional solvent was substantially replaced with dense carbon dioxide,

which led to the expansion of the solution volume. Hence, a completely homogenous reaction mixture was created that contained carbon dioxide, substrate, catalyst, organic solvent, and oxidant. The pressure required was on the order of 5 to 9 MPa, and the carbon dioxide mole fraction in the organic solvent ranged from 0.65 to 0.8. In several experiments, use of carbon dioxide-expanded organic solvents resulted in rate enhancement for reactions of dioxygen oxidation of alkenes and phenols with metal complexes of Schiff base (general structure of $R_1R_2C=N-R_3$) and porphyrin ligands (interconnected pyrrole-like subunits).

Solubility of Lipids in Supercritical Carbon Dioxide

Experimental Techniques

As previously mentioned, reduction in mass-transfer limitations and facilitation of reaction product separation are potential advantages of using supercritical carbon dioxide as a reaction medium. Both of these advantages are heavily influenced by the solubility of the reactants and products in supercritical carbon dioxide; hence, knowledge of solubility over a range of temperatures and pressures is important. Fortunately, solubility data are available for oleic acid + supercritical carbon dioxide [Zou et al., 1990; Foster et al., 1991; Nilsson et al., 1991; Maheshwari et al., 1992; Yu et al., 1992; Škerget et al., 1995]. However, solubility of pelargonic acid and azelaic acid in supercritical carbon dioxide could not be located. Although group contribution methods exist to predict solubility of compounds in a supercritical fluid [Gardeler and Gmehling, 2004], solubility can be also determined experimentally. In some cases, solubility cannot be determined experimentally due to several potential factors such as unavailability of solute standards

or cost of standards. However, pelargonic acid and azelaic standards are readily available and are not overly expensive.

There are three main experimental techniques for determining solubility of compounds in supercritical fluids: dynamic, static, and recirculating [Maxwell, 1996]. All three techniques are based upon the same principle: attainment of equilibrium between solute and supercritical fluid. In a dynamic system, the supercritical fluid passes through the solute at a rate in which equilibrium is attained. In a static process, experiments are conducted in vessel containing a fixed amount of solute, and the pressure or temperature is adjusted until a portion, or all, of the solute dissolves in the supercritical fluid. The recirculating method consists of an apparatus operating with a fixed volume of fluid that is continuously recycled through the system until equilibrium is obtained.

Most solubility measurements for solid lipids have been determined using the dynamic technique [Maxwell, 1996]. The dynamic technique has also been used to evaluate solubility of liquid-phase lipids such as oleic acid [Nilsson et al., 1991]. Figure 3.8 shows a diagram of a dynamic apparatus. The carbon dioxide is delivered from the solvent cylinder to a pump or compressor where it is compressed and heated. For the apparatus shown in Figure 3.8, the carbon dioxide flows from the compressor to a coil in a constant-temperature bath, which ensures that the solvent is at the required temperature. Then the carbon dioxide enters the pressure vessel that contains the lipid and dissolves a portion of it. Then the solute + supercritical fluid passes through a heated micrometering valve where the pressure is reduced nearly (or completely) to atmospheric pressure. The micrometering valve controls the flow of the expanded carbon dioxide as well as the pressure in the extraction vessel. Hence, the micrometering valve assembly is often

referred to as a back-pressure regulator. As the carbon dioxide expands, the solute precipitates and is collected in a receiver. As the carbon dioxide exits the system, a flow meter and flow totalizer are used to record the flow rate and total gas volume as a function of time. Advantages of the dynamic technique include:

- The apparatus can be composed of off-the-shelf equipment
- Sampling procedures are not complicated
- Solubility data can be generated relatively quickly
- Equilibrium or fractionating information can be obtained [Maxwell, 1996].

Disadvantages of the dynamic approach include:

- Obstruction of the micrometering valve by the solute
- Potential entrainment of liquid solutes
- Undetected phase changes
- If the pressure cell is in a vertical position at high pressure, the supercritical fluid density can become greater than the solute density, which may result in extrusion of the liquid solute from the pressure cell
- The solubility of the supercritical fluid in a liquid solute cannot be determined since only the supercritical fluid phase is sampled [Maxwell, 1996].

Researchers have used many modified forms of the dynamic apparatus in Figure 3.8. For example, Dobbs et al. (1986) added a second pressure cell in line with the first pressure cell. In that design, both cells were charged with solute, but the second pressure cell ensured that the supercritical fluid was saturated with solute.

Behavior of Lipids in Supercritical Carbon Dioxide

Many studies of lipid solubility/extraction are available in the literature and provide insightful information as to what can be expected from the solubility experiments in this work. For example, in the work by Sparks et al. (2006), lipids were extracted from rice bran at pressures of 20 to 35 MPa and temperatures of 45, 65, and 85°C. In terms of its fatty acid profile, rice bran contained over 40 % oleic acid. As illustrated in Figure 3.9, extraction efficiencies were directly proportional to pressure and inversely proportional to temperature. However, rice bran oil is a complex solute that is actually composed of many different molecules, so it is important to know the behavior that can be expected for pure lipids. Nilsson et al. (1991) evaluated the solubilities of methyl oleate, oleic acid, monoolein, diolein, and triolein in supercritical carbon dioxide at temperatures of 50 and 60°C and at pressures of 11 MPa to 30.9 MPa. The methyl oleate exhibited the highest solubility, presumably because it has the highest vapor pressure, and oleic acid had the next highest solubility. Triolein was least soluble. All of the compounds were more soluble in supercritical carbon dioxide at 50°C than at 60°C, which was the same behavior observed in the previously mentioned rice bran oil study. Nilsson et al. referred to this behavior as retrograde behavior, in which the solvent density had the dominant effect on solubility. Nonretrograde behavior, in which solubility increases with increasing temperature, can also occur. In the nonretrograde regime, the temperature effect on the vapor pressure has the dominant effect on solubility.

Both Hammam (1992) and Yu et al. (1994) studied the solubility of a variety of lipids in supercritical carbon dioxide and concluded that solubility depended not only on

the operating conditions, but also on the chemical structure of the solute. Chain length, degree of unsaturation, and presence of functional groups have all been found to affect solubility. For example, methyl palmitate showed a higher solubility in supercritical carbon dioxide than methyl stearate due to the shorter chain length of the palmitate group [Inomata et al., 1989]. Though it had the same chain length, ethyl stearate had a lower solubility than ethyl oleate due to the double bond of the oleate group [Bharath et al., 1989]. However, molecular weight appeared to have a larger impact on solubility than degree of unsaturation. A polar carboxyl group can also impact solubility. Hammam (1992) found that trilaurin and palmitic acid had approximately the same solubility in supercritical carbon dioxide even though trilaurin had a larger molecular weight. Hammam suggested that the carboxyl group on the palmitic acid caused the molecule to be more polar, which caused a lower solubility.

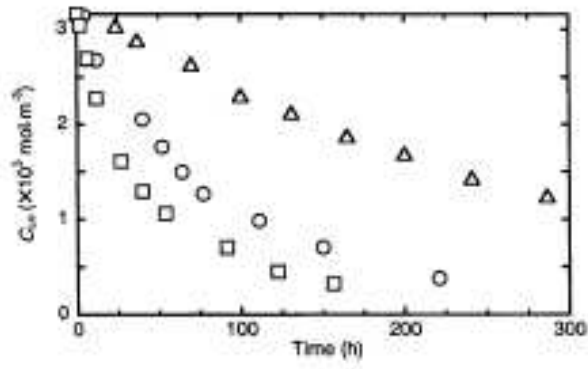


Figure 3.1: Changes in oleic acid concentration over time due to autoxidation: Δ , 333 K; \circ , 348 K; \square , 363 K [Takahashi et al., 2000]

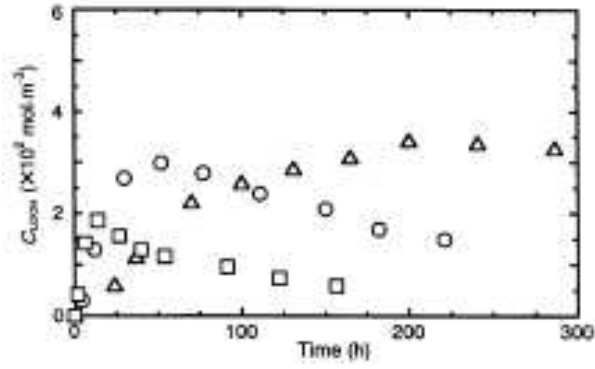


Figure 3.2: Changes in oleyl hydroperoxide concentration over time during autoxidation of oleic acid: Δ , 333 K; \circ , 348 K; \square , 363 K [Takahashi et al., 2000]

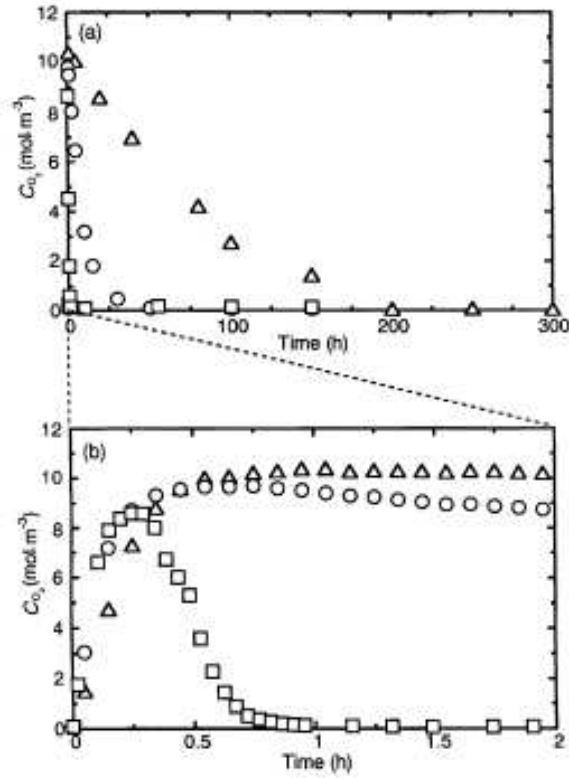


Figure 3.3: Changes in dissolved oxygen concentration for oleic acid autoxidation: (a) for complete reaction time, (b) for the first two hours of reaction time: Δ , 333 K; \circ , 348 K; \square , 363 K [Takahashi et al., 2000]

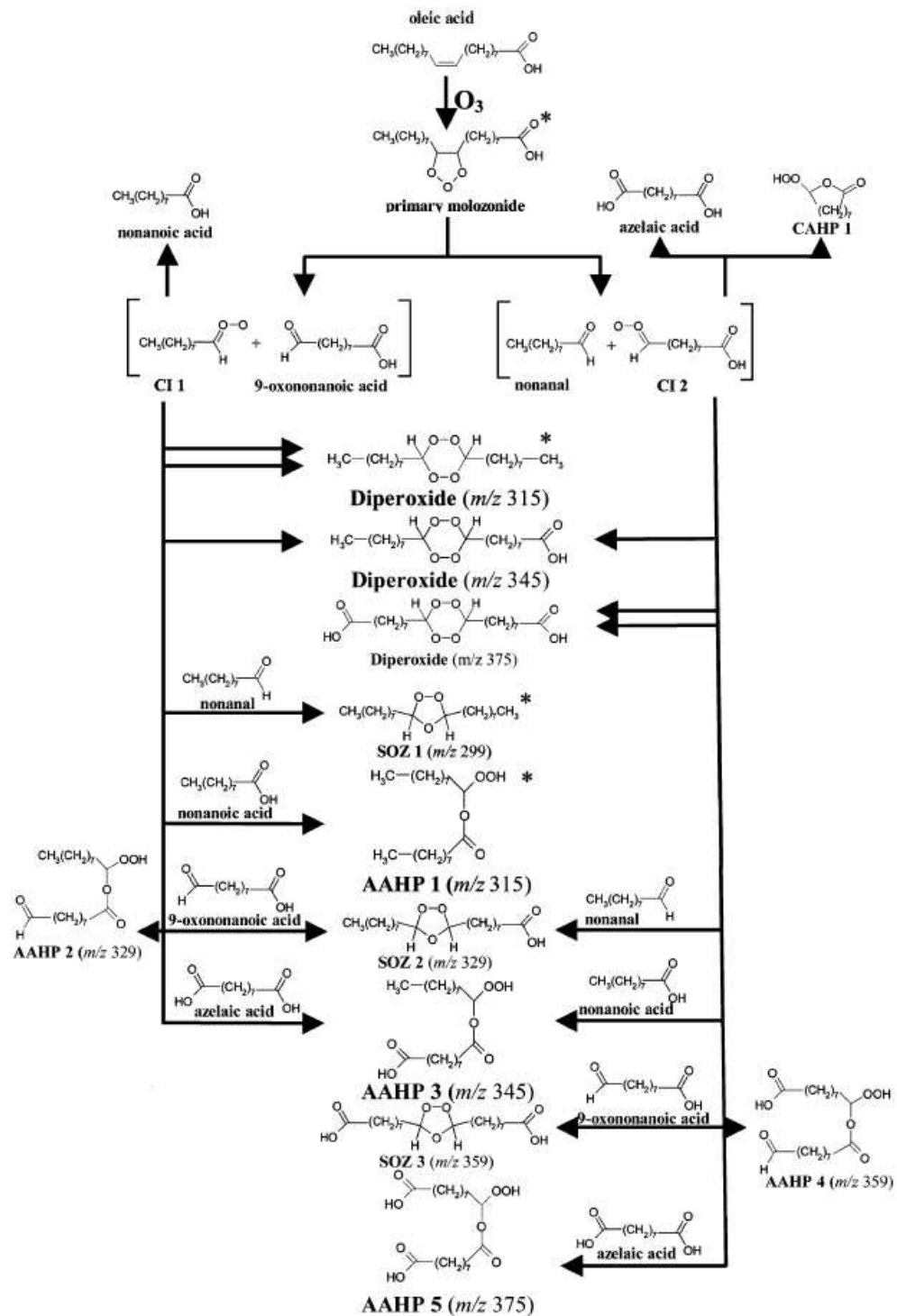


Figure 3.4: Proposed oleic acid ozonolysis mechanism where the asterisk denotes products that theoretically cannot be incorporated into an oligomer [Reynolds et al., 2006]

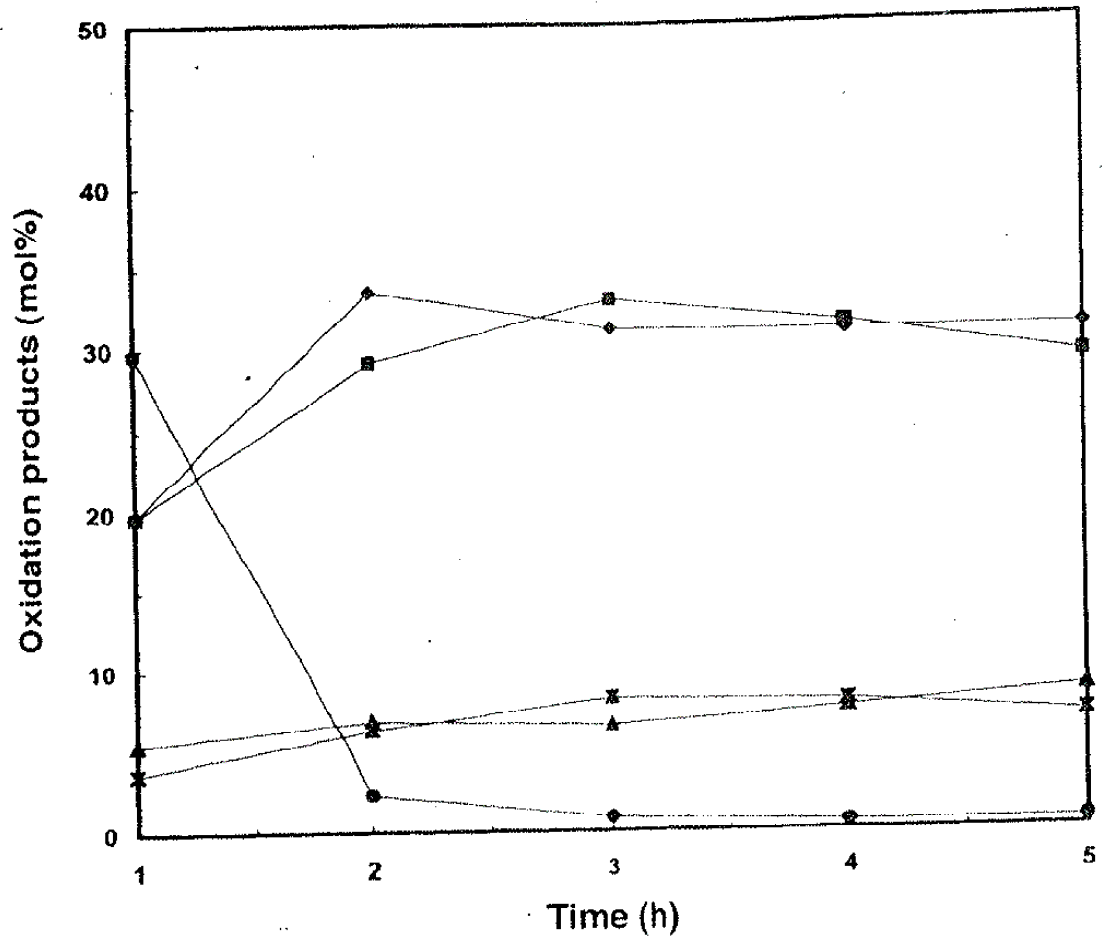


Figure 3.5: Oxidation of oleic acid with hydrogen peroxide with alumina-supported tungstic oxide catalyst: ♦, pelargonic acid; ■, azelaic acid, ▲, octanoic acid; ●, oleic acid; *, suberic acid [Noureddini and Kanabur, 1999]

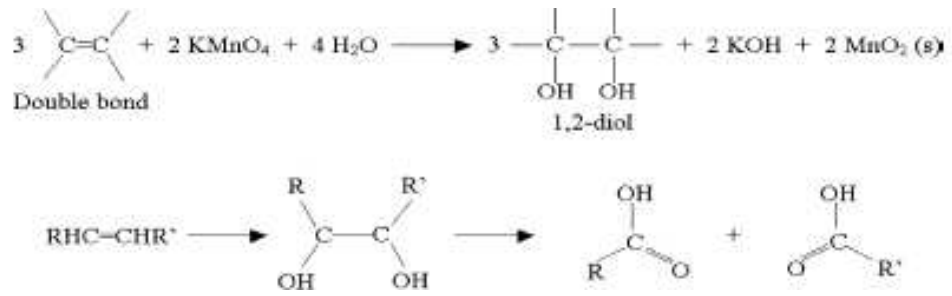


Figure 3.6: Hydroxylation of an olefin followed by oxidation into carboxylated species [Mercangöz et al., 2004]

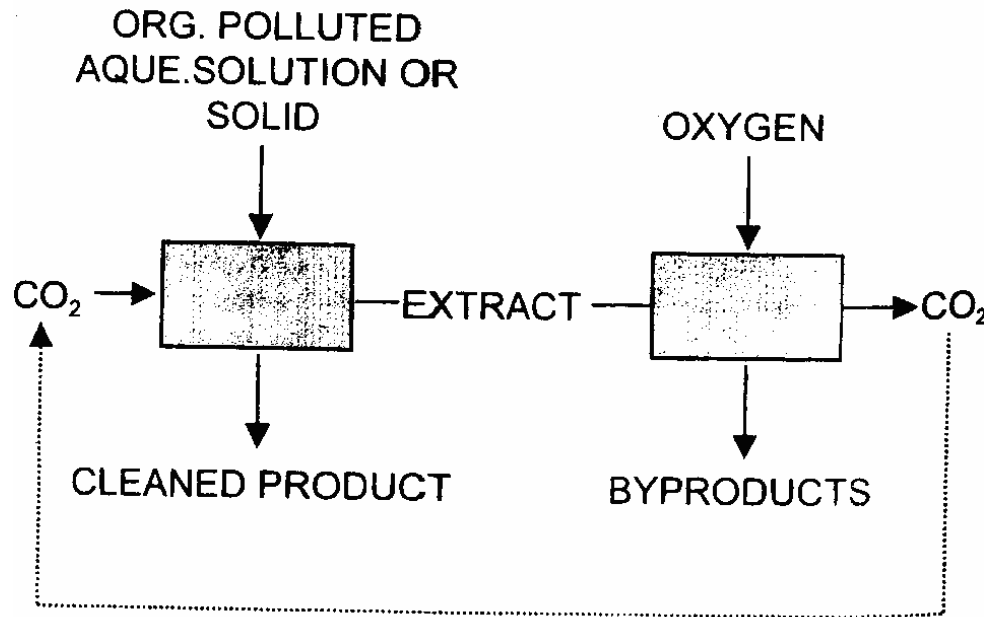


Figure 3.7: Combined extraction and reaction process for removal of organic pollutants [Kruse and Schmieder, 1998]

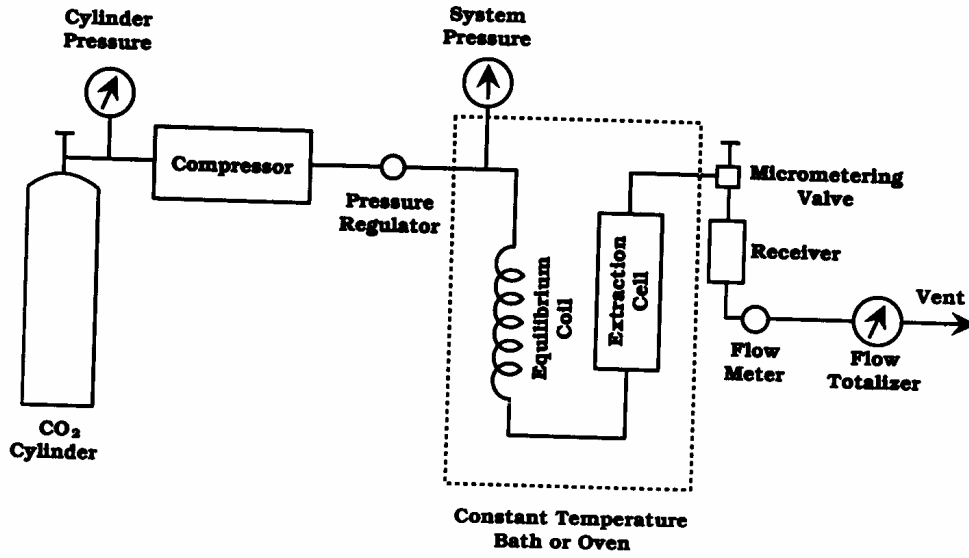


Figure 3.8: Dynamic apparatus for determining solubility in a supercritical fluid [Maxwell, 1996]

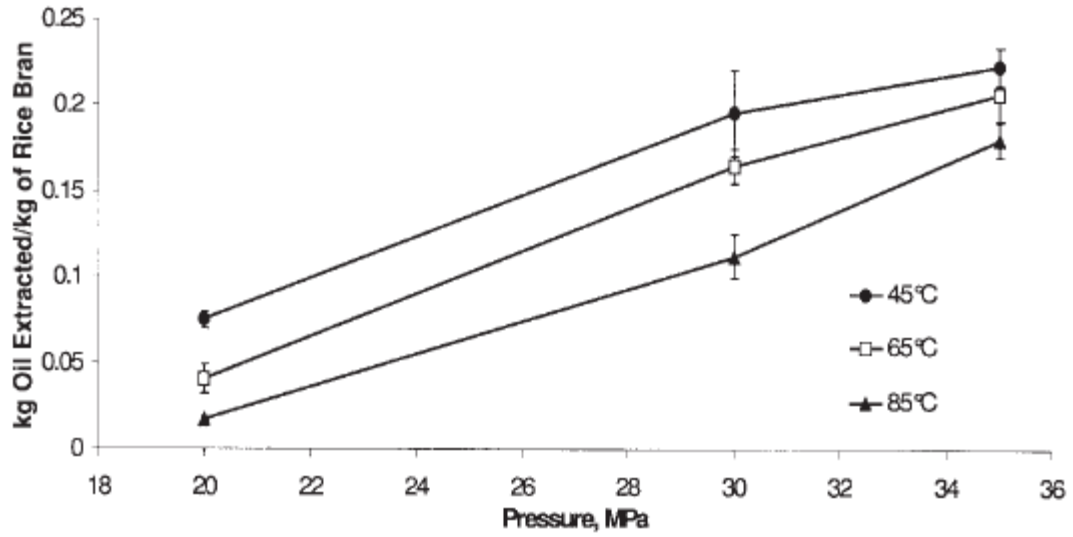


Figure 3.9: Supercritical CO₂ extraction yields based upon pressure at different temperatures where the error bars indicate mean \pm 1 SD ($n = 3$) [Sparks et al., 2006]

CHAPTER IV
METHODS AND MATERIALS

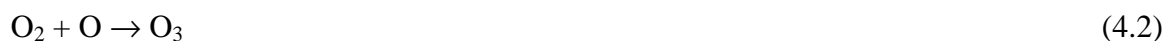
Introduction

Chapter IV provides descriptions of analytical procedures, experimental methods, and materials used throughout this study. However, specific details of procedures (i.e. flowrates, pressures, etc...) and materials are provided in subsequent chapters (VII-X) where the actual experiments are discussed.

Oxidizer Generation

Ozone Generation

Ozone was produced via a Model LC-1234 Ozone Generator from Ozonology, Inc. (Northbrook, IL). The ozone generator was equipped with an internal oxygen generator (Airsep Corporation Model AS-12; Buffalo, NY) capable of producing a stream of oxygen concentrated to 90 % \pm 5 % on a volume basis. Ozone (O₃) is formed in two sequential reactions: (1) an oxygen (O₂) molecule splits as a result of the reception of a photon and (2) the resulting oxygen atoms react with O₂ to form O₃. This reaction sequence is shown below.





Ozone (O_3 , CAS No. 10028-15-6) is created in nature by lightning strikes and ultraviolet (UV) light from the sun [Suslow, 2004]. Ozone is also produced by photochemical oxidation reactions of hydrocarbons, oxygen, and nitrogen [Graham, 1997]. Commercial ozone generators are available that utilize a UV light source, but these units have a lower ozone production capacity compared to corona discharge systems. In these systems, a high-voltage current is applied across a discharge gap (corona) in the presence of oxygen or air, splitting the oxygen molecules to form oxygen atoms [Suslow, 1998]. In the same manner previously described, the oxygen atoms combine with oxygen molecules to form ozone. The Model LC-1234 Ozone Generator is a corona-discharge unit and the amount of ozone produced was directly related to the amount of voltage applied to the corona and inversely related to the flowrate of oxygen across the corona. The voltage controller could be varied from 0 to 100 volts and the flowrate could be varied between 0 and 10 standard cubic feet per hour (SCFH). The ozone generator had four cells that could be utilized simultaneously to generate ozone. However, these streams could only be varied with respect to each other by changing the flowrate for each particular cell. The unit is equipped with only one corona, so the voltage was constant across all active cells. The gas flowrate for each cell was controlled by a rotameter.

The ozone concentration produced at a specific voltage and flowrate was determined with a Model HC Ozone Monitor (PCI Ozone & Control Systems, Inc.; West Caldwell, NJ) utilizing a UV-absorption type photometric technique. The monitor utilizes a sampling system containing a sample pump, ozone scrubber, solenoid valve,

and sample chamber. The monitor is able to alternate between the flow of an ozone-containing stream to that of an oxygen stream. By comparing the intensity of the UV light passing through the ozone stream to the UV light intensity passing through the oxygen stream, the ozone concentration can be calculated using Beer's Law. Figure 4.1 shows the ozone generator along with the ozone monitor. The ozone monitor was used to generate calibration curves showing how ozone concentration varied with voltage and flowrate. As Figure 4.2 shows, the concentration of ozone increases with increasing voltage and decreasing flowrate. After leaving the ozone monitor, the ozone was sent to a flask containing Carulite (manganese dioxide/copper oxide, Carus Chemical Company; Peru, IL), which served as a catalyst to decompose the ozone.

Potassium Permanganate

Typically, potassium permanganate (KMnO_4 , CAS No. 7722-64-7) is generated via a multi-reaction process. First, pyrolusite is combined with potassium nitrate or potassium hydroxide in the presence of heat and air to form potassium manganate. Then upon electrolytic oxidation in an alkaline medium, the potassium manganate is converted to potassium permanganate [USITC, 2005; Wikipedia, 2007b]. For this work, potassium permanganate was obtained from Sigma-Aldrich (Cat. # 399124-500g) and used without modification. The KMnO_4 was 99+% purity (ACS grade) with low mercury content. Figure 4.3 shows potassium permanganate crystals being moved via a stainless-steel scoopula.

Solubility in Supercritical Carbon Dioxide

A dynamic technique was used to determine solubility of pelargonic acid, azelaic acid, oleic acid, and potassium permanganate in supercritical carbon dioxide (SC-CO₂). Under the dynamic technique, the assumption is made that the solute solvent system reaches equilibrium as the solvent passes over the solute [Maxwell, 1996]. Figure 4.4 provides a schematic of the supercritical-fluid extractor, manufactured by Thar Technologies (Model SFE-100; Pittsburgh, PA), used for the solubility experiments. The system is rated for pressures up to 68 MPa and is equipped with a Coriolis mass-flow meter, dual-piston pump, backpressure regulator (BPR), and cyclone separator. A brief description of these major components now follows.

- **Coriolis Mass-Flow Meter:** The mass-flow meter is manufactured by Rheonik (Munich, Germany) and operates on the principle of the Coriolis effect which can be described as the inertial force exerted on an object as a result of movement relative to a rotating frame of reference [Rheonik, 2006]. The Rheonik mass-flow meter has two parallel measuring tubes that form an Omega shape. The tubes oscillate in opposing directions. Two high-mass cross bars mounted on vertical torsion rods drive the oscillating system and stabilize the torsional movement. When mass flows through the tubes, a Coriolis force is produced, which causes deflection in the top of the tubes. The deflection is detected as a phase shift between two electronic sensors mounted on the oscillating tubes. The mass flowing within the tubes is directly proportional to the extent of phase shift detected. The mass-flow meter has an accuracy of ± 0.20 %.

- **Dual-Piston Pump:** The P-50 pump is a high-pressure pump that incorporates a low dead volume head and check valves to ensure efficient pumping of carbon dioxide. As a piston moves back to refill the solvent chamber, a lower check valve opens to allow solvent to flow into the chamber while an upper check valve closes to seal the system fluid from entering the solvent chamber. Once a piston completes its filling cycle, it will move forward, causing the lower check valve to close. When the pressure in the chamber exceeds the system pressure, the upper check valve opens and solvent flows into the system. By utilizing two pistons, the P-50 is able to provide a continuous, pulse-free delivery of CO₂ up to a rate of 50 g·min⁻¹ (0.83 g·s⁻¹).
- **Backpressure Regulator:** The BPR is a precision valve attached to a motor controller with a position indicator. The maximum expected flowrate under liquid to atmospheric pressure drop conditions is 200 g·min⁻¹. The needle position is reported as 0 to 6000 counts with 0 counts corresponding to minimum flow and 6000 counts indicating a fully open system.
- **Cyclone Separator:** The cyclone separator removes solute molecules by causing the solute/CO₂ stream to flow in a spiral pattern inside of a 500 mL cylinder. Due to the centrifugal force, the solute molecules move outward and collide with the wall of the vessel [Copper and Alley, 1994]. Then the solute molecules tend to fall to the bottom of the cyclone due to

the influence of gravity, and the CO₂ is allowed to flow out of the top of the cyclone.

Temperature along with the dual-piston pump and backpressure regulator are controlled via computer using Instrument Control Module (ICM) with PID control.

For each solubility experiment, a portion of the compound of interest was suspended in a stainless steel equilibrium vessel (volume of 100 mL) using layers of glass wool (Fisher Scientific) and 2 mm diameter borosilicate glass beads (Chemglass, Vineland, NJ). The packing helps minimize channeling of the supercritical fluid and prevents entrainment of the solute [Maxwell, 1996; Lee et al., 1994]. Both ends of the equilibrium vessel were equipped with 5 µm stainless steel frits. The equilibrium vessel, equipped with a heating jacket, was allowed to reach the desired operating temperature of the experiment (± 1 K). Before entering the equilibrium vessel, the CO₂ passed through a heat exchanger, which raised the temperature of the solvent to the necessary value. By the time the CO₂ reached the equilibrium cell, it was in a supercritical state (SC-CO₂). The system was maintained at the desired pressure (± 0.2 MPa) via the backpressure regulator.

Once the solute/solvent mixture exited the equilibrium cell, it flowed to the cyclone separator where the pressure was reduced; hence, the CO₂ became a gas and separated from the solute. Then, 25 mL of an appropriate solvent (organic solvent in the case of fatty acids, water in the case of potassium permanganate) was used to dissolve the solute in the cyclone separator. The solute/solvent mixture was collected in a tared 40 mL amber glass vial. Specific methods of determining the amount of solute in the 40 mL vial vary based on solute type and are discussed in subsequent chapters. Between

experiments, the equilibrium vessel was taken offline, and SC-CO₂ was used to clean the tubing of the experimental apparatus.

Oxidation in Supercritical Carbon Dioxide

Oxidation experiments conducted in supercritical carbon dioxide utilized a 250 mL stainless steel reactor assembly manufactured by Thar Technologies (Model R250; Pittsburgh, PA). The reactor body is composed of 316 stainless steel while the cap is composed of Nitronic 60 stainless steel. The R250 is equipped with a magnetic stirrer as well as two 6.35 mm diameter single crystal sapphire windows to allow remote viewing of inside the reactor via a camera and light source. The reactor temperature is controlled by a process control package that also provides monitoring of reactor pressure. The reactor can attain a maximum pressure of 41.3 MPa and a maximum temperature of 150 °C. Since the process control package did not include a tachometer for the stirrer, the speed setting had to be determined manually via a NIST traceable, pre-calibrated photo/contact tachometer (Cat. No. 05-028-23, Fisher Scientific). First, reflective tape was cut into a 12.7 mm square and placed on the shaft of the stirrer. Then the photo signal light beam was directed at the tape on the rotating shaft. Three measurements were taken for each speed setting, and a calibration curve (Figure 4.5) was generated showing RPM as a function of speed setting. Although error bars indicating standard deviations are included in Figure 4.5, the values (≈ 0.2 RPM to ≈ 2 RPM) are so small that the error bars cannot easily be seen.

For the oxidation reactions, the R250 was used inline with part of the SFE-100 assembly previously described. Specifically, the P-50 solvent pump was used to deliver

carbon dioxide to the reactor. For the potassium permanganate oxidation experiments, a syringe pump (Teledyne Isco Model 100DX; Lincoln, NE) was used to add oleic acid into the R250 reactor. This particular model of syringe pump has a capacity of 100 mL and can provide pulseless delivery from 0.00001 to 60 mL·min⁻¹ over a pressure range of 0 to 68.95 MPa. Although the syringe pump can be operated in either constant-pressure or constant-flow mode, only the constant flow-mode was used for this study. The flow accuracy of the pump is a minimum of ± 0.5 %. Figure 4.6 provides an illustration of the experimental setup including the syringe pump. The pressure release valve shown in Figure 4.6 was used to depressurize the reactor at the end of experiments. An Erlenmeyer flask containing glass wool was used to collect any material that exited the reactor with the carbon dioxide.

Analytical Methods

Conversion of Reaction Products to Methyl Ester Derivatives

Fatty acids and their oxidation products are typically converted to methyl ester derivatives because the enhanced peak shape that results when gas chromatography (GC) is employed. The derivatization procedure used in this work is a modified form of that described by Christie (2003b). First, the lipid sample (up to 100 mg) was placed in a 20 mL test tube containing 1 mL of toluene (Optima, Fisher Scientific) and 2 mL of methanol (Optima, Fisher Scientific) containing 2 % sulfuric acid (Certified ACS Plus, Fisher Scientific). In the case of the potassium permanganate oxidation experiments, the lipid sample was already dissolved in the methanol/sulfuric acid solution prior to derivatization. The test tube was capped and placed in an incubator for overnight

(minimum eight hours) at 50°C. For free fatty acids, a reaction time of two hours at 50°C is required [Christie, 2003b]; however, the additional reaction time was included to ensure complete reaction. At the end of the reaction period, 4 mL of an aqueous solution containing 5 % NaCl was added followed by vortex mixing to quench the reaction. Then 5 mL of hexane (Optima, Fisher Scientific) was added to the vial followed by vortex mixing and centrifugation (Sorvall Model RT 6000D, Fisher Scientific) at 3000 RPM for 1 minute. Then an additional 4 mL of hexane was added to the vial followed by vortex mixing and centrifugation. Next, 1 mL of the upper organic layer containing the lipids was combined via vortex mixing with 0.5 mL of 1,3-dichlorobenzene (≥ 98 % purity, Fluka) in a GC sample vial. The 1,3-dichlorobenzene served as an internal standard for GC analysis.

Analysis of Fatty Acid Methyl Esters with Gas Chromatography

The fatty acid methyl ester derivatives described previously were analyzed with gas chromatography. Fatty acid methyl esters show considerable volatility below 300°C, so they are well suited for gas chromatographic analysis. The major components of a gas chromatograph are the gas supply, injector, oven, column, detector, and recording device [Rood, 1991] as shown in Figure 4.7. A high purity carrier gas such as helium, nitrogen, or hydrogen flows into the injector, through the column, and exits as it traverses the detector. Typically, a liquid (or gas) sample is introduced via syringe to the injector, which is heated to around 200 to 300°C. Upon exposure to the heat of the injector, the sample vaporizes and is carried into the column by the carrier gas. Most columns used today are wall-coated open tubular columns (capillary columns), although packed

columns are still used for some applications. Modern open tubular columns are made of fused silica, which gives the column enough flexibility so that it can be coiled very tightly. The column is contained in the oven where a very precise and reproducible temperature program is applied. As previously mentioned, the column walls are coated with a film, and the chemical characteristics of this film vary with the type of separation desired. Therefore, each compound in the sample will interact with the column differently and be “retained” by the column for a different length of time. The length of time a compound spends on the column before reaching the detector is referred to as its *retention time*.

The retention time of a compound is dependent upon many factors other than the type of coating on the column. These factors include carrier gas flowrate, column temperature, and column dimensions including length, internal diameter, and film thickness [Christie 2003c]. As compounds exit the column, they must traverse the detector. When a compound is sensed by the detector, an electrical signal is sent to a recording device such as a strip chart recorder or computer system. The signal from the detector appears as a series of peaks plotted as a function of time. This type of plot is called a chromatogram. Under ideal conditions, each peak represents an individual compound; however overlapping or convolution of peaks is not uncommon. The retention of a peak can be used for qualitative information, i.e. compound identification. The size of the peak can be used for quantitative purposes. This is due to the fact that the size of the peak can be related to the amount of sample exiting the column. The ratio of the size of the peak to the amount of the sample is known as a response factor. If standards are available, calibration curves can be generated for individual compounds.

The response factor from the calibration curve can be used to quantify compounds in samples. Due to the sensitivity of peak height and area to operating conditions, an internal standard is frequently added to the sample mixture. By measuring the peak height or area of each sample compound relative to the peak height or area of the internal standard, minor variations in operating conditions can be compensated for because the assumption can be made that any variation will affect the internal standard peak and the sample peaks in relatively the same way [Hargis, 1988a].

Many types of detectors are currently used in gas chromatography with the most common being the thermal conductivity detection (TCD), flame ionization detection (FID), thermionic emission detection (TED), flame photometric detection (FPD), electron capture detection (ECD), and mass spectrometry (MS). The type of sample being analyzed often dictates the type of detector employed. For example, a thermionic emission detector is well-suited for phosphorous- and nitrogen-containing compounds while an electron capture detector is ideal for electrophilic compounds such as nitriles, peroxides, and halogenated species [Hargis, 1988a]. For the ozone oxidation experiments, the Agilent 6890N GC (Palo Alto, CA) equipped with FID shown in Figure 4.8 was used to analyze the methyl ester derivatives of reaction products. An example of a flame ionization detector is shown in Figure 4.9. The mobile phase exiting the column is mixed with hydrogen before being burned in the presence of air. A positively charged cylinder is mounted above the negatively charged burner so that ions formed during the combustion migrate to the electrodes, causing a current to flow in an external circuit [Hargis, 1988a]. As a result of gas impurities, normal column bleed, and system contamination, a background signal is always present. Ionization of a compound in a

sample causes an increase in the detector current above the background level. The change in detector current is processed in the data recorder into a peak on a chromatogram. Advantages of FID include:

- capability of sensing a wide range of compounds
- wide linear range of 10^5 to 10^6 [Rood, 1991]
- insensitivity to water and temperature variations of the carrier gas [Hargis, 1988a]
- sensitive technique with detection limits down to 0.1 to 1 ng of analyte [Rood, 1991]

However, FID also has disadvantages. First, FID is a destructive detection method, and analytes cannot be recovered from the detector for further analysis. Second, FID response decreases as the degree of substitution for hydrogen in carbon-hydrogen bonds increases. Specifically, compounds with hydrogen substituted with halogens, oxygen, sulfur, and nitrogen result in a decrease in detector response [Rood, 1991].

The separation of reaction products from the ozone oxidation experiments was achieved with a fused-silica capillary column composed of stabilized poly(90 % biscyanopropyl/10 % cyanopropylphenyl siloxane) (SP-2380; Supelco, Bellefonte, PA). The dimensions of the column were 100 m in length \times 0.25 mm inner diameter \times 0.2 μ m film thickness. A calibration curve was prepared by injecting known concentrations of oleic acid, azelaic acid, and pelargonic acid standards. As previously mentioned, 1,3-dichlorobenzene was used as an internal standard. The method consisted of injecting 1 μ L of sample into the gas chromatograph with a split ratio of 100:1. The temperature program began at 110°C and ended at 240°C over a nonlinear temperature program (Table 4.1) totaling 99 min. The carrier gas was ultra high purity helium and the detector

gases were ultra high purity hydrogen and ultra zero grade air. All gases were obtained from Nexair (Memphis, TN). Both the injector and detector were set to a temperature of 260°C, and flow through the GC was maintained at a pressure of 0.27 MPa. All calibration curves generated had a minimum r^2 value of 0.995 using a linear fit. Sample peaks were identified based on matching of retention times with standard compounds.

For the potassium permanganate oxidation reactions, a Varian 3600 coupled with a Saturn 2000 mass spectrometer detector was used for product analysis. Figure 4.10 displays the actual GC-MS instrument used in this work. Although a mass spectrometer does not offer the wide linear response range of FID, it is a more sensitive technique than flame ionization detection and provides the capability of unknown product identification through two modes: electron impact (EI) and chemical ionization (CI). The fundamental requirement for either mode is that the sample molecules must be charged so that their paths can be manipulated via electric and magnetic fields. Hence, radicals and neutral molecules are unresponsive to mass spectrometers [Downard, 2004].

The basic principle of mass spectrometry is that molecules in the vapor phase are bombarded with electrons to form charged ions, which can then fragment in different ways to give smaller charged species. This process is referred to as *electron impact*. However, the fragmentation of charged molecules is not random because splitting tends to occur at weaker bonds, such as those adjacent to particular functional groups [Christie, 2003c]. The most common way in which ions are produced is through the loss of an electron, as shown in Eq. (4.4) [Downard, 2004].



where M is a molecule, e is an electron, and M^+ is a radical cation in that it is an odd electron species with a positive charge and is referred to as the *molecular ion*. The molecular ion has the same mass as the molecular weight of the starting molecule. It should be noted that not all ions formed are positive ions because some electronegative molecules can attract an electron during electron impact. Eq. (4.5) shows this type of reaction.



The molecular ion M^+ still has a mass equivalent to the molecular weight of the starting molecule. As mentioned previously, fragmentation typically accompanies electron impact. Once the molecular ion is formed it can dissociate into smaller mass fragments if sufficient energy has been delivered to the molecule from ionization. As shown in Eqs. (4.6) and (4.7), the positively charged molecular ion formed in Eq. (4.4) can fragment in at least two ways [Downard, 2004]:

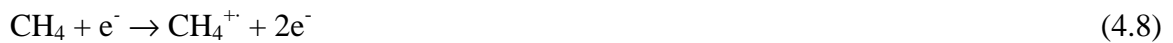


and



In Eq. (4.6), the molecular ion dissociates to form an even electron fragment (F^+) and a radical (R^\cdot). In Eq. (4.7), the molecular ion dissociates to produce a smaller mass fragment ($F^{+\cdot}$) and a neutral molecule (N). However, no matter which type of fragmentation occurs, only the charged fragments are detected. Therefore, the most useful aspect of electron impact is the use of fragmentation ions in both identification and quantification of analytes. Calibrations were based upon the analysis of reference compounds, and all calibration curves generated had a minimum r^2 value of 0.995.

In chemical ionization, a reagent gas is ionized followed by a transfer of charge from the ionized gas to the sample molecule [Downard, 2004]. Typical reagent gases include methane, ammonia, isobutane, hydrogen, and propane [Harrison, 1992]. If methane is used as the reagent gas, then the primary ion that forms is given by:



where CH_4^+ is the primary ion. Then carbocations are formed from the primary ion.

For example, the following reaction can occur:



where CH_5^+ is the carbocation. Then the carbocation can react with a sample molecule in the following ways:



and



where $[\text{M} + \text{H}]^+$ and $[\text{M} + \text{CH}_5]^+$ are the product ions. Although chemical ionization can produce some fragmentation, it is considered a “softer” ionization method compared to electron impact, so it is very useful in determining molecular weight of molecules [Christie, 2003c].

The Saturn 2000 mass spectrometer utilized a quadrupole ion trap design. Essentially, the quadrupole ion trap can serve as both an ion store in which gaseous ions can be confined for a period of time and also as a mass spectrometer with a wide mass range and variable mass resolution [March, 1997]. As shown in Figure 4.11, a quadrupole ion trap consists of two conical lenses and one ring electrode. Ions are stored in the volume between the conical lenses. This volume is bounded by the end caps of the

conical lenses and the center of the ring electrode. By changing the voltages across the entrance and exit trap electrodes, ions can flow into the trap and be stored for a period of time. Then the ions can be selectively released to the detector. Ions can be stored until an adequate density is acquired for ejection and analysis. Due to the relatively short path to the detector that the ions must travel as well as the ability to store ions, quadrupole ion traps can lead to very low detection limits [Downard, 2004].

The chromatographic separation of reaction products from the potassium permanganate oxidation experiments was obtained using a Rtx-5MS column (30 m in length \times 0.25 mm inner diameter \times 0.25 μ m film thickness) manufactured by Restek (Bellefonte, PA). The stationary phase of the column consisted of crosslinked 5 % diphenyl/95 % dimethyl polysiloxane. The injector was operated at 280°C in splitless mode with 1 μ L injection volume. The oven was programmed with an initial temperature of 50°C, held for 3 minutes and was then ramped to 150°C at 10°C/min, then ramped to 190°C at 1°C/min, and finally ramped to 280°C at 10°C/min and held for 2 min. Helium served as the carrier gas, and the gas cylinders utilized a Built in Purifier, (BIP[®], AirGas; Radnor, PA). The chromatographic system utilized the NIST library to aid in compound identification. The temperature program of the oven is shown in Table 4.2.

The multiple peaks from the total ion chromatograms were identified using CI spectra to determine molecular weight. Isobutane was used as the reagent gas for CI mode. For isobutane, the primary ion formed is the t-butyl ion ($C_4H_9^+$) with a minor yield of $C_3H_3^+$ [Harrison, 1992]. Quantification of methyl ester derivatives of reaction products was performed while in EI mode using calibration curves obtained from standard compounds. For EI mode, the mass range considered was from an m/z of 50 to

an m/z of 450 with a background m/z of 49. The unit m/z refers to the *mass-to-charge ratio*, which is the ratio of the dimensionless mass number (m) of an ion divided by the number of its elementary charges (z). For a singly charged ion ($z = 1$), the mass-to-charge scale directly reflects the m scale. Although singly charged ions often occur, doubly, triply, or higher charged ions can occur depending upon the ionization method employed [Gross, 2004]. The mass range considered for CI mode was 120 to 450 m/z with a background mass of 65 m/z . To extend the life of the rhenium filament, the mass spectrometer did not begin analysis until after solvent peaks had eluted the system.

Determination of KMnO_4 Concentration with UV/VIS Spectroscopy

The concentration of potassium permanganate in water was determined using a LAMBDA 25 UV/VIS Spectrophotometer (PerkinElmer; Waltham, MA). This particular model of spectrophotometer (shown in Figure 4.12) has a scanning range from 190 to 1100 nm (± 0.1 nm) with a fixed 1 nm bandwidth and utilizes a double-beam design [PerkinElmer, 2004]. An example of a double-beam design is shown in Figure 4.13. The beam of the spectrophotometer is split and passed alternately through the sample and reference cells. The beam chopper is a rotating half-mirror and is used to alternately pass the beam through a reference and sample cell. Since the two path lengths are the same, the detector sees alternating segments of radiation that have traversed the cells. Absorbance is determined by a comparison of the two segments. Since the cell signals are compared frequently, the system automatically corrects for changes in source intensity or detector response. A very useful application of the double-beam design is wavelength scanning. By changing the position of the grating, the wavelength reaching

the cells is altered [Hargis, 1988b]. The PerkinElmer LAMBDA 25 utilizes two sources: tungsten and deuterium. Prior to analyzing potassium permanganate samples, the instrument had to be calibrated. By using the wavelength scan function, it was determined that 510 nm was a suitable wavelength for analysis. Then standard solutions of potassium permanganate in water were prepared and analyzed on the spectrophotometer. The resulting calibration curve is shown in Figure 4.14. Over the range of concentrations used to create the calibration curve, absorbance shows to be a linear function of concentration.

Table 4.1: GC-FID temperature program used for analysis of oleic acid ozonolysis products

Oven Ramp	Ramp Rate/ °C .min ⁻¹	Next Temperature/ °C	Hold Time/ min.	Run Time/ min.
Initial	-	110	2	2
Ramp 1	10	140	4	9
Ramp 2	2	220	0	49
Ramp 3	2	240	40	99

Table 4.2: GC-MS temperature program used for analysis of products generated from oleic acid oxidation with potassium permanganate

Oven Ramp	Ramp Rate/ °C·min ⁻¹	Next Temperature/ °C	Hold Time/ min.	Run Time/ min.
Initial	-	50	3	3
Ramp 1	10	150	0	13
Ramp 2	1	190	0	53
Ramp 3	10	280	2	64



Figure 4.1: LC-1234 Ozone Generator equipped with a Model HC Ozone Monitor utilized for this study

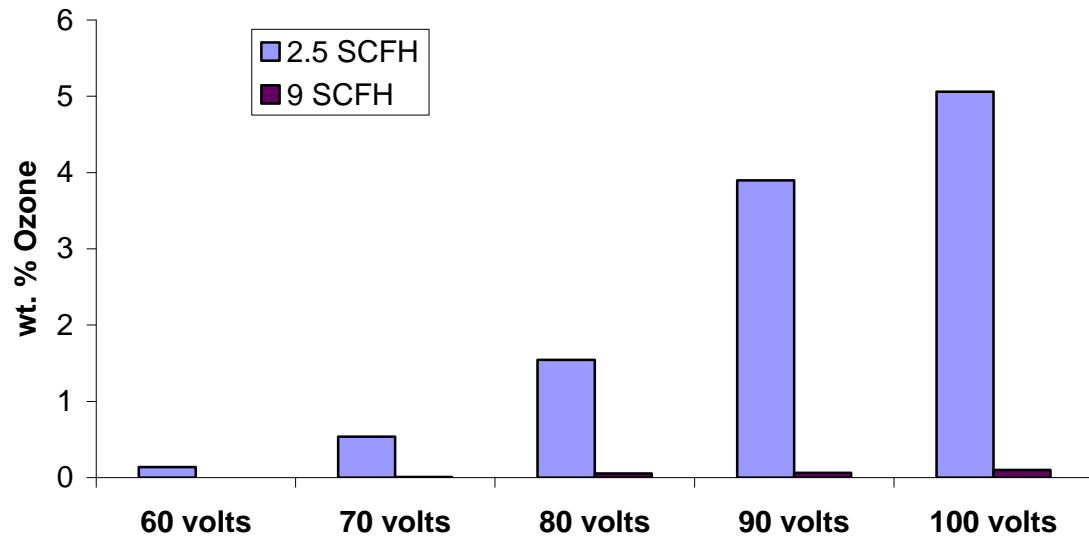


Figure 4.2: Ozone generator calibration data



Figure 4.3: Potassium permanganate crystals

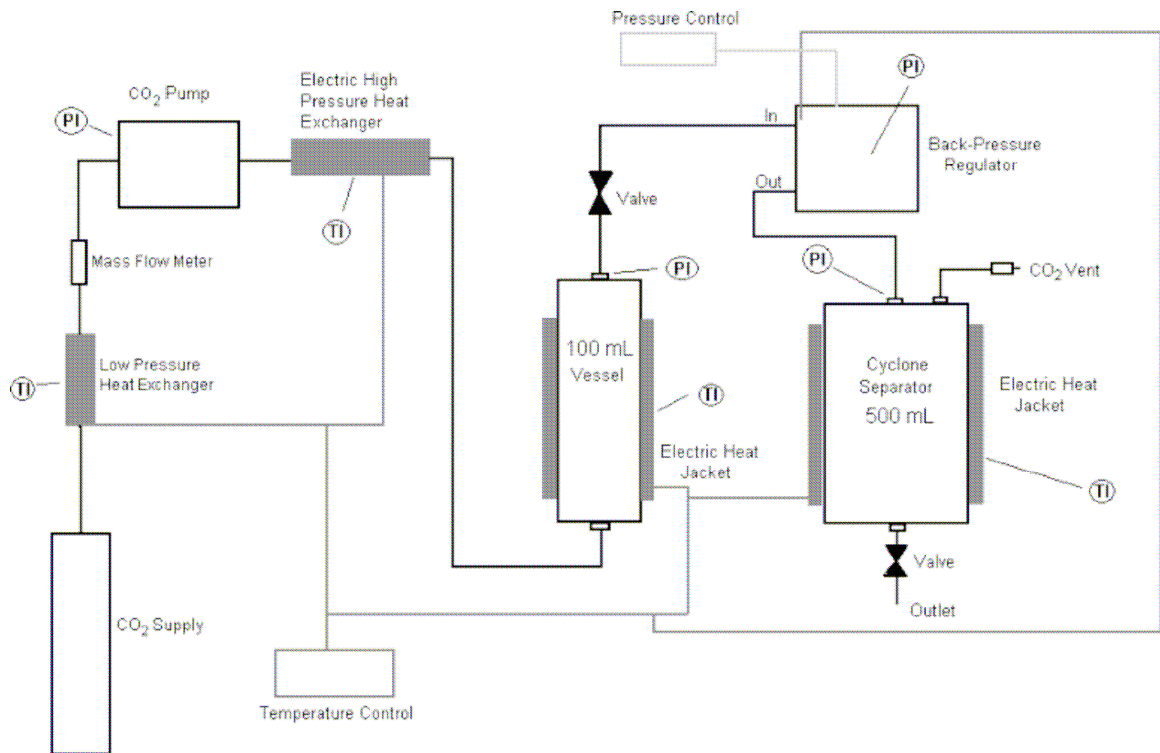


Figure 4.4: Experimental apparatus used for solubility experiments

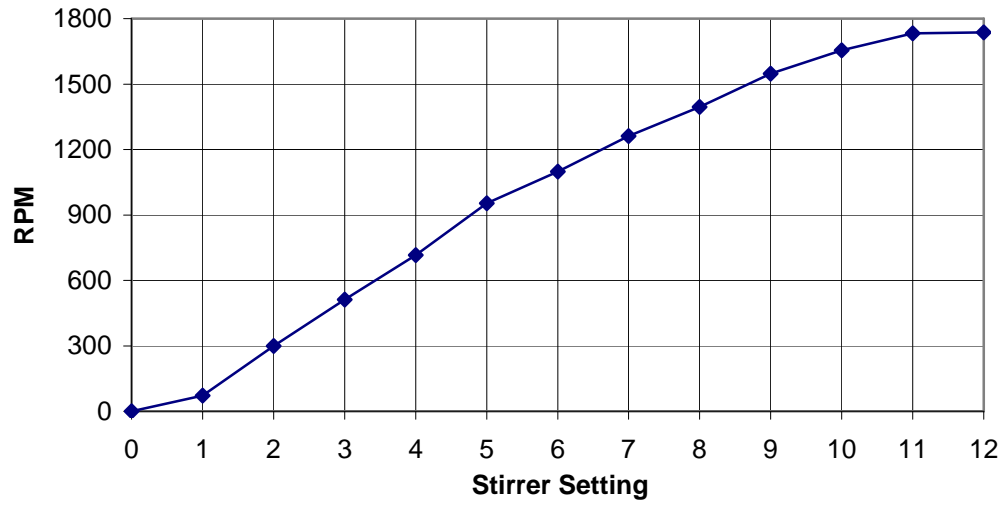


Figure 4.5: Magnetic stirrer calibration curve generated using photo/contact tachometer

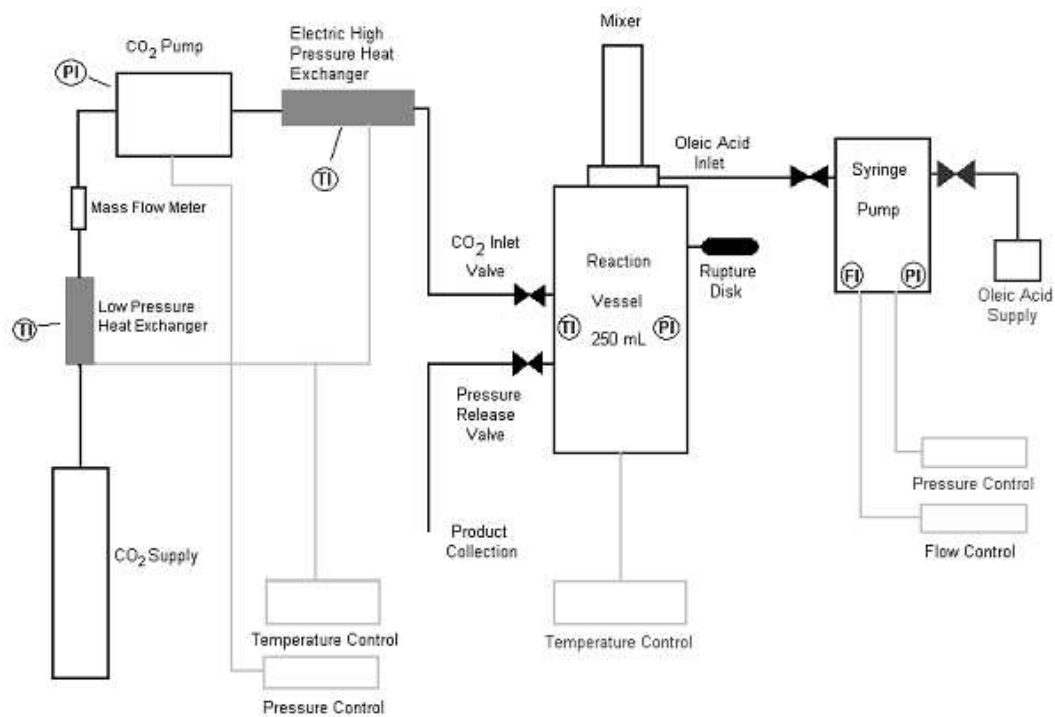


Figure 4.6: Experimental apparatus used for oxidation reactions in SC-CO₂

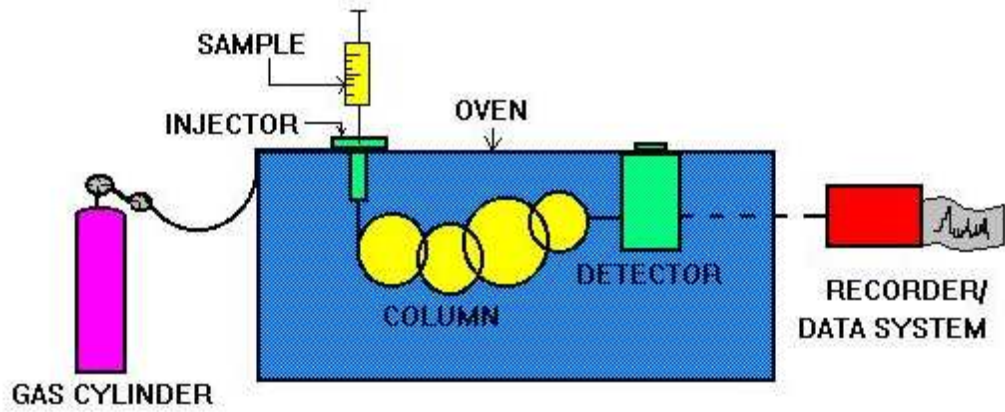


Figure 4.7: Major components of a gas chromatograph [Punrattanasin and Spada, 1997]



Figure 4.8: Agilent 6890N GC-FID used in this work

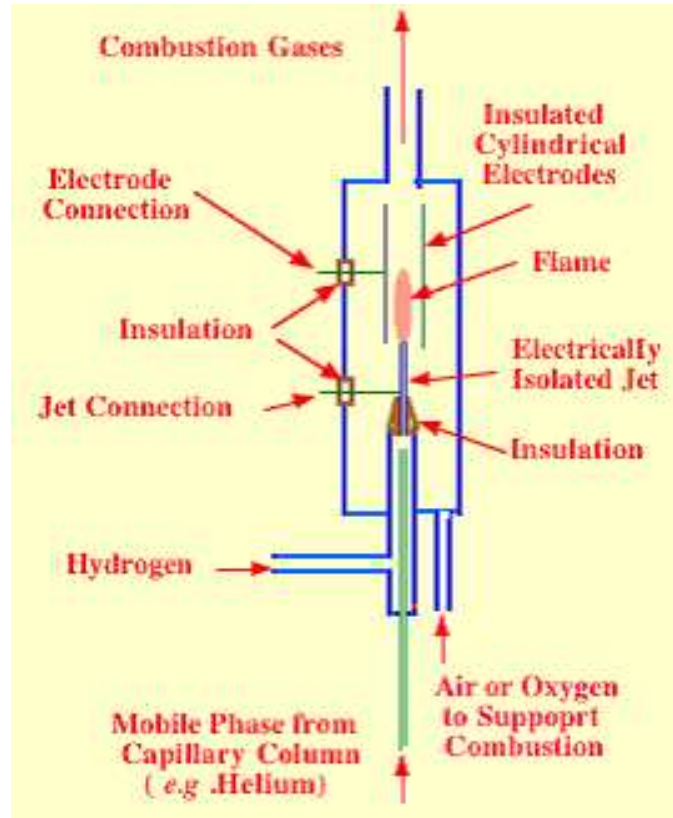


Figure 4.9: Illustration of a flame ionization detector [Scott, 2007]



Figure 4.10: Varian 3600 GC with Saturn 2000 Mass Spectrometer used in this study

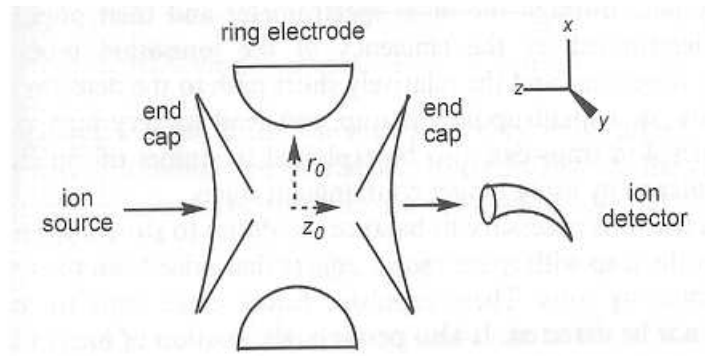


Figure 4.11: Schematic of a quadrupole ion trap [Downard, 2004]



Figure 4.12: LAMBDA 25 UV/VIS Spectrophotometer used for determining potassium permanganate concentration

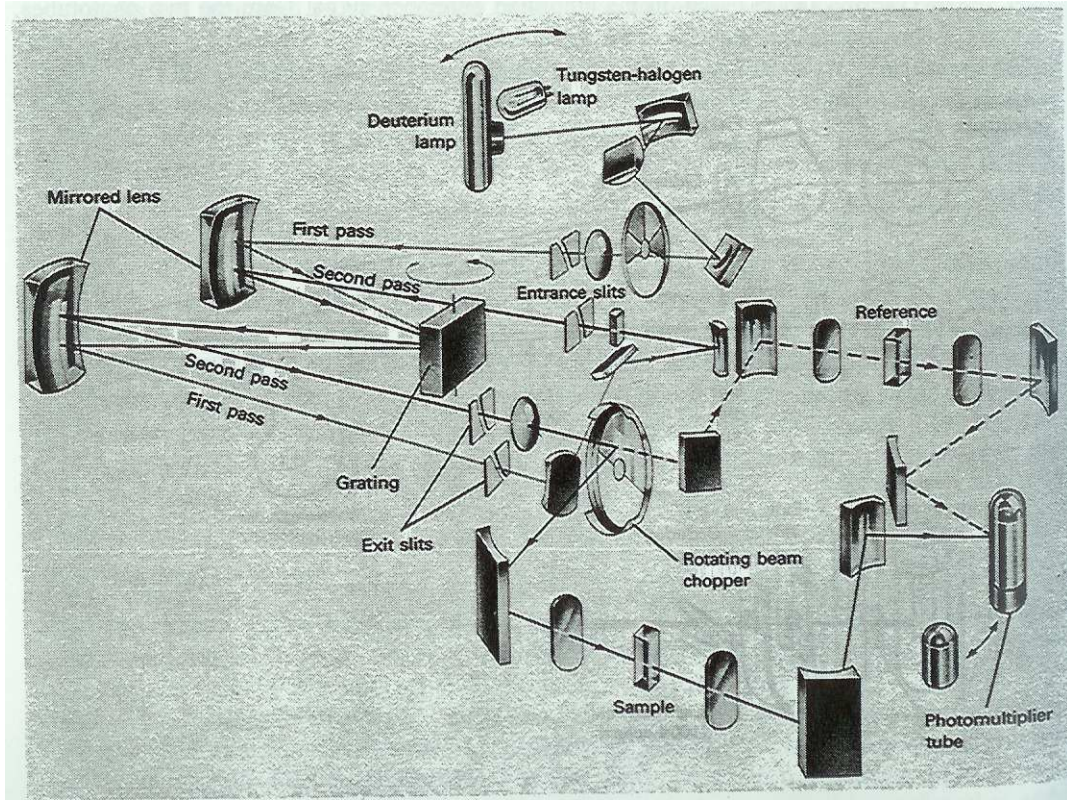


Figure 4.13: UV/VIS spectrophotometer double-beam design [Hargis, 1988b]

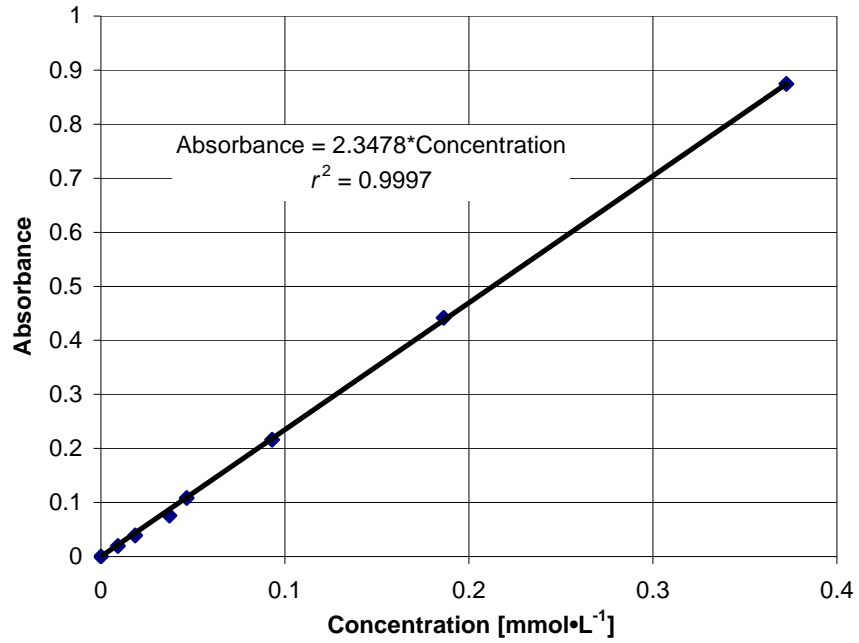


Figure 4.14: UV/VIS spectrophotometer calibration curve

CHAPTER V

SOLUBILITY MODELING THEORY

Introduction

The purpose of this chapter is to provide a theoretical background for the solubility models appearing in later chapters. Most models can be classified as being either semi-empirical or equation-of-state based. Three of the most common semi-empirical methods are those developed by Chrastil (1982), Méndez-Santiago and Teja (1999), and Bartle et al. (1991). Although many types of equations of state exist, the Peng-Robinson equation of state (PR-EoS; Peng and Robinson, 1976) is the most commonly used EoS in predicting solubility of solids and liquids in supercritical fluids [Yu et al., 1994]. Therefore, it is the only EoS considered in this work.

Semi-Empirical Methods

Chrastil's model, one of the first density-based models proposed, is based upon the theory that at equilibrium a solvato complex is formed between associating solute and solvent molecules [Chrastil, 1982]. Chrastil's theory led to the development of a model that relates the solubility of the solute and the density of the pure solvent. This relationship is provided in Eq. (5.1):

$$c_2 = \rho_1^k \exp\left(\alpha + \frac{\beta}{T}\right) \quad (5.1)$$

where c_2 is the solubility of solute in $\text{kg}\cdot\text{m}^{-3}$, ρ_1 is the supercritical fluid density in $\text{kg}\cdot\text{m}^{-3}$, k is an association number, α is a function of the association number and molecular weights of the solute and supercritical fluid, β is a function of the heat of solvation and heat of vaporization, and T is temperature. The association constant k shows the dependence of the solubility on density and parameter β reflects the dependence of the solubility on temperature [Güçlü-Üstündağ and Temelli, 2000]. According to Chrastil's equation, a log-log graph of c_2 versus ρ_1 for isothermal data should give a straight line. However, Chrastil's method has several limitations. If the solute solubility is very high (greater than 100 to 200 $\text{kg}\cdot\text{m}^{-3}$), the density term in Eq. (5.1) must be corrected due to the influence of the solute [del Valle and Aguilera, 1988]. Also, Chrastil's equation is not valid over a wide range of temperature [Chrastil, 1982]. Due to these limitations, several modified forms of Chrastil's equation have been developed.

As mentioned previously, a log-log plot of c_2 versus ρ_1 yields a straight line for isothermal data with an intercept of

$$I = \alpha + \frac{\beta}{T} \quad (5.2)$$

In studying the solubility of vegetable oil in supercritical carbon dioxide, del Valle and Aguilera (1988) found that when values of I for a series of isotherms were plotted against $1/T$, a straight line should be obtained. The slope of this line would be equivalent to β in Eq, (1) which, as previously mentioned, is a function of the heats of solvation and vaporization of the solute. To recompense for the change in the heat of vaporization with temperature, they proposed the following modification to Chrastil's equation:

$$c_2 = \rho_1^k \exp\left(\alpha + \frac{\beta}{T} + \frac{\gamma}{T^2}\right) \quad (5.3)$$

Adachi and Lu (1983) modified Chrastil's equation to better model the solubility of triacylglycerols. Note that both Chrastil and del Valle and Aguilera assumed the association number k to be constant and independent of density or temperature. Adachi and Lu (1983) changed the association number to a polynomial that is a second-order function of the supercritical fluid density. They proposed that the association constant k be expressed as:

$$k = e_0 + e_1\rho_1 + e_2\rho_1^2 \quad (5.4)$$

Therefore, the Adachi-Lu equation can be expressed as follows:

$$c_2 = \rho_1^{(e_0 + e_1\rho_1 + e_2\rho_1^2)} \exp\left(\alpha + \frac{\beta}{T}\right) \quad (5.5)$$

They found that by using Eq. (5.5) instead of Eq. (5.1) a significant reduction in variation between experimental and calculated solubility data could be achieved for some systems.

A widely used density-based model is that proposed by Méndez-Santiago and Teja (1999). An advantage of Chrastil's model (and its modified forms by del Valle and Aguilera and by Adachi and Lu) is that properties of the solute are not required. However, methods proposed later by Méndez-Santiago and Teja (1999) require the sublimation pressure of the solid. They proposed a model based on the theory of dilute solutions in which the so-called enhancement factor is a function of the density of the solvent. The Méndez-Teja equation can be expressed as

$$T \ln E = T \ln \frac{y_2 P}{P_2^{sub}} = A + B\rho_1 \quad (5.6)$$

where T is absolute temperature, E is the enhancement factor, y_2 is the solute mole fraction, P is total pressure, P_2^{sub} is the sublimation pressure of the solute, ρ_1 is the density of the supercritical fluid, and A and B are regressed constants. The enhancement factor represents the ratio of the actual solubility to the ideal solubility, i.e., that calculated according to the ideal-gas law (P_2^{sub} / P) [Prausnitz et al., 1999]. The Méndez-Teja equation is an abbreviated form of the following expression:

$$T \ln E = - \left[A + B (\rho_1 - \rho_{c,1}) \right] + \frac{V_2 (P - P_2^{sub})}{R} - T \ln \phi_1 \quad (5.7)$$

where $\rho_{c,1}$ is the critical density of the solvent, V_2 is the molar volume of the solute, ϕ_1 is the fugacity coefficient of the solvent, and all other terms are the same as those defined for Eq. (5.6). Although Harvey (1990) proposed that a plot of $T \ln E$ versus ρ_1 should yield a straight line if the last two terms on the right-hand side of Eq. (5.7) are neglected, Méndez-Santiago and Teja (1999) actually tested the validity of the approximation. An advantage of this model is that solubility data at different temperatures can be represented by a single straight line, and this can be attributed to the regression constants A and B in Eq. (5.6) being independent of temperature. Therefore, this model is excellent for determining consistency of solubility data across different isotherms. Although, Méndez-Santiago and Teja noticed no upper density limit of Eq. (5.6) in terms of linear behavior, they noticed a lower density limit of about $0.5\rho_c$ of the solvent.

In many instances, the sublimation pressure of the solid is not available, so Méndez-Santiago and Teja (1999) proposed a modified version of the method for cases in

which the sublimation pressure was unknown. This model is obtained by substituting a two-constant Antoine equation for P_2^{sub} into equation (5.6):

$$T \ln y_2 P = A' + B' \rho_1 + C' T \quad (5.8)$$

where A' , B' , and C' are regressed constants. All other variables in Eq. (5.8) are the same as defined in Eq. (5.6).

Bartle et al. (1991) also proposed a model relating the enhancement factor of the solute to the density of the solvent:

$$\ln E = A + C \rho_1 \quad (5.9)$$

where A and C are regressed constants. Since the sublimation pressure of solids is not always available, Bartle et al. approximated the enhancement factor as follows:

$$E \approx \frac{y_2 P}{P_{ref}} \quad (5.10)$$

where y_2 is the mole fraction of the solute, P is the total pressure and P_{ref} is the reference pressure, which is typically (and arbitrarily) taken to be 0.1 MPa. The use of a reference density as a corrective term is typically incorporated into Eq. (5.9) to make A less sensitive to experimental errors in solubility data and also to variations caused by extrapolation to zero density [Ghiasvand et al., 1999]. Therefore, Eq. (5.9) can be expressed as:

$$\ln \frac{y_2 P}{P_{ref}} = A + C (\rho_1 - \rho_{ref}) \quad (5.11)$$

where ρ_{ref} is the reference density (typically and arbitrarily taken to be $700 \text{ kg}\cdot\text{m}^{-3}$) and all other terms are the same as previously defined. In this work, the critical density of carbon dioxide was used as the reference density. The constant C relates to the solvation

of the solute by the supercritical fluid and is assumed to be independent of temperature.

The term A comes from the vapor pressure of the solute and can be expressed as follows:

$$A = a + \frac{b}{T} \quad (5.12)$$

where a and b are constants and T is temperature [Ghiasvand et al., 1999]. Therefore, an alternative expression of the Bartle equation is the following:

$$\ln \frac{y_2 P}{P_{ref}} = a + \frac{b}{T} + C(\rho_1 - \rho_{ref}) \quad (5.13)$$

Dimensionless Forms of the Models [Sparks, 2007b]

In literature, the units used for solute concentration and density vary, so regressed constants for Eqs (5.1), (5.3), and (5.5) are dependent upon the units used to obtain them.

Also, Chrastil-type equations are dimensionally inconsistent. For example, solute concentration and solvent density can be expressed in $[\text{kg}\cdot\text{m}^{-3}]$. Since the value of the association constant k is usually different from 1 and not an integer [Chrastil, 1982], the density term of Eq. (5.1) will be raised to a power other than 1. Therefore, the units of the left-hand side of Eq. (5.1) do not match the units of the right-hand side. To compensate for this inconsistency, dimensionless variables can be used. Hence, Eqs.

(5.1), (5.3), and (5.5) can be rewritten as follows:

$$c_2^* = \rho_{r,1}^k \exp\left(\alpha + \frac{\beta}{T_r}\right) \quad (5.14)$$

$$c_2^* = \rho_{r,1}^k \exp\left(\alpha + \frac{\beta}{T_r} + \frac{\gamma}{T_r^2}\right) \quad (5.15)$$

$$c_2^* = \rho_{r,1}^{(e_0 + e_1 \rho_{r,1} + e_2 \rho_{r,1}^2)} \exp\left(\alpha + \frac{\beta}{T_r}\right) \quad (5.16)$$

where:

$$c_2^* = \frac{c_2}{\rho_{c,1}}; \quad \rho_{r,1} = \frac{\rho_1}{\rho_{c,1}}; \quad T_r = \frac{T}{T_{c,1}} \quad (5.17)$$

For calculation purposes, the critical density of carbon dioxide was 467.6 [kg/m³] (NIST, 2007) and its critical temperature was 304.2 [K] (CHEMCAD, 2005).

The equations for Méndez-Santiago and Teja and for Bartle et al. are dimensionally consistent. However, there are still advantages to express them in dimensionless or reduced form. The main one is that parameters obtained by authors using different units will be identical and thus easier to compare. Eqs. (5.6) and (5.8) are expressed in terms of reduced variables, as follows:

$$T_r \ln E = A^* + B^* \rho_{r,1} \quad (5.18)$$

$$T_r \ln y_2 P_r = A'' + B'' \rho_{r,1} + C'' T_r \quad (5.19)$$

where P_r is reduced pressure and A^* , A'' , B^* , B'' , C^* , and C'' are regressed constants [Sparks et al., 2007a]. Finally, the Bartle equations can be expressed in terms of dimensionless variables as follows:

$$\ln \frac{y_2 P}{P_{ref}} = A + C (\rho_{r,1} - 1) \quad (5.20)$$

$$\ln \frac{y_2 P}{P_{ref}} = a + \frac{b}{T_r} + C (\rho_{r,1} - 1) \quad (5.21)$$

where, for convenience, the arbitrary reference density has been taken to be the critical density of carbon dioxide.

Equation of State Approach

The Peng-Robinson equation of state (PR-EoS) is a cubic equation of state of the van der Waals type. Therefore, the pressure is expressed as the sum of a repulsion pressure, P_R , and an attraction pressure, P_A , as shown in Eq. (5.22).

$$P = P_R + P_A \quad (5.22)$$

Peng and Robinson (1976) proposed the following equation:

$$P = \frac{RT}{v-b} - \frac{a}{v(v+b)+b(v-b)} \quad (5.23)$$

where P is pressure, R is the gas constant, T is the absolute temperature, v is the molar volume, and a and b are equation parameters. In Eq. (5.23), the repulsion portion is the first term on the RHS and the attraction portion is the second term on the RHS. The parameters a and b are determined by the following equations:

$$a = a_c \alpha = \left(0.45724 \frac{R^2 T_c^2}{P_c^2} \right) \left(1 + m(1 - \sqrt{T_r}) \right)^2 \quad (5.24)$$

$$b = 0.07780 \frac{RT_c}{P_c} \quad (5.25)$$

where m is a quadratic function of the acentric factor ω as shown in Eq. (5.26) and the subscripts c and r denote critical and reduced values respectively.

$$m = 0.37464 + 1.54226\omega - 0.26992\omega^2 \quad (5.26)$$

The parameters a and b are typically determined by mixing rules. To account for the composition dependence of parameters a and b , van der Waals mixing rules were used. Since only binary systems were analyzed in this work, the mixing rules can be expressed as follows:

$$a_{mix} = \sum \sum x_i x_j a_{ij} = a_{11}x_1^2 + a_{22}x_2^2 + 2a_{12}x_1x_2 \quad (5.27)$$

$$b_{mix} = \sum \sum x_i x_j b_{ij} = b_{11}x_1^2 + b_{22}x_2^2 + 2b_{12}x_1x_2 \quad (5.28)$$

where x_i is the mole fraction of component i in the fluid phase. The values for the cross coefficients a_{12} and b_{12} are obtained from the following expressions:

$$a_{12} = \sqrt{a_{11}a_{22}}(1 - k_{12}) \quad (5.29)$$

$$b_{12} = \left(\frac{b_{11} + b_{22}}{2} \right) (1 - c_{12}) \quad (5.30)$$

where k_{12} is the binary interaction parameter and c_{12} is the size parameter [Škerget, et al., 2002]. Typically, c_{12} is set to zero, especially in the case of mixtures of nonpolar components [Prausnitz, et al., 1999].

The solubility of a nonvolatile solid in a supercritical fluid may be expressed as

$$y_2 = \frac{\hat{\phi}_2^s P_2^{sub}}{\hat{\phi}_2 P} \exp\left(\frac{V_2^{sol} (P - P_2^{sub})}{RT} \right) \quad (5.31)$$

where y_2 is the mole fraction of solute, P_2^{sub} the sublimation pressure of the solid at the system temperature (T), $\hat{\phi}_2^s$ the fugacity coefficient at the sublimation pressure and system temperature, $\hat{\phi}_2$ the fugacity coefficient of the vapor phase, P the system pressure, V_2^{sol} the molar volume of the solid, and R is the gas constant [Škerget, et al., 2002]. The basis for Eq. (5.31) is the assumption that the solid is in equilibrium, which can be expressed in terms of fugacity:

$$f_2^s = f_2^V \quad (5.32)$$

where f_2^s is the fugacity of the solute in the solid phase and f_2^v is the fugacity of the solute in the vapor phase. Since the solid is pure, f_2^s can be expressed as

$$f_2^s = P_2^s \phi_2^s \exp\left(\frac{V_2^{sol} (P - P_2^{sub})}{RT}\right) \quad (5.33)$$

When f_2^v is expressed in terms of $\hat{\phi}_2$, the following relationship results:

$$f_2^v = \phi_2 y_2 P \quad (5.34)$$

By combining Eqs. (5.33) and (5.34) and solving for the solute mole fraction y_2 , Eq.

(5.31) is obtained. In the case of nonvolatile solids, the sublimation pressure is so small

that $\hat{\phi}_2^s$ is approximately unity [Prausnitz, et al., 1999], and since $P \gg P_2^{sub}$, Eq. (5.31) can be

simplified to the following form:

$$y_2 = \frac{P_2^{sub}}{\hat{\phi}_2 P} \exp\left(\frac{V_2^{sol} P}{RT}\right) \quad (5.35)$$

If literature values are available for a binary system, then an objective function can be

utilized to obtain the binary interaction parameter k_{12} . The objective function used for

this work is written as

$$OF = \sqrt{\frac{\sum_{i=1}^{N_p} (y_{i,calc} - y_{i,exp})^2}{N_p}} \quad (5.36)$$

where N_p is the total number of experimental points, $y_{i,calc}$ is the solute mole fraction

calculated from the equation of state, and $y_{i,exp}$ is the experimental solute mole fraction

[Caballero, et al., 1992].

Use of cubic equations of state such as the PR-EoS can be difficult due to their

complexity compared to other methods such as semi-empirical models. Since $\hat{\phi}_2$ is a

function of y_2 , an iterative solution technique is necessary. Also, obtaining the critical properties of a solid such as its critical temperature and pressure from literature can be problematic because of the difficulty of reaching the critical point of many solids experimentally to establish the values. Therefore, group contribution methods such as the Ambrose method or Joback's modification of the Lydersen method are often used to estimate the required properties [Reid et al., 1987]. In the case of nonvolatile solids, sublimation pressure data can also be difficult locate. Other challenges can arise from the type of system being investigated. For example, in highly nonideal systems, the interaction parameters display a temperature dependence, and equations of state do not fit the data equally well at all temperatures and pressures, especially in the near-critical region [Škerget, et al., 2002].

CHAPTER VI
EVALUATION OF DENSITY-BASED MODELS FOR THE SOLUBILITY OF
SOLIDS IN SUPERCRITICAL CARBON DIOXIDE AND FORMULATION OF A
NEW MODEL [Sparks et al., 2007b]

Introduction

Whether a supercritical fluid is being used as an extraction solvent or as a reaction media, the ability to estimate the solubility of compounds in the supercritical fluid is crucial in determining proper operating conditions. Although several methods exist to experimentally determine solubility, models are often used to provide correlations [Maxwell, 1996; Sauceau et al., 2003]. Most models can be classified as being either semi-empirical or equation-of-state based; however, semi-empirical models are often utilized because their relative ease of application compared to equations of state. The most common semi-empirical models are based upon providing a correlation between solubility and density; hence, they are referred to as density-based models. Three of the most common semi-empirical methods are those developed by Chrastil (1982), Méndez-Santiago and Teja (1999), and Bartle et al. (1991), and their theoretical development can be found in Chapter V. In this study, Chrastil's equation and its modifications, the methods of Méndez-Teja, and Bartle's equations were compared in terms of their ability

to estimate the solubility of solid compounds in supercritical carbon dioxide. The methods are also compared in terms of relative complexity and possible limitations.

Methodology

To compare the efficacy of the models in estimating solubility, each model was applied to several solid compounds that have experimental solubility in supercritical carbon dioxide readily available in literature. The compounds considered in this work were naphthalene, fluorene, hydroquinone, anthracene, and cholesterol. Table 6.1 provides a summary of the experimental solubility results for each compound along with the appropriate reference.

Three isotherms were considered for each of the five solid-CO₂ systems. Table 6.2 provides physical properties for these solid compounds and for carbon dioxide. Sublimation pressures were determined with Antoine's equation in the form

$$\log P^{sat} = A - \frac{B}{T} \quad (6.1)$$

where P^{sat} is in Pa and T is in K and A and B are the Antoine constants. Values for the Antoine's constants shown in Table 6.2 were determined from sublimation pressure data. With the exception of the critical temperature and pressure of cholesterol, all other physical properties were obtained from the CHEMCAD (2005) component database. The critical pressure and temperature for cholesterol were obtained from Huang et al. (2004).

The percent average error (% AVERR) was determined for each compound for each isotherm with each model. The % AVERR can be written as:

$$AVERR(\%) = \frac{\sqrt{\frac{\sum_{i=1}^N (y_{i,calc} - y_{i,exp})^2}{N}}}{\sum_{i=1}^N y_{i,exp}} \times 100 \times N \quad (6.2)$$

where N is the number of data points, $y_{i,exp}$ is the experimental solubility of the solid for experimental point i , and $y_{i,calc}$ is the calculated solubility corresponding to point i . The constants for the semi-empirical models were determined by using the Solver tool in Excel (Microsoft; Redmond, WA) by minimizing the following objective function:

$$OF = \sqrt{\frac{\sum_{i=1}^N (y_{i,calc} - y_{i,exp})^2}{N}} \quad (6.3)$$

Modeling Results

A comparison of the original Chrastil's equation (Eq. 5.1) with the dimensionless form is shown in Table 6.3. The dimensionless form of Chrastil's equation provides very similar average error to the original form, as expected. In the original Chrastil equation, k is already dimensionless, so its value should not be affected by switching to dimensionless variables. The parameters are readily related by comparing Eq. (5.1) and Eq. (5.14); the dimensionless form of α and β are given by the following equations:

$$\beta|_{dimen} = \frac{\beta}{T_{c,1}}; \quad \alpha|_{dimen} = \alpha - (k - 1) \ln p_{c,1} \quad (6.4)$$

As can be seen from Table 6.3, the regressed k values for Eq. (5.1) and Eq. (5.14) are very similar. Also, if α and β calculated from Eq. (6.4) are compared to the values in

columns 8 and 9 of Table 6.3, it will be noted that the values are quite similar and the small differences can be attributed to minor inconsistencies in the Solver tool.

When a similar analysis was done for all models, their dimensionless form yielded similar results to their non-dimensionless counterparts. Therefore, for the remainder of this paper, only results from dimensionless models will be reported. However, tables showing results for both traditional and dimensionless equations can be found in Appendix B.

It should be noted that two entries exist for cholesterol. This is because the solubility data for the 308.15 K isotherm exhibit a different curvature (convex) than the other two isotherms (concave), as shown in Figure 6.1. Due to the difference in curvature, the effectiveness of most of the models considered in this study was reduced when all three cholesterol isotherms were used. The first cholesterol entry corresponds to all three isotherms while the second one (last in each Table) corresponds to results ignoring the convex (308.15 K) isotherm.

Table 6.4 provides modeling results for the dimensionless form of the del Valle-Aguilera equation. In many cases the del Valle-Aguilera equation provided a better fit than Chrastil's equation. The most notable improvement in average error was seen in the cholesterol data, particularly the 308.15 K isotherm. However, to determine if this improvement is due to the ability of the del Valle-Aguilera equation to better compensate for temperature effects or just simply because it has one more adjustable parameter, the results of the Adachi-Lu equation must be considered.

Table 6.5 shows the results for the Adachi-Lu equation. In most cases, use of the Adachi-Lu equation resulted in a lower average error compared to either Chrastil's

equation or the del Valle-Aguilera equation. The primary exception is with the cholesterol isotherm of 308.15 K. When all three cholesterol isotherms are taken into account, the Adachi-Lu equation provides a similar average error to Chrastil's equation. However, when the 308.15 K isotherm is removed, the Adachi-Lu equation performs better than Chrastil's equation. Although the Adachi-Lu equation has five adjustable parameters, it does not perform as well as the del Valle-Aguilera equation for the cholesterol case. However, this is to be expected because, as previously mentioned, the additional adjustable parameters of the Adachi-Lu equation correct for different effect than the additional adjustable parameter of the del Valle-Aguilera equation. Therefore, the improvement seen by the del Valle-Aguilera equation must be due to its ability to better account for temperature effects than either Chrastil's equation or the Adachi-Lu equation.

As previously described, Adachi and Lu modified the term for the association constant k in the Chrastil equation so that it became a quadratic function of density. However, when values of k are calculated according to Eq. (5.4) for several solid-supercritical carbon dioxide systems [Adachi and Lu, 1983] and plotted against reduced density, an interesting trend can be observed. Though k was generated from a quadratic function, as shown in Figure 6.2, the change of k with density is somewhat linear for each compound. Therefore, the Adachi-Lu equation can be modified to the following form:

$$c_2 = \rho_1^{(e_0 + e_1 \rho_1)} \exp\left(\alpha + \frac{\beta}{T}\right) \quad (6.5)$$

with the corresponding dimensionless form being:

$$c_2^* = \rho_{r,1}^{(e_0 + e_1 \rho_{r,1})} \exp\left(\alpha + \frac{\beta}{T_r}\right) \quad (6.6)$$

The only difference between Eq. (6.5) and the Adachi-Lu equation is that k is expressed as a linear function of density as follows:

$$k = e_0 + e_1 \rho_1 \quad (6.7)$$

Table 6.6 shows the average error resulting from Eq. (6.6). As expected, the average error with one less adjustable parameter is similar to that obtained by using the original Adachi-Lu equation. Therefore, Eq. (6.6) provides a better account of the dependence of the association constant k on density compared to the original Chrastil equation but is not as complex as the Adachi-Lu equation. However, Eq. (6.6) also has the same weakness as the original form in that it does not provide a better compensation for the effect of temperature, unlike the del Valle-Aguilera equation. This weakness is reflected in the high average error for the previously discussed 308.15 K isotherm for cholesterol. These observations prompted the proposal of a new density-based model for solubility of solids in supercritical fluids. The new model is presented in the next section.

As previously mentioned, the original form of the Méndez-Teja equation requires sublimation pressure data. If application of Eq. (5.6) or its dimensionless form (Eq. 5.18) results in high error, a possible cause is poor quality vapor pressure data as opposed to simply being an ineffective model. Table 6.7 shows the average error for the dimensionless form of the Méndez-Teja equation (Eq. 5.18). Compared to Chrastil's equation, the average error resulting from the Méndez-Teja equation is higher at every isotherm for each compound. This could be due to poor vapor pressure data; however, the Méndez-Teja equation has only two adjustable parameters, whereas Chrastil's

equation has three. Therefore, the Méndez-Teja equation is not as robust as Chrastil's equation and its more complex modifications in terms of regression.

Since vapor pressure data are not required for the modified form of the Méndez-Teja equation, it is easier to apply to solute-supercritical fluid systems. Table 6.8 shows the average error resulting from Eq. (5.19). In each case, the modified Méndez-Teja equation provides a lower average error than the original form (Eq. 5.18).

At some isotherms, the modified Méndez-Teja equation performed better than Chrastil's equation. For example, at the 348 K isotherm of hydroquinone, the solubility estimated by the modified Méndez-Teja equation resulted in a lower deviation than Chrastil's equation or any of its more complex modifications, such as Eqs. (5.15) and (5.16). In addition to not being subjected to the effect of poor vapor-pressure data, the modified Méndez-Teja equation has one more adjustable parameter than the original form. As previously mentioned, Méndez-Santiago and Teja noticed a lower density limit of about $0.5\rho_{c,1}$ in terms of the ability of their proposed linear equations to adequately predict solubility behavior. For the data sets considered in this study, only naphthalene and fluorene have multiple solubility values at or below $0.5\rho_{c,1}$. Figures 6.3 and 6.4 show the experimental data for naphthalene and fluorene, respectively, along with calculated solubility values generated by the dimensionless form of the modified Méndez-Teja equation (Eq. 5.19). Above a reduced density of about 1.1, the naphthalene isotherms collapse to a straight line, indicating good consistency. However, below a reduced density of 1.1, differences among isotherms increase. As shown in Figure 6.3, below a reduced density of about 0.6, all of the experimental values are below the solubility predicted by Eq. (5.19). In the case of fluorene, the estimated solubility matches the

experimental values fairly well, but below a reduced density of 0.9, all the experimental values are below the model values, as shown in Figure 6.4. Therefore, there does appear to be a limitation for the Méndez-Teja group of equations in terms of lower density limit.

The dimensionless form of the Bartle equation (Eq. 5.20) is similar in structure to the dimensionless Méndez-Teja equation (Eq. 5.18); however, in most cases, Eq. (5.20) yields considerable higher average error than Eq. (5.19) when single parameters are used for all temperatures. Traditionally, Bartle's equation is applied to individual isotherms and regression constants are obtained for each isotherm. In their original paper, Bartle et al. did not propose a specific form for the dependence of the parameters with temperature. Instead, they calculated the parameters for each individual isotherm and presented them in an extensive table (their Table 4). The modified form (Eq. 5.13) of Bartle's equation has three adjustable parameters and compensates for the effect of temperature better. The average error of the dimensionless form of Bartle's equation (Eq. 5.21) is provided in Table 6.9. In general, the modified Bartle equation provides a lower average error than both the original and modified forms of the Méndez-Teja equation and, in some cases, it yields lower error than Chrastil's equation.

New Density-Based Model

Both the Adachi-Lu equation and its linear modification and the del Valle-Aguilera equation provide an improvement over Chrastil's equation, but as has been shown, cases exist where equations of the Adachi-Lu type are better than the del Valle-Aguilera equation and vice versa. The Adachi-Lu equation corrects the effect of density on solubility while the del Valle and Aguilera equation corrects the effect of temperature

on solubility. Therefore, a combination of the two corrections is proposed here. Adachi and Lu correction, however, goes from a constant association number, k , to a quadratic relationship between k and $\rho_{c,1}$. According to the results presented here, a linear relationship between k and $\rho_{c,1}$ seems to suffice. Combining Eq. (6.6) with the del Valle-Aguilera equation results in the following dimensionless expression:

$$c_2^* = \rho_{r,1}^{(e_0+e_1\rho_{r,1})} \exp\left(\alpha + \frac{\beta}{T_r} + \frac{\gamma}{T_r^2}\right) \quad (6.8)$$

Table 6.10 shows the average error resulting from Eq. (6.8). In general, Eq. (6.8) provides a lower average error than the individual models it is based upon.

If the full Adachi-Lu equation is combined with the del Valle-Aguilera to create an equation with six adjustable parameters, the following dimensionless expression is obtained:

$$c_2^* = \rho_{r,1}^{(e_0+e_1\rho_{r,1}+e_2\rho_{r,1}^2)} \exp\left(\alpha + \frac{\beta}{T_r} + \frac{\gamma}{T_r^2}\right) \quad (6.9)$$

In general, Eq. (6.9) provides even lower average error (shown in Table 6.11) than Eq. (6.8). However, the gain in efficacy is not justified by the additional complexity introduced in the equation. Also, achieving convergence via the objective function can be difficult because of the inherent complexity of the resulting equation. Ease of convergence relies upon the quality of the initial estimates of the adjustable parameters.

To compare all the equations in the same basis, the overall average error was determined for each compound using each model, and the results are shown in Figure 6.5. The overall average error was determined in the same fashion as the average error, except the summations of the objective function (Eq. 6.3) and the average error (Eq. 6.2) are

taken over the entire range of isotherms for each compound. As seen in Figure 6.5, Eq. (6.9) provides the lowest overall average error across all solutes considered.

Conclusions

Semi-empirical methods based upon the Méndez-Teja equation, Bartle's equation, and Chrastil's equation and its modifications were evaluated in terms of their ability to accurately estimate solid solubility in supercritical carbon dioxide. The solids considered for this study were naphthalene, anthracene, fluorene, hydroquinone, and cholesterol. Although naphthalene, anthracene, and fluorene are similar in structure, the solubilities of these compounds can vary greatly. Hydroquinone and cholesterol both contain –OH functional groups which can affect solubility in carbon dioxide. To estimate the solubility of these compounds in supercritical carbon, many of the above mentioned models have been used in literature. However, one of the models proposed in this study, a combination of the Adachi-Lu equation and the del Valle-Aguilera equation, provided the best fit in terms of lowest average error. The results of this study also show that semi-empirical models can be expressed in terms of dimensionless variables without loss of effectiveness.

Table 6.1: Sources of solid + supercritical carbon dioxide solubility data

Compound	<i>T</i> /K	<i>N</i>	<i>P</i> /MPa	$\rho_{CO_2}^a$ /kg·m ⁻³	Mol. Frac. ×10 ⁴	Reference
Naphthalene	308.15	22	6.08 – 33.44	162.64 – 945.45	2.4 – 187	Tsekhanskaya et al., 1964
	318.15	20	6.28 – 31.41	152.26 – 898.41	4.7 – 294	
	328.15	22	7.70 – 32.42	190.53 – 866.04	11 – 550	
Fluorene	308.15	6	8.37 – 41.45	589.91 – 977.58	4.15 – 27.2	Johnston et al., 1982
	323.15	9	6.99 – 41.45	171.6 – 929.64	0.109 – 43.6	
	343.15	8	8.37 – 48.34	185.8 – 897.5	0.688 – 91.8	
Hydroquinone	333	11	10 – 35	291 – 864 ^b	0.07 – 0.338	García-González et al., 2002
	348	11	10 – 35	234 – 809 ^b	0.09 – 0.424	
	363	11	10 – 35	203 – 753 ^b	0.1 – 0.5594	
Anthracene	303.15	4	10.43 – 41.45	780.95 – 993.33	0.292 – 0.795	Johnston et al., 1982
	323.15	10	9.06 – 41.45	289.85 – 929.64	0.035 – 1.72	
	343.15	9	11.81 – 41.45	335.54 – 864.57	0.142 – 3.49	
Cholesterol	308.15	7	12.36 – 27.89	774.19 – 918.04	0.139 – 0.555	Wong and Johnston, 1986
	313.15	7	10.09 – 27.6	635.16 – 896.14	0.708 – 2.5	
	333.15	7	10.1 – 27.33	296.13 – 808.3	0.291 – 3.8	

^a NIST, 2007.

^b García-González et al., 2002.

Table 6.2: Physical properties of solid compounds and carbon dioxide

Compound	T_c/K	P_c/MPa	ω	$\rho/kg\cdot m^{-3}$	$MW/g\cdot mol^{-1}$	A	B	Vapor Pressure Reference
Naphthalene	748.35	4.05	0.3020	1027	128.174	13.593	3742.6	Růžička et al., 2005
Fluorene	870	4.70	0.3390	1381.2	166.22	14.205	4561.8	Johnston et al., 1982
Hydroquinone	823	7.45	0.6823	988.254	110.12	15.451	5426.1	Jordan, 1954
Anthracene	873	2.90	0.4892	1230.2	178.23	12.147	4397.6	Johnston et al., 1982
Cholesterol	1168.23	4.155	0.9477	858.023	386.662	2.3272	1606.5	Wong and Johnston, 1986
Carbon Dioxide	304.2	7.382	0.231	-	44.01	-	-	-

Table 6.3: Chrastil equation modeling results

Comp.	T/K	Normal (Eq. 5.1)				Dimensionless (Eq. 5.14)			
		k	α	β/K	AVERR %	k	α	β	AVERR %
Naph.	308.15				12.86				12.58
	318.15	3.871	-0.919	-6.65E+03	12.11	3.869	16.621	-21.736	12.25
	328.15				5.76				5.83
Fluor.	308.15				8.92				9.02
	323.15	4.035	-10.661	-4.56E+03	7.5	4.040	8.047	-15.052	7.45
	343.15				5.06				5.05
Hydroq.	333				6.79				6.79
	348	2.613	-12.487	-2.59E+03	5.45	2.613	-2.569	-8.502	5.45
	363				6.97				6.97
Anthrac.	303.15				10.92				10.83
	323.15	4.352	-14.028	-5.21E+03	9.31	4.352	6.579	-17.124	9.35
	343.15				8.55				8.54
Chol.	308.15				118.27				114.34
	313.15	6.503	-19.108	-7.81E+03	39.43	6.754	15.254	-26.391	40.41
	333.15				13.40				13.57
Chol.	313.15				14.79				14.78
	333.15	6.786	-27.437	-5.67E+03	13.18	6.776	8.103	-18.602	13.17

Table 6.4: del Valle-Aguilera (Eq. 5.15) modeling results

Comp.	T/K	k	α	β	γ	AVERR %
Naph.	308.15	3.870	1.23E+02	-2.44E+02	1.16E+02	11.31
	318.15					7.83
	328.15					5.66
Fluor.	308.15	4.037	17.179	-34.769	10.625	8.76
	323.15					7.31
	343.15					5.05
Hydroq.	333	2.617	11.976	-41.78	19.008	6.6
	348					5.28
	363					6.99
Anthrac.	303.15	4.36	19.008	-43.982	14.48	8.65
	323.15					9.04
	343.15					8.51
Chol.	308.15	6.809	-9.60E+02	2.04E+03	-1.09E+03	8.62
	313.15					14.82
	333.15					13.2
Chol.	313.15	6.776	7.53	-17.385	-0.646	14.78
	333.15					13.17

Table 6.5: Adachi-Lu (Eq. 5.16) modeling results

Comp.	T/K	e_0	e_1	e_2	α	β	AVERR %
Naph.	308.15	2.817	2.268	-0.879	15.719	-20.893	10.49
	318.15						10.63
	328.15						2.96
Fluor.	308.15	2.978	2.499	-0.927	7.306	-14.478	8.40
	323.15						5.47
	343.15						2.11
Hydroq.	333	0.920	2.863	-1.058	-3.074	-7.997	4.8
	348						5.84
	363						4.34
Anthrac.	303.15	7.026	-1.297	0.085	5.646	-16.477	11.87
	323.15						7.55
	343.15						7.73
Chol.	308.15	-8.172	15.07	-4.045	15.205	-25.752	114.04
	313.15						39.95
	333.15						10.35
Chol.	313.15	-0.739	3.542	-0.212	10.489	-20.001	13.55
	333.15						6.4

Table 6.6: Eq. (6.6) modeling results

Comp.	T/K	e_0	e_1	α	β	AVERR %
Naph.	308.15	5.2	-0.651	15.933	-21.114	10.93
	318.15					10.7
	328.15					3.98
Fluor.	308.15	6.18	-0.893	7.486	-14.752	8.13
	323.15					5.93
	343.15					3.01
Hydroq.	333	3.183	-0.308	-2.837	-8.229	5.92
	348					6.75
	363					8.36
Anthrac.	303.15	6.708	-0.976	5.636	-16.455	11.99
	323.15					7.57
	343.15					7.66
Chol.	308.15	5.529	0.491	15.692	-26.647	114.34
	313.15					40.49
	333.15					12.84
Chol.	313.15	-0.223	2.86	10.577	-20.082	13.51
	333.15					6.33

Table 6.7: Méndez-Teja (Eq. 5.18) modeling results

Comp.	T/K	A*	B*	AVERR %
	308.15			43.35
Naph.	318.15	3.86	3.197	18.4
	328.15			25.15
	308.15			11.21
Fluor.	323.15	4.569	4.059	6.85
	343.15			4.63
	333			72.9
Hydroq.	348	2.913	3.105	38.65
	363			29.19
	303.15			33.86
Anthrac.	323.15	4.33	4.417	13
	343.15			12.76
	308.15			193.55
Chol.	313.15	12.237	1.221	58.82
	333.15			96.79
Chol.	313.15	10.92	2.38	52.74
	333.15			79.53

Table 6.8: Modified Méndez-Teja (Eq. 5.19) modeling results

Comp.	T/K	A''	B''	C''	AVERR %
Naph.	308.15				12.63
	318.15	-34.751	3.586	24.621	10.5
	328.15				3.59
Fluor.	308.15				6.54
	323.15	-28.789	4.019	15.9	4.65
	343.15				3.81
Hydroq.	333				6.56
	348	-16.566	2.737	1.818	4.98
	363				10.12
Anthrac.	303.15				15.18
	323.15	-33.653	4.561	16.19	8.2
	343.15				9.67
Chol.	308.15				188.63
	313.15	-33.537	4.759	16.315	28.85
	333.15				22.36
Chol.	313.15				17.96
	333.15	-33.499	4.825	16.354	15.18

Table 6.9: Modified Bartle (Eq. 5.21) modeling results

Comp.	T/K	<i>a</i>	<i>b</i>	<i>C</i>	AVERR %
Naph.	308.15	26.413	-28.5	3.364	12.72
	318.15				10.19
	328.15				3.17
Fluor.	308.15	17.048	-21.300	3.641	11.81
	323.15				4.93
	343.15				4.25
Hydroq.	333	5.323	-12.918	2.387	4.21
	348				4.94
	363				7.42
Anthrac.	303.15	15.661	-23.54	3.88	19.06
	323.15				6.71
	343.15				7.76
Chol.	308.15	24.979	-34.081	5.326	111.01
	313.15				41.41
	333.15				13.34
Chol.	313.15	14.236	-21.932	4.672	19.46
	333.15				14.66

Table 6.10: Eq. (6.8) modeling results

Comp.	T/K	E_0	e_1	α	β	γ	AVERR %
Naph.	308.15	5.152	-0.628	1.18E+02	-2.36E+02	1.12E+02	9.50
	318.15						5.44
	328.15						3.76
Fluor.	308.15	6.365	-0.971	23.48	-49.409	18.716	7.29
	323.15						5.39
	343.15						2.97
Hydroq.	333	3.274	-0.353	15.224	-49.596	23.647	5.61
	348						6.84
	363						8.6
Anthrac.	303.15	6.795	-1.007	19.362	-46.161	16.027	10.3
	323.15						6.94
	343.15						7.69
Chol.	308.15	-0.214	2.856	-9.76E+02	2.08E+03	-1.11E+03	6.16
	313.15						13.51
	333.15						6.33
Chol.	313.15	-0.223	2.86	12.668	-24.524	2.357	13.51
	333.15						6.33

Table 6.11: Eq. (6.9) modeling results

Comp.	T/K	E_0	e_1	e_2	α	β	γ	AVERR %
Naph.	308.15	2.538	2.595	-0.974	1.18E+02	-2.36E+02	1.13E+02	9.03
	318.15							5.59
	328.15							2.63
Fluor.	308.15	2.128	3.495	-1.215	25.517	-53.834	21.228	7.97
	323.15							4.12
	343.15							1.93
Hydroq.	333	0.668	3.306	-1.222	19.937	-60.740	30.166	4.30
	348							5.61
	363							4.13
Anthrac.	303.15	6.28	-0.507	-0.129	19.587	-46.623	16.287	10.41
	323.15							6.95
	343.15							7.57
Chol.	308.15	-0.784	3.604	-0.232	-9.74E+02	2.07E+03	-1.11E+03	6.11
	313.15							13.56
	333.15							6.4
Chol.	313.15	-0.739	3.542	-0.212	12.618	-24.525	2.400	13.55
	333.15							6.4

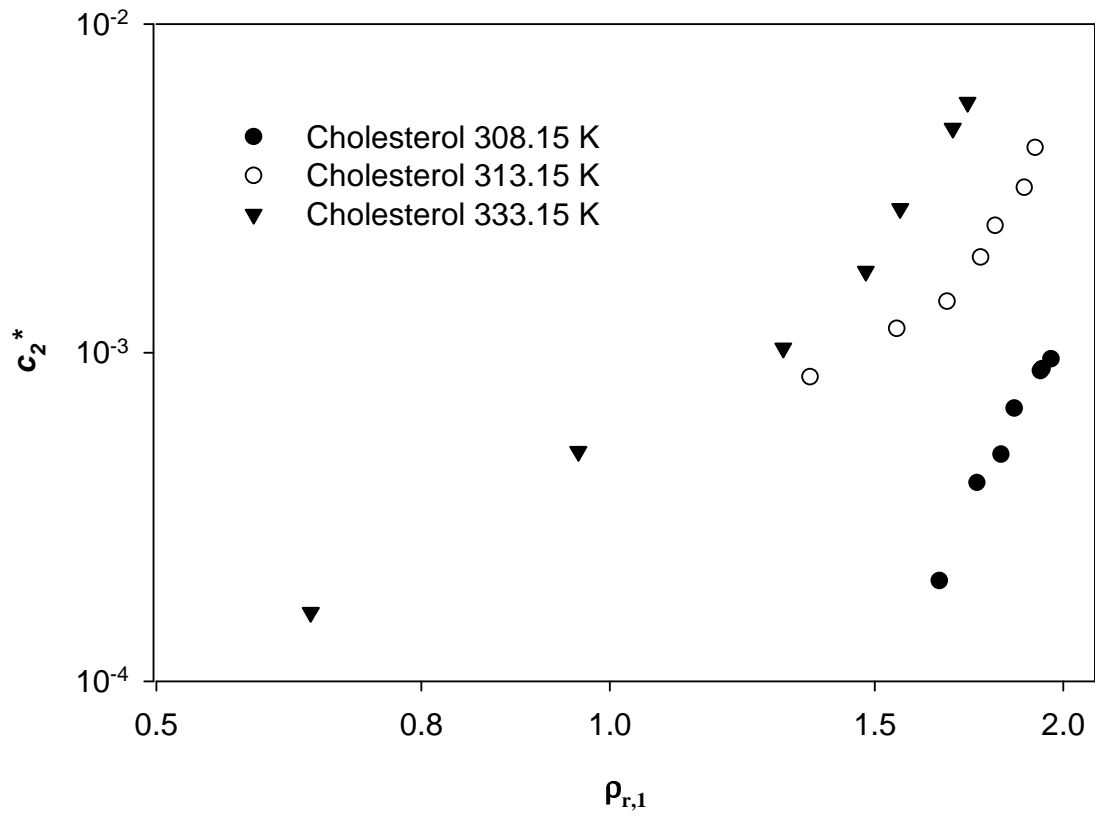


Figure 6.1: Plot of cholesterol solubility in SC-CO₂ at pressures between 10.09 MPa and 27.89 MPa

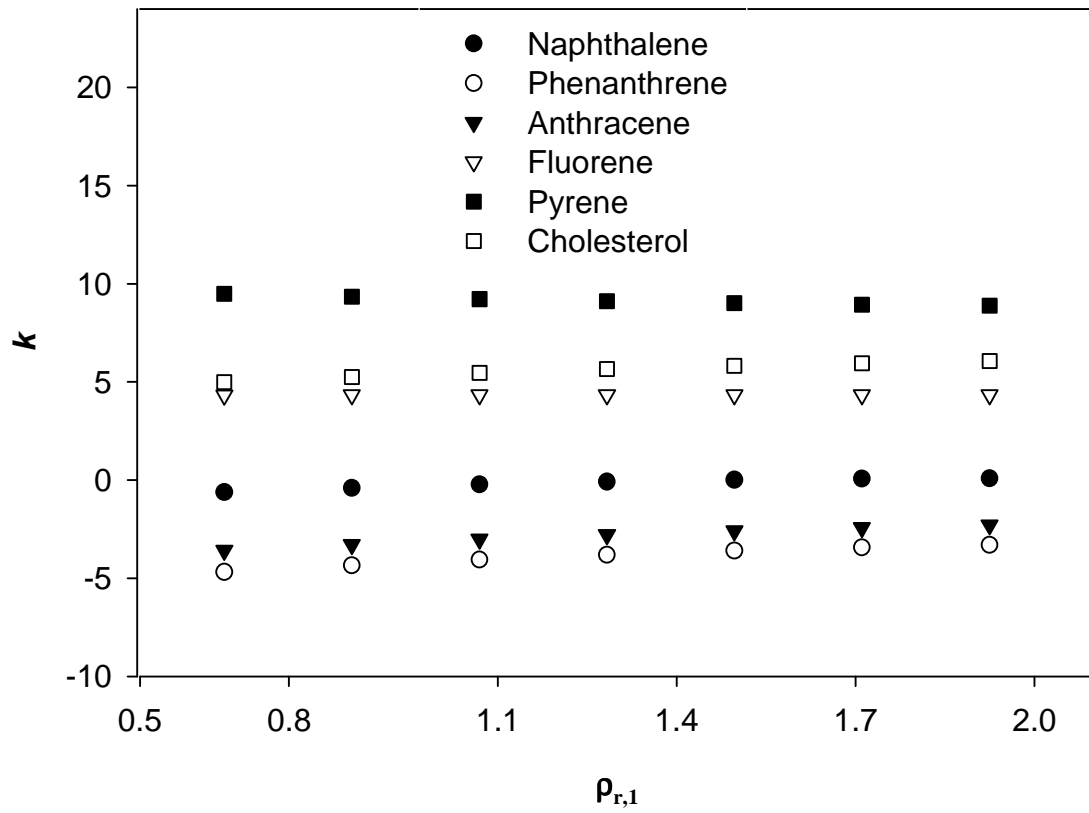


Figure 6.2: Variation of the association constant k with density

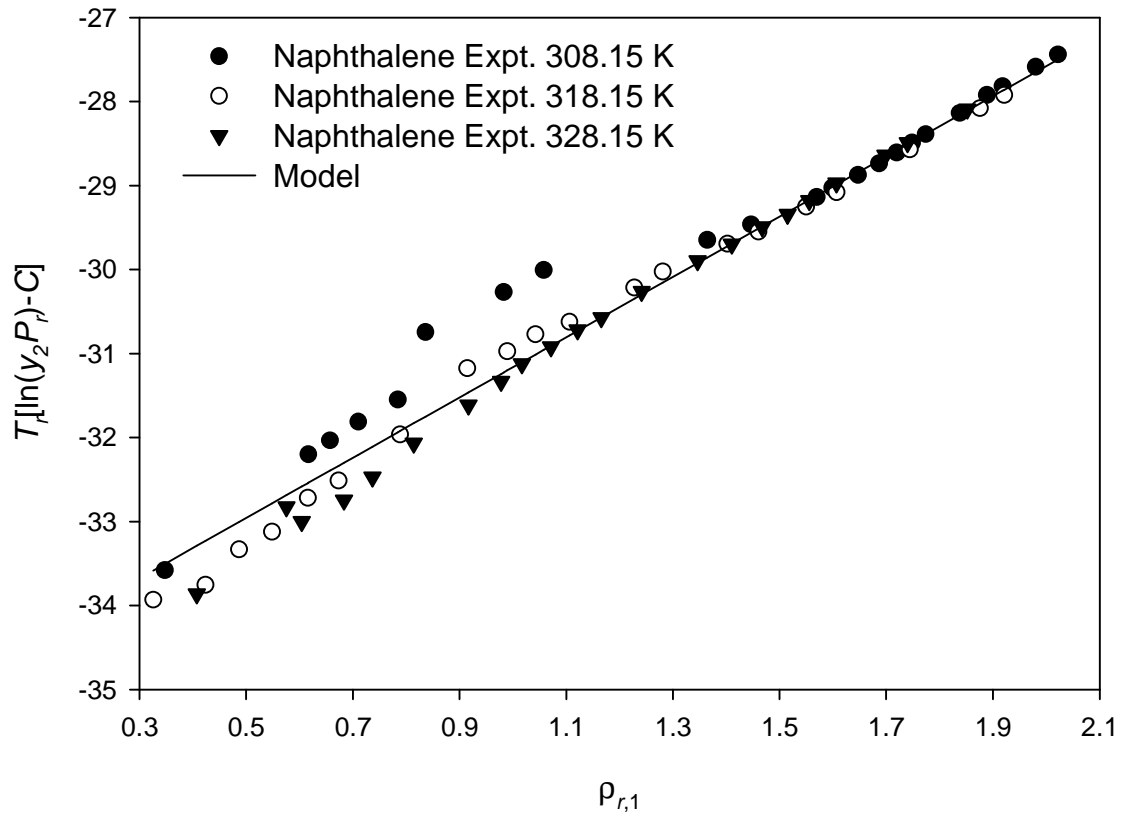


Figure 6.3: Experimental naphthalene solubility and values estimated by Eq. (5.19) for pressures between 6.08 MPa and 33.44 MPa

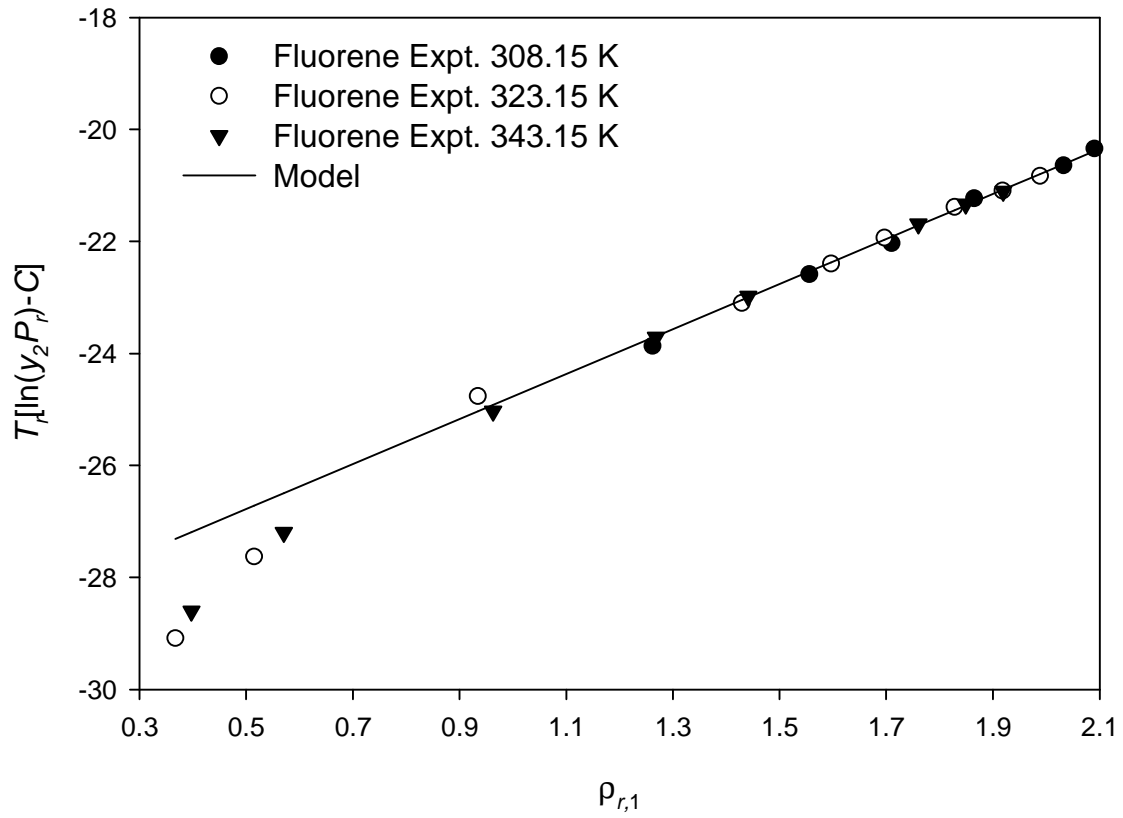


Figure 6.4: Experimental fluorene solubility and values estimated by Eq. (5.19) for pressures between 6.99 MPa and 48.34 MPa

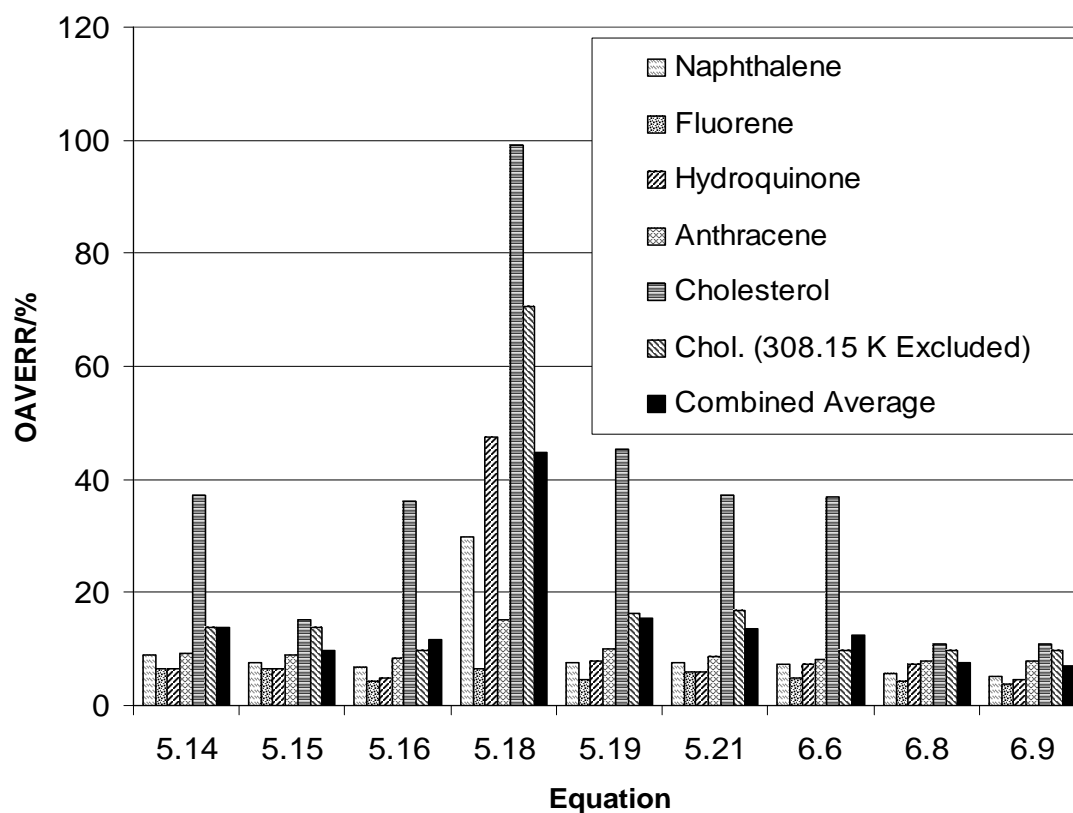


Figure 6.5: Overall average error of models studied

CHAPTER VII
SOLUBILITY OF AZELAIC ACID IN SUPERCRITICAL CARBON DIOXIDE

[Sparks et al., 2007c]

Introduction

Azelaic acid is one of the major oxidation products of oleic acid and can be used to formulate a wide variety of products, such as polyurethanes and polyamides [Hill, 2000]. Azelaic acid is also used in medicine for the topical treatment of skin conditions such as *acne rosacea*, a chronic acneiform disorder affecting the skin [Macasai, 1996]. Due to the versatility of diacids such as azelaic acid, new sources and production pathways are being pursued [Kroha, 2004]. In this research, the alternate production pathway of azelaic acid was oxidation of oleic acid in supercritical carbon dioxide. A key thermophysical variable to know is the solubility of the reactants and reaction products in the supercritical medium. In this study, the solubility of azelaic acid in supercritical carbon dioxide was determined at 313.15 K and 333.15 K over a pressure range of 10 MPa to 30 MPa. Azelaic acid is a solid at these temperatures and pressures.

Experimental Methods

Materials

Azelaic acid ($\text{HOOC}(\text{CH}_2)_7\text{COOH}$, CAS No. 123-99-9) was supplied by Sigma-Aldrich (minimum 99.0 % purity), and methanol (HPLC grade) was obtained from Fisher

Scientific. NexAir (Memphis, TN) provided carbon dioxide (99.5 % purity) and nitrogen (ultrahigh purity). The carbon dioxide (CO₂) was further purified by passing it through a 2 μm filter (Valco Instrument Company, Inc., Houston, TX). All other chemicals were used without further purification.

Procedure

A dynamic technique was used to determine azelaic acid solubility in supercritical carbon dioxide (SC-CO₂). Under the dynamic technique, the assumption is made that the solute-solvent system reaches equilibrium as the solvent passes over the solute [Maxwell, 1996]. Figure 4.4 provides a schematic of the supercritical-fluid extractor, manufactured by Thar Technologies (model SFE-100, Pittsburgh, PA), used for the solubility experiments. The system is equipped with a Coriolis mass-flow meter, dual-piston pump, backpressure regulator, and cyclone separator. A complete description of the experimental apparatus is provided in Chapter IV.

A portion of ≈ 5 g of azelaic acid was suspended in a stainless steel equilibrium vessel (volume of 100 mL) using layers of glass wool (Fisher Scientific) and 2 mm diameter borosilicate glass beads (Chemglass, Vineland, NJ). The packing helps minimize channeling of the supercritical fluid and prevents entrainment of the solute [Maxwell, 1996; Lee, 1994]. The equilibrium vessel, equipped with a heating jacket, was allowed to reach the desired operating temperature (± 1 K) of the experiment. Before entering the equilibrium vessel, the CO₂ passed through a heat exchanger, which raised the temperature of the solvent to the necessary value. By the time the CO₂ reached the

equilibrium cell, it was in a supercritical state (SC-CO₂). The system was maintained at the desired pressure (± 0.2 MPa) via the backpressure regulator.

Azelaic acid solubility was determined at 313.15 K and 333.15 K and at pressures ranging from 10 MPa to 30 MPa; experiments were performed in triplicates. For each experiment, a total of 0.6 kg of SC-CO₂ was allowed to flow through the equilibrium cell. The mass of liquefied carbon dioxide used was measured with a Coriolis mass flow meter, and a dual-piston pump propelled the CO₂ at a flow rate of 25 g·min⁻¹ (0.42 g·s⁻¹). To ensure that equilibrium had been achieved, preliminary solubility experiments were performed at several flow rates ranging from 0.33 g·s⁻¹ to 0.50 g·s⁻¹ at constant pressure. The solubilities determined from these experiments were independent of flow rate. Once the solute/solvent mixture exited the equilibrium cell, it flowed to the cyclone separator where the pressure was reduced; hence, the CO₂ became a gas and separated from the azelaic acid. Because azelaic acid is readily soluble in alcohols, a methanol wash of 25 mL was used to dissolve the azelaic acid in the cyclone separator [Azelaic Acid, 1996]. The azelaic acid/methanol mixture was collected in a tared 40 mL amber glass vial, and then the methanol was removed using a TurboVap model LV (Caliper Life Sciences, Hopkinton, MA), which evaporated the solvent using a stream of nitrogen. Once the methanol was removed, the vial was weighed with a balance (Mettler Toledo Model AB265-S/FACT, Columbus, OH) to determine the mass (± 0.01 mg) of azelaic acid collected from the experiment. Between experiments, the equilibrium vessel was taken offline, and SC-CO₂ was used to clean the tubing of the experimental apparatus.

Results and Discussion

The solubility results of azelaic acid in SC-CO₂ are summarized in Table 7.1. The density of CO₂ was obtained from the NIST fluid property database [NIST, 2007]. In general, as pressure was elevated at constant temperature, the solubility of azelaic acid in SC-CO₂ increased. At lower pressures, the solubility at 333.15 K is lower than the solubility at 313.15 K. However, the crossover pressure occurs between 16.7 MPa and 20.0 MPa, and from that point forward, solubility was higher at 333.15 K than at 313.15 K. This indicated that the vapor pressure of azelaic acid began to have a dominant effect on solubility. Modeling is often used to correlate solubility data. Two approaches are generally found in the literature: the so-called semi-empirical methods, many of which derived from the one originally proposed by Chrastil (1982) and the equation-of-state methods.

Semi-empirical Methods

As discussed in Chapter V, Chrastil developed a theory based on the law of mass action applied to the formation of a solvate complex between a solute molecule and a number of solvent (SCF) molecules [Chrastil, 1982]. This theory leads to the following equation for the solubility of component 2 (solid or liquid) in component 1 (SCF):

$$c_2 = \rho_1^k \exp\left(\alpha + \frac{\beta}{T}\right) \quad (7.1)$$

so that a log-log graph of c_2 versus ρ_1 for isothermal data should give a straight line. In Eq. (7.1), c is the concentration of solute in the supercritical fluid, ρ is the density of the supercritical fluid, k is an association number, α is a function of the molecular weights of

the solute and supercritical fluid, β is a function of the heat of solvation and heat of vaporization, and T is temperature. Later, this equation was slightly modified to include a more accurate effect of temperature [del Valle and Aguilera, 1988].

$$c_2 = \rho_1^k \exp\left(\alpha + \frac{\beta}{T} + \frac{\gamma}{T^2}\right) \quad (7.2)$$

where the γ term offsets variation of the heat of vaporization with temperature and the other variables are the same as previously defined for Eq. (7.1).

As shown in Figure 7.1, a log-log graph of c_2 versus ρ_1 for isothermal data does show a linear relationship. This plot clearly shows that concentration of azelaic acid in the SC-CO₂ increases with increasing density. The values for k , α , and β in Eq. (7.1) were determined to be 3.86, -16.27, and -4439.06, respectively, via multi-linear regression using Polymath 5.1 (Polymath Software; Willimantic, CT). For the regression analysis, c and ρ were both expressed in kg·m⁻³, and T was expressed in K. Also, Figure 7.1 illustrates that the concentration of azelaic acid is generally higher at 333.15 K than at 313.15 K. The error bars therein correspond to one standard deviation calculated based on the three measurements done at the corresponding temperature and pressure (as mentioned before, each solubility measurement was done in triplicate).

In the above methods, no properties of the solute are required. Other methods have been proposed later by Méndez-Santiago and Teja (1999) that require the sublimation pressure of the solid, which is not always available. They proposed to plot the so-called enhancement factor as a function of the density of the solvent in the following form

$$T \ln E = T \ln \frac{y_2 P}{P_2^{sub}} = A + B \rho_1 \quad (7.3)$$

where T is absolute temperature, E is the enhancement factor, y is the solute mole fraction, P is total pressure, P_2^{sub} is the sublimation pressure of the solute, ρ is the density of the supercritical fluid, and A and B are regressed constants. This should give a straight line. The enhancement factor represents the ratio of the actual solubility to the ideal solubility, i.e., that calculated according to the ideal-gas law (P_2^{sub} / P). The main advantage of this model is that solubility data at different temperatures can be represented by a single straight line.

They also proposed a modified version of the method for cases in which the sublimation pressure was unknown. This is obtained by substituting a two-constant Antoine equation for P_2^{sub} into equation (7.3):

$$T \ln y_2 P = A' + B' \rho_1 + C' T \quad (7.4)$$

where A' , B' , and C' are regressed constants. All other variables in Eq. (7.4) are the same as defined in Eq. (7.3).

A two-step procedure is needed in this case. First, constants A' , B' , and C' should be determined for a given data set by a regression method; then, a plot of $T (\ln y_2 P - C')$ versus ρ_1 is prepared and should give a straight line. This method (original or modified version) provides an excellent tool to test consistency of data taken at different temperatures. For this study, Eq. (7.4) was used to model the results. The values for A' , B' , and C' were determined to be -8746.98 K, $2.52 \text{ K} \cdot \text{m}^3 \cdot \text{kg}^{-1}$, and 11.54, respectively, via multi-linear regression using Polymath 5.1 (Polymath Software; Willimantic, CT). For

the regression analysis, P , ρ , and T were expressed in MPa, $\text{kg}\cdot\text{m}^{-3}$, and K, respectively. Figure 7.2 shows that the data points for both isotherms follow a single trend, indicating good consistency of the data over the range of temperatures tested. A variant of the Méndez-Teja approach using reduced variables is presented by Sparks et al. [2007a]. The main advantage of this variant is that the model parameters have no units.

Equation-of-State (EoS) Methods

In this approach, the solubility is obtained from the following phase-equilibrium equation:

$$y_2 = \frac{P_2^{sub}}{\hat{\phi}_2 P} \exp\left(\frac{V_2^{sol} P}{RT}\right) \quad (7.5)$$

where the variables in the pre-exponential factor are sublimation pressure of the solid, fugacity coefficient of the solid in the supercritical fluid phase, and total pressure, while those in the exponential argument are molar volume of the solid, universal gas constant, and absolute temperature. This equation comes from an exact thermodynamic equation and is subjected to two standard and fully justified assumptions, both stemming from the fact that sublimation pressures are usually extremely low: (a) $P \gg P_2^{sub}$, and (b) at T and P_2^{sub} , $f_2^{sub} \approx P_2^{sub}$. All variables in Eq. (5), except $\hat{\phi}_2$, can be readily obtained. Obtaining $\hat{\phi}_2$, however, entails some complexity. Cubic equations of state are normally used to this end, although other types have been used by some authors as recently reviewed in the literature [Valderrama. 2003]. Some of the difficulties of EoS in general and cubic EoS in particular are: (a) $\hat{\phi}_2$ is a function of y_2 , and thus iteration is required; (b) the critical

point of most pure solids of interest is unreachable and, thus, their critical properties are virtual variables (usually they are estimated by group contribution methods); (c) the sublimation pressure of solid solutes normally encountered in supercritical extraction processes is hard to measure and thus has to be also estimated; and (d) the choice of the proper EoS and mixing rules is not trivial given the myriad of choices available nowadays. Item (a) above is rather minor given the increased capacity of computers and computer software; the others remain to be a challenge. In this work, the Peng-Robinson EoS and van der Waals mixing rules, with one binary interaction parameter (in the combination rule for parameter a), have been chosen for modeling purposes. The best interaction parameter was found by minimizing an objective function (Eq. 6.3) as defined by Caballero et al. (1992) and they were 0.132 at 313.15 K and 0.165 at 333.15 K. Physical properties of carbon dioxide and azelaic acid used for the EoS calculations are available in Appendix C. These properties include critical temperature (T_c), critical pressure (P_c), acentric factor (ω), molecular weight (MW), sublimation pressure (P^{sub}), normal boiling point (T_B), and density (ρ). Figure 7.3 shows how the experimental solubility data compare to those predicted by the Peng-Robinson EoS. (Error bars shown are the same as in Figure 7.1.) The solubility data at 333.15 K fit the EoS model better than the 313.15 K data. This could be due to the increased variance of the data at 313.15 K. Figure 7.3 also illustrates that, in general, azelaic acid solubility increased as pressure was increased.

Conclusions

The solubility of azelaic acid in supercritical carbon dioxide has been determined experimentally. To the author's knowledge, this is the first set of reported data for this system. The solubility varied from an azelaic acid mole fraction of $0.42 \cdot 10^{-6}$ at 333.15 K and 10.0 MPa to $10.12 \cdot 10^{-6}$ at 313.15 K and 26.7 MPa. Due to the low solubility of azelaic acid in SC-CO₂, determining the extracted amount of azelaic acid gravimetrically resulted in large variations in the data (especially the 313.15 K data set). In general, the solubility of azelaic acid increased with increasing temperature only after exceeding the crossover pressure that occurred between 17 MPa and 20 MPa. Both the semi-empirical methods and the equation of state approach to modeling the data provided good correlations.

Table 7.1: Solubility of azelaic acid in supercritical carbon dioxide^a

<i>T/K</i>	<i>P/MPa</i>	$\rho/\text{kg}\cdot\text{m}^{-3}$	average Solubility/ $10^6 y_2$
313.15	10.0	628.61	1.47 ± 0.09
	13.3	750.23	1.96 ± 0.94
	16.7	803.71	3.44 ± 1.21
	20.0	839.81	1.69 ± 0.61
	23.3	867.59	3.57 ± 2.46
	26.7	890.40	3.33 ± 2.66
	30.0	909.89	7.17 ± 4.19
333.15	10.0	289.95	0.42 ± 0.13
	13.3	525.73	1.72 ± 0.16
	16.7	657.00	2.80 ± 0.17
	20.0	723.68	3.92 ± 0.26
	23.3	768.62	4.84 ± 0.92
	26.7	802.74	10.12 ± 3.89
	30.0	829.71	8.37 ± 0.77

^a \pm uncertainties refer to one standard deviation (σ)

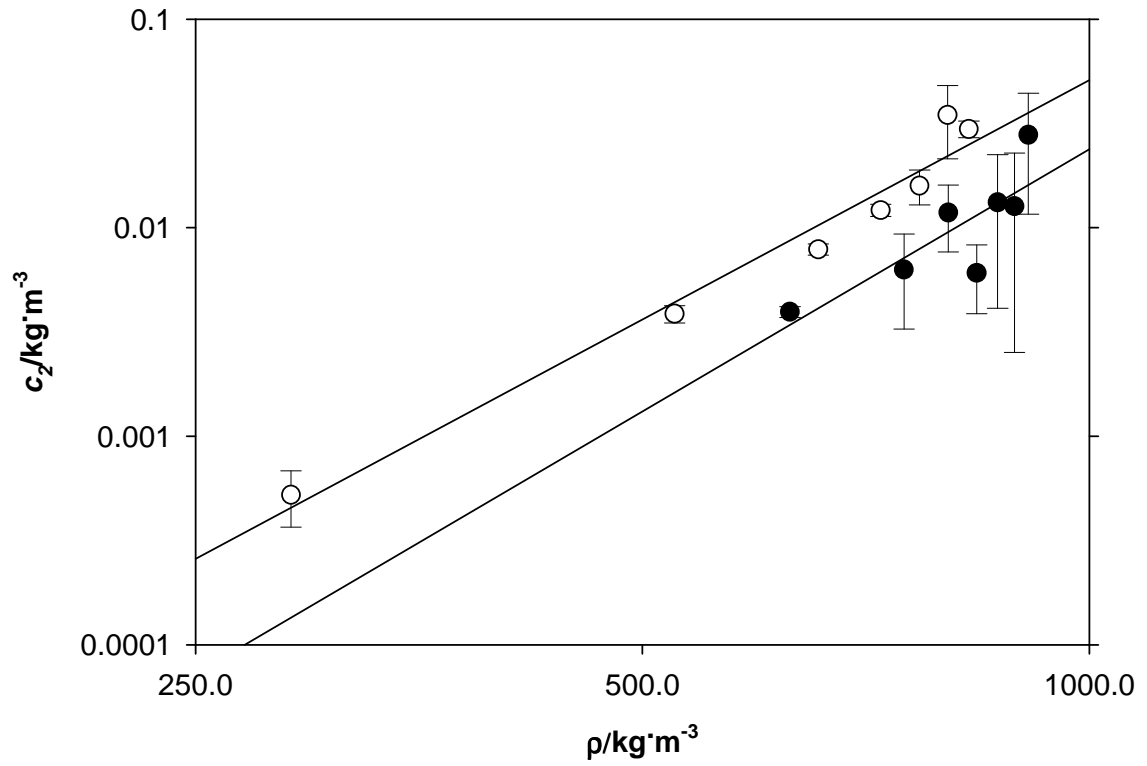


Figure 7.1: Chrastil plot of azelaic acid solubility in SC-CO₂: ●, 313.15 K; ○, 333.15 K; —, Chrastil Model Prediction

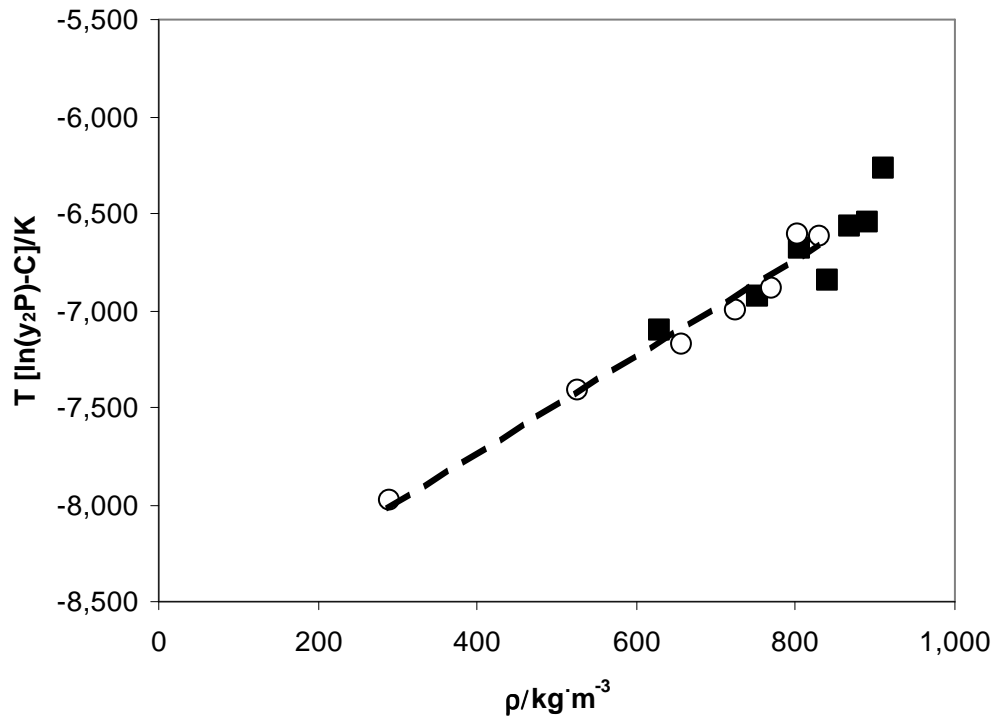


Figure 7.2: Méndez-Teja plot resulting from multi-linear regression of Eq. (7.4): ■, 313.15 K; ○, 333.15 K; - - -, Model Prediction

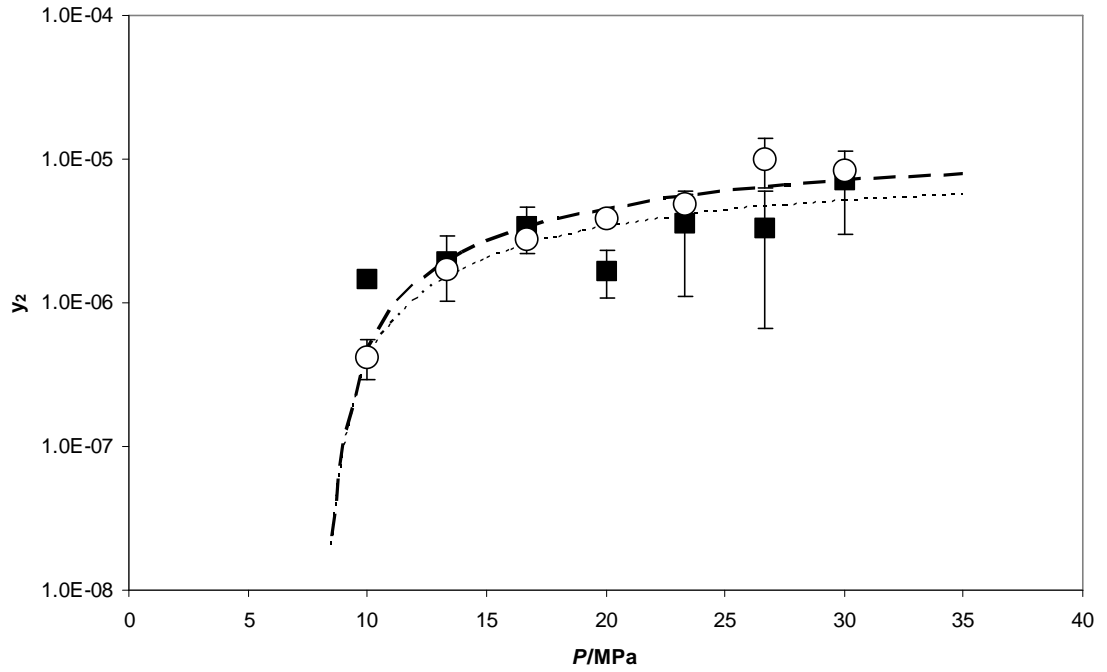


Figure 7.3: Experimental and EoS-predicted solubilities of azelaic acid in SC-CO₂: ■, 313.15 K; ○, 333.15 K; ---, 313.15 K EoS Prediction; —, 333.15 K EoS Prediction

CHAPTER VIII
SOLUBILITY OF NONANOIC (PELARGONIC) ACID IN SUPERCRITICAL
CARBON DIOXIDE [Sparks et al., 2007d]

Introduction

From an economic point of view, the goal of most chemical processes is to convert low-value materials into more valuable ones. Monounsaturated fatty acids, such as *cis*-13-docosenoic acid (erucic acid, CAS No. 112-86-7) and *cis*-9-octadecenoic acid (oleic acid, CAS No. 112-80-1) can be oxidized to form compounds ranging from epoxides, aldehydes, monoacids, and diacids. For example, oleic acid can be oxidized to produce an equimolar mixture of nonanoic acid (pelargonic acid, CAS No. 112-05-0) and nonanedioic acid (azelaic acid, CAS No. 123-99-9). Pelargonic acid forms esters with alcohols that can be used as plasticizers and lubricating oils. Azelaic acid can be used to formulate polymers and pharmaceutical products [Hill, 2000; Pelargonic Acid, 1996; Agrice, 1999; Macsai, et al., 1996]. Pelargonic acid is also used as a chemical intermediate for synthetic flavors, cosmetics, pharmaceuticals, and corrosion inhibitors [ChemicalLand21, 2007]. Additionally, it is used in modifying alkyd resins to prevent discolor and to keep flexibility and resistance to aging since saturated pelargonic acid will not be oxidized. C8 - C12 straight- and saturated-chain fatty acids such as pelargonic acid are capable of removing the waxy cuticle of broad-leaved, grassy weeds,

thus causing tissue death. Therefore, they are used as active ingredient of environment-friendly and fast-acting herbicides [ChemicalLand21, 2007].

Due to the increase in demand for dibasic acids, such as azelaic acid, more uses for the co-product pelargonic acid are being researched [Noureddini and Rempe, 1996]. A recent study has shown that pelargonic acid is an excellent solvent for extracting ethanol from water [Boudreau and Hill, 2006]. Due to the value of the oxidation products, there is a strong economic incentive to carry out this oxidation reaction industrially.

Oxidation via ozonolysis is the most well-known method of producing azelaic and pelargonic acids from oleic acid [Goebel et al, 1957]. This reaction takes place in the liquid phase; therefore, the ozone and the oxygen have to be transferred to the liquid phase. Typically, the limiting step in the process is the mass transfer of these reactants into the liquid. By having the reactants in a single phase, the mass-transfer limitations are removed, and this can be accomplished by carrying out the reaction in a supercritical-fluid medium, such as supercritical carbon dioxide [Brennecke, 1993]. Knowledge of the solubilities of the reactants and products in the supercritical fluid is crucial in determining reactor operating conditions and the feasibility of separating the products via supercritical fluid fractionation. In this study, the solubility of pelargonic acid in supercritical carbon dioxide was determined at 313.15 K and 333.15 K over a pressure range of 10 MPa to 30 MPa. Pelargonic acid is a liquid at these experimental conditions.

Experimental Methods

Materials

Pelargonic acid ($\text{CH}_3(\text{CH}_2)_7\text{COOH}$, minimum 96 % purity) and oleic acid ($\text{CH}_3(\text{CH}_2)_7(\text{CH})_2(\text{CH}_2)_7\text{COOH}$; \approx 99 % purity) were supplied by Sigma-Aldrich, and hexane (Optima grade) was purchased from Fisher Scientific. Nitrogen (ultra-high purity) and carbon dioxide (99.5 % purity) were obtained from NexAir (Memphis, TN). Carbon dioxide was provided as a liquid in cylinders equipped with a diptube and it was further purified by passing it through a 2 μm filter (Valco Instrument Company, Inc.; Houston, TX). Additional purification of all other chemicals was not carried out.

Procedure

Solubility of pelargonic acid, a liquid at room temperature, in supercritical carbon dioxide (SC-CO_2) was determined using a dynamic technique. The dynamic method is based on the assumption that the solute-solvent system reaches equilibrium as the solvent flows over the solute [Maxwell, 1996]. The solubility experiments used a supercritical-fluid extractor manufactured by Thar Technologies (Model SFE-100; Pittsburgh, PA). Chapter IV provides a complete description of the experimental apparatus, along with a diagram of the experimental setup (Figure 4.4). The system was equipped with a Coriolis mass-flow meter, dual-piston pump, backpressure regulator, and cyclone separator.

A quantity of \approx 10 g of pelargonic acid was placed in a stainless-steel equilibrium vessel (volume of 100 mL) packed with alternating layers of 2 mm diameter borosilicate glass beads (Chemglass; Vineland, NJ) and glass wool (Fisher Scientific). The packing was necessary to reduce channeling of the SC-CO_2 and prevent pelargonic acid

entrainment [Maxwell, 1996; Lee et al., 1994]. The temperature (± 1 K) of the equilibrium vessel was increased to the prescribed operating value using a heating jacket. CO₂ was pumped through a heat exchanger to raise its temperature prior to entering the equilibrium cell. Upon entering the equilibrium vessel, the CO₂ was in a supercritical state at the desired pressure (± 0.2 MPa), which was maintained by a backpressure regulator.

Pelargonic acid solubility experiments were performed in triplicates at 313.15 K and 333.15 K and at a pressure of 10 MPa to 30 MPa. Approximately 0.3 kg of SC-CO₂ was allowed to flow over the pelargonic acid in each experiment. A Coriolis mass-flow meter was used to quantify the mass (± 0.2 %) of liquid CO₂ used. The CO₂ was delivered by a dual-piston pump at a flow rate of 0.25 g·s⁻¹. To confirm that equilibrium had been reached, preliminary experiments were conducted at flow rates ranging from 0.167 g·s⁻¹ to 0.33 g·s⁻¹ at constant pressure. These preliminary experiments indicated that solubilities were not a function of SC-CO₂ flow rate. The solute-solvent mixture flowed from the equilibrium vessel to the cyclone separator through a valve and the backpressure regulator undergoing a continuous expansion. Consequently, the pressure was reduced resulting in a phase separation; the gaseous CO₂ exited the system while the pelargonic acid was deposited on the vessel walls. The cyclone separator was rinsed with 25 mL of hexane to dissolve the pelargonic acid. The pelargonic acid + hexane mixture was collected in a tared, 40 mL amber glass vial, and then the hexane was removed using a TurboVap Model LV (Caliper Life Sciences; Hopkinton, MA). This device evaporated the solvent (hexane) using a stream of nitrogen. The vials were then reweighed to measure the mass of pelargonic acid that had dissolved in the SC-CO₂. After each

extraction, the system was cleansed with an additional 0.3 kg of SC-CO₂. The balance used to tare and reweigh the vials was Mettler Toledo Model AB265-S/FACT (± 0.01 mg; Columbus, OH).

Results and Discussion

Solubility Results

The solubility results of pelargonic acid in SC-CO₂ are summarized in Table 8.1. The density of CO₂ was obtained from the NIST fluid property database [NIST, 2007]. In general, as pressure was increased at constant temperature, the solubility of pelargonic acid in SC-CO₂ increased. The results show that solubility at 333.15 K is greatly dependent upon pressure; in fact, an overall increase in solubility of over two orders of magnitude was observed. For the pressure range considered in this study, the solubility at 333.15 K is slightly lower than the solubility at 313.15 K. This means that all solubilities were measured at conditions where the density effects dominate over the temperature effects, i.e., below the crossover point. As detailed in Chapter VII, the solubility of azelaic acid in supercritical carbon dioxide has been determined for various pressures and temperatures. Since the pelargonic acid and azelaic acid solubility experiments were conducted at the same densities and temperatures, the separation factor of the two compounds can be determined. According to Chrastil (1982), the separation factor can be defined as follows:

$$\mu_{AB} = \frac{c_A}{c_B} \quad (8.1)$$

where μ_{AB} is the separation factor and c_A and c_B are the concentrations of the solutes. The

separation factor is based upon the assumption that the solute molecules behave independently of each other [Chrastil, 1982]. Taking pelargonic acid to be c_A and azelaic acid to be c_B , the separation factor ranges from approximately 267 (313.15 K, 10 MPa) to 4073 (333.15 K, 10 MPa). Based upon these values of the separation factor, supercritical fluid fractionation of pelargonic acid and azelaic acid appears feasible.

Modeling

The solubility data did not fit well to Chrastil's semi-empirical equation, which is based on the law of mass action applied to the formation of a complex between a molecule of solute and a number of solvent molecules [Chrastil, 1982]. A log-log plot of solubility versus density produced a slightly curved line rather than a straight line. The Chrastil equation for the solubility of component 2, c_2 (solid or liquid), in component 1 (SCF) is:

$$c_2 = \rho_1^k \exp\left(\alpha + \frac{\beta}{T}\right) \quad (8.2)$$

A modification of the Chrastil equation proposed by Adachi and Lu was used as basis in the modeling [Adachi and Lu, 1983]. The Adachi-Lu equation is:

$$c_2 = \rho_1^{(e_0 + e_1 \rho_1 + e_2 \rho_1^2)} \exp\left(\alpha + \frac{\beta}{T}\right) \quad (8.3)$$

In Eqs. (8.2) and (8.3), c_2 is the concentration of solute in the supercritical fluid, ρ_1 is the density of the supercritical fluid, α is a function of the association number and the molecular weights of the solute and supercritical fluid, β is a function of the enthalpy of solvation and enthalpy of vaporization, and T is temperature. The dimensionless

association number is the exponent of the density (referred to as k in the original Chrastil equation) and shows the dependence of the solubility on density. In the Adachi-Lu version of the model, k is a function of density. As seen in Eq. 8.3, they chose the following function:

$$k = e_0 + e_1\rho_1 + e_2\rho_1^2 \quad (8.4)$$

The approach used here is a modified Adachi-Lu method in two ways. First, both the Chrastil equation and its Adachi-Lu modification are dimensionally inconsistent, as per the argument that follows. Typical values of the association number k are between 4 and 10. Therefore, the units of the left-hand side (LHS) of either equation are, for example, $[\text{kg}\cdot\text{m}^{-3}]$, while the units of the right-hand side (RHS) are $[\text{kg}\cdot\text{m}^{-3}]$ raised to a power different from 1 (typically between 4 and 10). Therefore, the units of the LHS and those of the RHS do not match. To overcome this inconsistency, dimensionless variables have been introduced, as indicated below. The second modification has to do with the form of the function for k used by Adachi-Lu in Eq. (8.4). The Chrastil equation has been shown to work fine in many instances. If the fit is not as good as necessary or expected, then a first correction would be to assume that the association number varies linearly with density (rather than being a constant, as Chrastil assumed). Adachi and Lu decided to use a quadratic form for the association number, which might be necessary in extreme cases. Figure 8.1 shows how the association number varies with density for a number of systems analyzed by Adachi and Lu. Constants e_0 , e_1 , and e_2 are those reported by Adachi and Lu. Since pelargonic acid is a liquid, only liquid solutes (at

experimental conditions) have been included in Figure 8.1. It can be observed that a first-degree polynomial would be enough for these systems.

Based on the above analysis, the model chosen to fit the pelargonic solubility data is as follows:

$$c_2^* = \rho_{r,1}^{(e_o + e_1 \rho_{r,1})} \exp\left(\alpha + \frac{\beta}{T_r}\right) \quad (8.5)$$

where:

$$c_2^* = \frac{c_2}{\rho_{c,1}}; \quad \rho_{r,1} = \frac{\rho_1}{\rho_{c,1}}; \quad T_r = \frac{T}{T_{c,1}} \quad (8.6)$$

For calculation purposes, the critical density of carbon dioxide was $467.6 \text{ kg}\cdot\text{m}^{-3}$ and its critical temperature was 304.2 K [NIST, 2007]. The values for model parameters were regressed via Excel (Microsoft; Redmond, WA) by minimizing an objective function based on the relative deviation between the experimental solubility and the predicted solubility and are presented in Table 8.2 along with the objective function (OF) value. The objective function can be expressed as follows:

$$OF = \sum_{i=1}^{N_p} \left[\frac{c_{i,2} - c_{i,calc}}{c_{i,2}} \right]^2 = \sum_{i=1}^{N_p} \left[\frac{c_{i,2}^* - c_{i,calc}^*}{c_{i,2}^*} \right]^2 \quad (8.7)$$

where N_p is the total number of experimental points, $c_{i,2}$ is the experimental solute concentration at the i^{th} experimental point, $c_{i,calc}$ is the predicted solute concentration at the i^{th} point, $c_{i,2}^*$ is the normalized experimental solute concentration at the i^{th} experimental point, and $c_{i,calc}^*$ is the normalized predicted solute concentration at the i^{th} point. Table 8.2 also provides the objective function values for the dimensionless forms

of the Adachi-Lu equation and Chrastil's equation. The dimensionless Adachi-Lu equation and Eq. (8.5) provide considerably better correlation than the dimensionless form of Chrastil's equation. The additional parameter of the dimensionless Adachi-Lu equation provides a slightly better correlation than that of Eq. (8.5); however, that slight difference does not justify the complexity of adding a parameter.

Figure 8.2 illustrates that the concentration of pelargonic acid generally increases as the density of SC-CO₂ increases. The error bars correspond to one standard deviation calculated based on the three measurements done at the corresponding temperature and pressure. As Figure 8.2 illustrates, the estimated solubilities calculated from Eq. (8.5) correlate quite well with the experimental data.

Apparatus Validation

Since no literature values for pelargonic acid solubility in SC-CO₂ could be found, it was imperative to ensure that the experimental technique was adequate. Therefore, oleic acid (also a liquid at room temperature) was used for validation purposes. Solubility data for oleic acid were generated and compared to literature values. A summary of literature and experimental solubility values for oleic acid in supercritical carbon dioxide is available in Appendix D. Experiments were performed at 323.15 K and at pressures of 10 MPa to 25 MPa. The procedure was identical to that used for the pelargonic acid experiments, including equilibrium determination and runs in triplicate. The oleic acid results are presented in Figure 8.3. A log-log graph of c_2^* versus $\rho_{r,1}$ for the oleic acid data shows a linear relationship for the data produced from this work and for the literature values [Nilsson et al., 1991; Maheshwari et al., 1992; Škerget et al.,

1995]. Since no standard deviations were provided in the work of Nilsson et al. or Škerget et al. (1995), standard deviations are only provided for the experimental values and the study by Maheshwari et al. (1992). For this work, the error bars correspond to one standard deviation calculated from experiments done in triplicate. The experimental results show good agreement with the literature values, especially with the data of Nilsson et al. (1991) and Maheshwari et al. (1992). In both studies, a flow-through technique was used. However, in the work by Škerget et al. (1995), a static method was employed.

Conclusions

The solubility of pelargonic acid in supercritical carbon dioxide has been determined experimentally. The solubility varied from a concentration of 0.14 ± 0.07 $\text{kg}\cdot\text{m}^{-3}$ at 333.15 K and 10.0 MPa to 25.39 ± 0.61 $\text{kg}\cdot\text{m}^{-3}$ at 313.15 K and 30.0 MPa. In general, the solubility of pelargonic acid increased with increasing pressure at constant temperature. Overall, the solubility was higher at 313.15 K than at 333.15 K. The solubility data were modeled with a semi-empirical equation intermediate to Chrastil's equation and the Adachi-Lu equation. To avoid dimensional inconsistency, the proposed model was expressed in terms of normalized concentration and reduced density and temperature. The model provided a better fit than Chrastil's equation and was comparable to the Adachi-Lu equation. Since this is believed to be the first reported data of pelargonic acid solubility in SC-CO₂, the validity of the experimental approach was verified with oleic acid with good results.

Table 8.1: Solubility of pelargonic acid in supercritical carbon dioxide^{a,b}

<i>T</i> /K	<i>P</i> /MPa	ρ /kg·m ⁻³	Average Solubility <i>c</i> ₂ /kg·m ⁻³	Average Solubility 10 ³ <i>y</i> ₂
313.15	10.0	628.61	16.09 ± 0.43	7.07 ± 0.19
	13.3	750.23	21.26 ± 0.68	7.82 ± 0.25
	16.7	803.71	21.84 ± 1.17	7.50 ± 0.4
	20.0	839.81	23.23 ± 1.09	7.63 ± 0.36
	23.3	867.59	24.01 ± 0.65	7.64 ± 0.21
	26.7	890.40	24.66 ± 0.99	7.64 ± 0.30
	30.0	909.89	25.39 ± 0.61	7.70 ± 0.18
333.15	10.0	289.95	0.14 ± 0.07	0.13 ± 0.07
	13.3	525.73	4.68 ± 0.72	2.47 ± 0.38
	16.7	657.00	16.05 ± 2.34	6.75 ± 0.98
	20.0	723.68	19.72 ± 0.68	7.52 ± 0.26
	23.3	768.62	21.3 ± 1.18	7.65 ± 0.42
	26.7	802.74	21.06 ± 1.02	7.24 ± 0.35
	30.0	829.71	21.3 ± 1.86	7.09 ± 0.61

^a average values for solute concentration (*c*₂) and mole fraction (*y*₂) taken from triplicate runs

^b ± uncertainties refer to one standard deviation (σ)

Table 8.2: Modeling results

Compound	Solubility Constants for Eq. (8.5)				Eq. (8.5) OF	Adachi-Lu OF	Chrastil OF
	e_0	e_1	α	β			
Pelargonic Acid	8.23	-2.71	-6.66	1.8	0.12	0.10	1.31

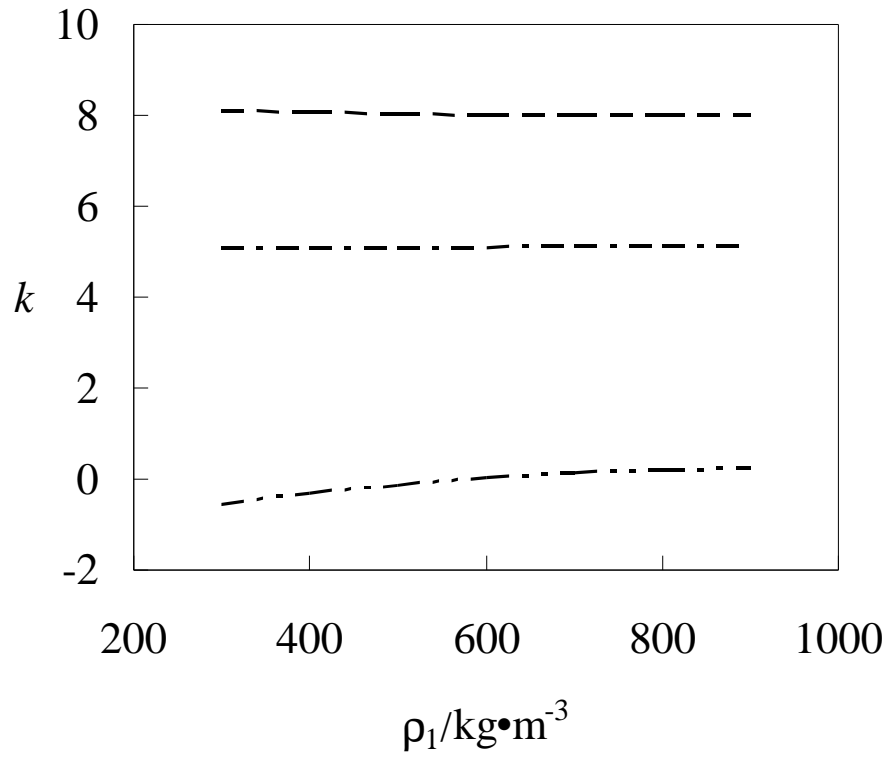


Figure 8.1: Dependence of k on density: - - -, oleic acid; - · - · -, triolein; - · · - · -, trilinolein

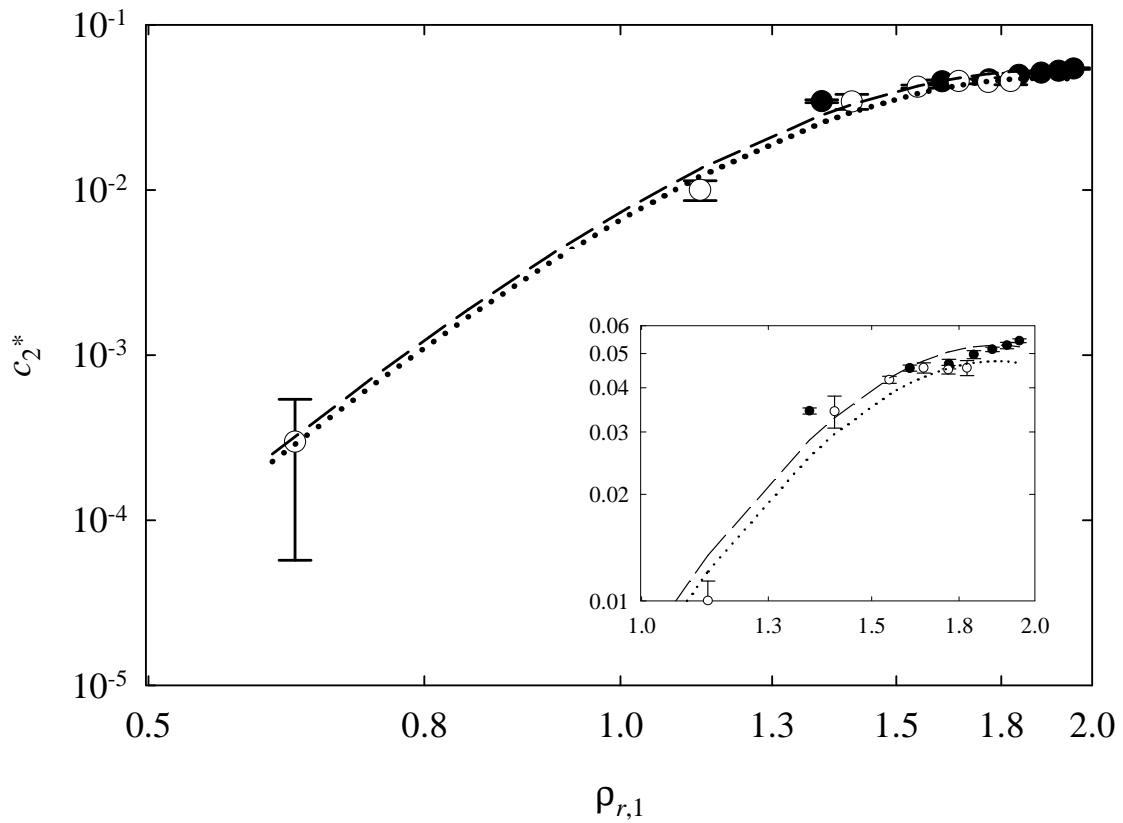


Figure 8.2: Plot of pelargonic acid solubility (c_2^*) in SC-CO₂ vs. solvent density ($\rho_{r,1}$):
 ●, 313.15 K; ○, 333.15 K; --, 313.15 K model prediction; •••, 333.15 K model prediction where the inset shows an enlarged view of top log cycle and the error bars correspond to uncertainties of one standard deviation (σ) taken from triplicate runs

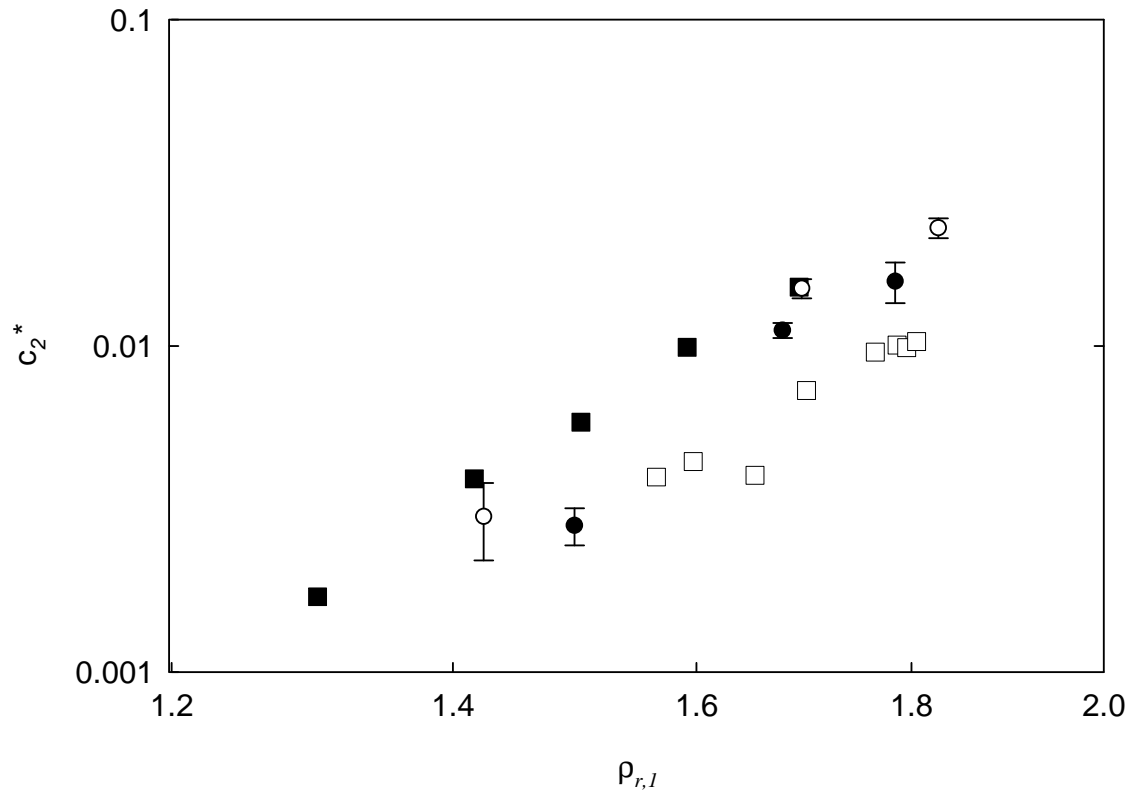


Figure 8.3: Plot of oleic acid solubility (c_2^*) in SC-CO₂ vs. solvent density ($\rho_{r,1}$) at 323.15 K: ■, Nilsson et al., 1991; ○, Maheshwari et al., 1992; ●, this work; □, Škerget et al., 1995 where the error bars correspond to uncertainties of one standard deviation (σ) taken from triplicate runs

CHAPTER IX
OXIDATION OF OLEIC ACID WITH OZONE

Introduction

One of the most common unsaturated fatty acids is oleic acid, and, as discussed in Chapter III, it can be oxidized with ozone to produce azelaic acid (a diacid) and pelargonic acid (a monoacid). Although ozonolysis of oleic acid is currently the most economical method to generate azelaic and pelargonic acid, the efficiency of the process could be improved in terms of both the oxidation reaction and product separation. Since oleic acid is a liquid and ozone is a gas, the oxidation occurs in multiphase reactors. To establish contact between the two reactants, countercurrent mixing is used. Since the reactants are in two separate phases, the ozone must diffuse into the liquid phase, which results in mass-transfer limitations. In terms of product separation, distillation is typically used to remove the pelargonic acid, and the remaining mixture is extracted with hot water. The azelaic acid is soluble in hot water, but as temperature is reduced, the solubility drops rapidly. Therefore, azelaic acid is removed from the aqueous extract via crystallization [Goebel et al., 1957; Kadesch, 1979]. Both crystallization and distillation can be energy-intensive, resulting in high operating costs.

By incorporating a supercritical fluid into the process, the ozonolysis of oleic acid could be made more efficient in terms of the oxidation itself and separation of reaction products. If the reactants can be solubilized into a single phase, then mass-transfer

limitations could be avoided. Gases such as oxygen and ozone are completely miscible with supercritical carbon dioxide [Brennecke, 1993]. Additionally, studies have shown that oleic acid has some degree of solubility in supercritical carbon dioxide [Zou et al., 1990; Foster et al., 1991; Nilsson et al., 1991; Maheshwari et al., 1992; Yu et al., 1992; Škerget et al., 1995]. Carbon dioxide is an ideal reaction medium for oxidation reactions because it is already oxidized; hence, it will not react with ozone to form oxidation products. As shown in Chapters VII and VIII, the solubilities of azelaic acid and pelargonic in supercritical carbon dioxide can differ by several orders of magnitude. Therefore, these products could be separated using a supercritical fractionation. Industrially, this would at least reduce the need for distillation and crystallization.

The objective of this study was to evaluate the impact of supercritical carbon dioxide on the ozonolysis of oleic acid. As discussed in Chapter III, incorporation of supercritical fluids into a reaction system has been shown to affect reaction rate, reaction products, and selectivity so these areas were particularly studied.

Experimental Methods

Materials

The following lipids were purchased from Sigma-Aldrich: oleic acid (*cis*-9-octadecenoic acid; CAS No. 112-80-1; $\text{CH}_3(\text{CH}_2)_7\text{CH}=\text{CH}(\text{CH}_2)_7\text{COOH}$; $\approx 99\%$ purity), pelargonic acid (nonanoic acid; CAS No. 112-05-0; $\text{CH}_3(\text{CH}_2)_7\text{COOH}$; minimum 96 % purity), methyl oleate (methyl *cis*-9-octadecenoate; CAS No. 112-62-9; $\text{CH}_3(\text{CH}_2)_7\text{CH}=\text{CH}(\text{CH}_2)_7\text{COOCH}_3$; $\geq 99\%$ purity), methyl pelargonate (methyl nonanoate; CAS No. 1731-84-6; $\text{CH}_3(\text{CH}_2)_7\text{COOCH}_3$; $\geq 99.8\%$ purity), azelaic acid

(nonanedioic acid; CAS No. 123-99-9; $\text{COOH}(\text{CH}_2)_7\text{COOH}$; $\geq 99\%$ purity), and dimethyl azelate (dimethyl nonanedioate; CAS No. 1732-10-1; $\text{CH}_3\text{OOC}(\text{CH}_2)_7\text{COOCH}_3$; 80 % purity). 1,3-Dichlorobenzene ($\geq 99.0\%$ purity) was also purchased from Sigma-Aldrich. Hexane (HPLC grade), toluene (Optima grade), methanol (HPLC grade), and sulfuric acid (technical grade) were purchased from Fisher Scientific. Ozone was generated via corona discharge with oxygen in a Model LC-1234 Ozone Generator from Ozonology, Inc. (Northbrook, IL). NexAir (Memphis, TN) provided carbon dioxide (99.5 % purity), which was further purified by passing it through a 2 μm filter (Valco Instrument Company, Inc., Houston, TX). All other chemicals were used without further purification.

Procedure

Traditional Oxidation

The goal of the traditional oxidation experiments was to provide benchmarks in terms of conversion, reaction rate, and products formed. For these experiments, reaction conditions were similar to those used for the industrial process. A quantity of 48 g of oleic acid was combined with 303 g of pelargonic acid in a 500 mL jacketed reaction vessel (Chemglass Model CG-1928-01; Vineland, NJ) equipped with Morton indentations, which provided better mixing. The contents of the reactor were then mixed using a magnetic stir bar and heated to 40°C using an Isotemp Model 145D Dry-Bath Incubator (Fisher Scientific) to circulate water through the reactor jacket. Then the reactor was capped with a lid (Chemglass Model CG-1944-01; Vineland, NJ) equipped with three 24/40 necks and one #7 Chem-Thread neck. Upon reaching 40°C, ozone was

sparged into the reactor from the ozone generator at a mass fraction of 5.06 % in oxygen (0.0417 SCFM or 1.18 SLM) using a bubble stone. The ozone was delivered to the reactor using tubing inserted through a 0.635 cm wide hole drilled through a 24/40 PTFE stopper. Only 0.635 cm OD (outer diameter) PTFE tubing was used throughout these experiments. Unreacted ozone left the reactor through a separate neck equipped with another drilled PTFE stopper and traveled to a Model HC Ozone Monitor (PCI Ozone & Control Systems, Inc.; West Caldwell, NJ). The ozone generator and monitor are discussed in detail in Chapter IV and are shown in Figure 4.1. Upon leaving the ozone monitor, the unreacted ozone was sent to a flask containing Carulite (manganese dioxide/copper oxide; Carus Chemical Company; Peru, IL), which served as a catalyst to decompose the oxidant. Ozone was supplied to the reactor for 2.5 hours. Then the stream of ozone in oxygen was turned off at the generator while the reaction mixture was heated to 80°C. Oxygen (no ozone) was then supplied to the reactor for an additional 3.5 hours for a total reaction time of 6 hours.

One of the 24/40 necks was outfitted with a sampling adapter equipped with a PTFE-silica-PTFE septum. Samples were collected using an 18-gauge needle (Popper Deflected Noncoring Septum Penetration Needle; Fisher Scientific) that was 30.5 cm in length connected to a 20 mL Luer-lock syringe (Perfektum Micro-Mate Interchangeable Syringe; Fisher Scientific). Temperature was monitored via a thermometer placed through the Chem-Thread neck. Figure 9.1 shows the 500 mL reactor system. In preliminary experiments, a rubber septum (as shown in Figure 9.1) was used for sampling. However, the ozone degraded the rubber, which led to sample contamination.

Therefore, the rubber septum was replaced with a sampling adapter equipped with a PTFE-silica-PTFE septum, which was resistant to oxidation.

Oxidation in Supercritical Carbon Dioxide

For the supercritical fluid experiments, 1 g of solid oleic acid was placed into a 250 mL stainless steel reaction vessel (Model R250; Thar Technologies; Pittsburgh, PA), and then the vessel was sealed with a Nitronic 60 stainless steel cap equipped with a magnetic stirrer. The reaction assembly is shown in Figure 9.2. For these experiments, a batch configuration was required. Therefore, ozone was fed into the reactor at a mass fraction of 5.06 % in oxygen until the pressure inside the reactor equaled the output pressure of the ozone generator, which was approximately 0.28 MPa. Then the reactor was heated while carbon dioxide was fed into the reactor using a dual-piston pump (Model P-50; Thar Technologies; Pittsburgh, PA) until the required pressure was reached. By the time the desired reaction temperature and pressure were attained, oleic acid (melting point of $\approx 13^{\circ}\text{C}$) was a liquid. Achieving the reaction temperature and pressure required approximately 20 minutes. Then stirring at 1000 RPM was initiated, and the reaction time was started. Reactions were conducted at pressures of 10 to 35 MPa and temperatures of 40 and 60°C for 12 hours. At the end of the reaction period, agitation was stopped and heating was turned off. Then the reactor was depressurized in a step-wise manner by sending the gas phase through a back-pressure regulator (Thar Technologies; Pittsburgh, PA) where the pressure was reduced. Then the stream went to a cyclone separator where the gas phase exited the system and passed through Carulite to destroy any unreacted ozone.

Analysis of Reaction Products

The methyl ester derivatives of samples were used for product analysis. Samples (up to 100 mg) were placed in toluene and converted to methyl ester derivatives via acid-catalyzed esterification with 2 % by weight sulfuric acid in methanol at 50°C overnight. At the end of the derivatization, the fatty acid methyl esters were extracted with hexane. This derivatization method was based upon the technique described by Christie (2003b). Then a solution of 1,3-dichlorobenzene was added as an internal standard prior to analysis with gas chromatography with flame ionization detection (GC-FID). Prior to sample analysis, the GC-FID (6890N; Agilent; Palo Alto, CA) was calibrated with external standards of methyl oleate, methyl pelargonate, and dimethyl azelate with 1,3-dichlorobenzene as an internal standard. Complete details of the sample preparation technique and a discussion of the GC method can be found in Chapter IV.

Results and Discussion

Oxidation of oleic acid using the traditional ozonolysis method resulted in complete conversion of oleic acid within 2 hours (120 minutes), which was before the end of the first phase of the reaction (2.5 hours). The second phase of the reaction was not needed because of the high concentration (5.06 % by weight ozone in oxygen) of ozone used in the first phase. In the industrial process, the initial ozone stream is only about 1.75 % ozone by weight in oxygen [Goebel et al., 1957]. Figure 9.3 shows a plot of how oleic acid concentration varied with time. The error bars correspond to standard deviations of duplicate measurements. It is apparent that oleic acid concentration was a

linear function of time. Hence, the reaction is zero-order and the linear function can be expressed as the following [Fogler, 1999]:

$$C_{OA} = C_{OA0} - kt \quad (9.1)$$

with

$$r_{OA} = -k \quad (9.2)$$

where C_{OA} is the concentration of oleic acid, C_{OA0} is the initial oleic acid concentration, t is time, k is the rate constant, and r_{OA} is the rate of reaction of oleic acid. Therefore, the slope of the line is $-k$. Based on Figure 9.3, the rate of the disappearance of oleic acid is $0.077 \text{ mol}\cdot\text{s}^{-1}\cdot\text{m}^{-3}$. The zero-order reaction indicated that the rate of oleic acid ozonolysis was independent of oleic acid concentration. Hence, the reaction mixture was probably mass-transfer limited despite mixing and sparging.

The only products detected with GC-FID were pelargonic acid and azelaic acid. Based upon GC analysis, the initial mass of the reaction system (oleic acid + pelargonic acid) was 351.4 g, and the final mass of the reaction system (pelargonic acid + azelaic acid) was 341.5 g. Therefore, 97.2 % of the initial mass was accounted for by GC analysis. The “missing” mass could be attributed to aldehydes that were formed as reaction intermediates between oleic acid consumption and formation of pelargonic acid and azelaic acid. Aldehydes such as pelargonaldehyde are known to be volatile, so they could have been carried out of the reaction mixture with the unreacted ozone + oxygen stream. Since only liquid phase products were analyzed in this study, any volatile components carried off by unreacted ozone + oxygen would not be detected by GC-FID. Control experiments in which azelaic acid and pelargonic acid were subjected to

ozonation for 12 hours at 40°C did not result in significant degradation of the target reaction products.

Unfortunately, no reaction of oleic acid with ozone was ever observed in the supercritical carbon dioxide. The main reason for this is likely the inability to get ozone into the reactor at a sufficient enough concentration for a measurable reaction to occur. Since the ozone was only 5.06 % by weight ozone in oxygen and could be delivered into the reactor at a maximum pressure of 0.28 MPa, the total amount of ozone available for reaction with oleic acid was miniscule, especially considering the fact that ozone is not stable and decomposes. Once the carbon dioxide was added to the reactor, the concentration of ozone was diluted even further.

Conclusions

The traditional method of oleic acid ozonolysis has been performed. Complete conversion of oleic acid was achieved in less than 2 hours. The two observed products were azelaic acid and pelargonic acid. Based upon a mass balance of the initial compounds versus the observed products, 97.2 % of mass was accounted for by pelargonic acid and azelaic acid. The remaining mass could be due to volatile aldehydes that were swept out of the reaction system by the exiting ozone + oxygen stream. The traditional ozonolysis reaction was zero-order with a reaction rate constant of 0.077 mol·s⁻¹·m⁻³. Based upon the apparent order of the reaction, the ozonolysis of oleic acid was mass-transfer limited. No reaction was observed for the ozonolysis of oleic acid in supercritical carbon dioxide. This could be due in part to the lack of sufficient ozone for reaction.



Figure 9.1: Reactor assembly for oleic acid ozonolysis at ambient pressure



Figure 9.2: Reactor assembly for oleic acid ozonolysis in supercritical carbon dioxide

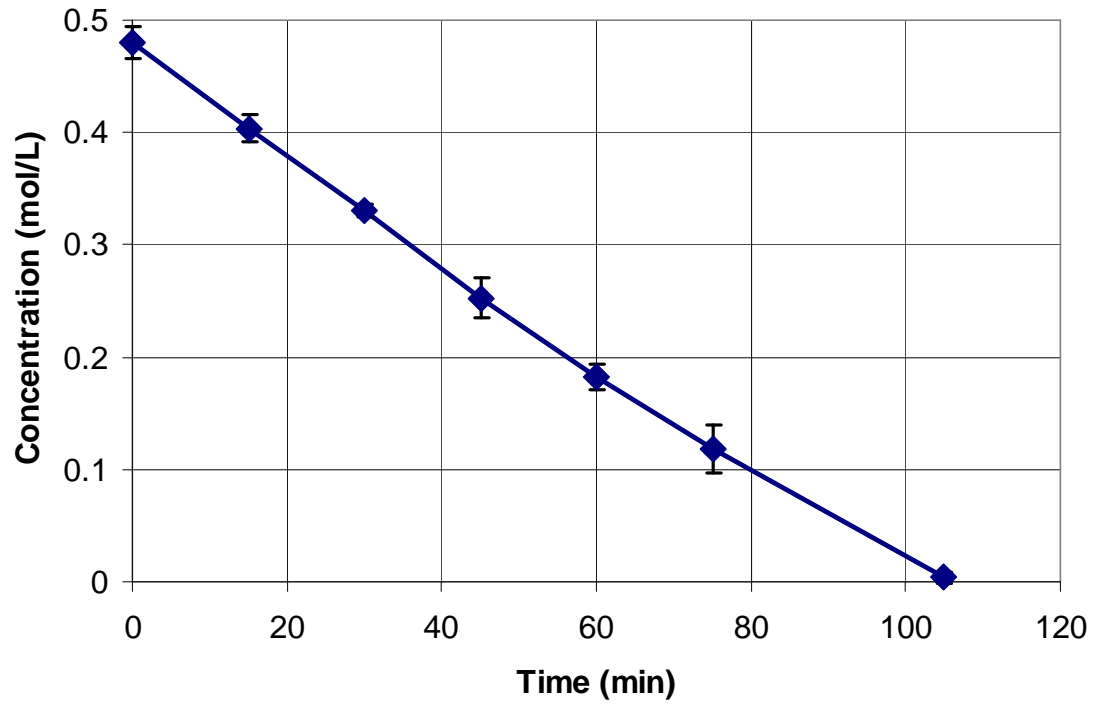


Figure 9.3: Change of oleic acid concentration over time at a temperature of 40°C and an ozone mass concentration of 5.06 % in oxygen (1.18 SLM)

CHAPTER X

OXIDATION OF OLEIC ACID WITH POTASSIUM PERMANGANATE

Introduction

The major industrial sources of azelaic acid and pelargonic acid are from the oxidation of oleic acid [Chemical Market Reporter, 2001]. Ozone has been used as the oxidizer for this process since the 1950s because it is a very powerful oxidizer that leads to good yields of azelaic and pelargonic acid and does not require any type of catalyst. Other oxidizers, particularly hydrogen peroxide and potassium permanganate, have been studied as alternatives to ozonation. However, these oxidizers have several disadvantages compared to ozone. First, they are not as potent of an oxidizer as ozone. In terms of oxidation potential, ozone has one of the highest at 2.07 volts while hydrogen peroxide and potassium permanganate have values of 1.77 and 1.67 volts, respectively [Mountain High Water, 2007]. Second, to obtain reasonable rates of reaction, studies have shown that the use of hydrogen peroxide [Noureddini and Kanabur, 1999; Santacesaria et al., 2003] requires a catalyst, and emulsifiers or phase-transfer catalysts are necessary for use with potassium permanganate [Foglia et al., 1977; Garti and Avni, 1981]. And good yields of azelaic acid and pelargonic acid can be achieved by the countercurrent mixing of oleic acid with ozone [Goebel et al, 1957].

As discussed in Chapter III, a recent study by Mercangöz et al. (2004) investigated the use of sub/supercritical carbon dioxide as reaction medium for the

oxidation of soybean oil with aqueous potassium permanganate. Soybean oil is primarily composed of unsaturated fatty acids, so the authors monitored consumption of the double bonds with time. In a control reaction between oleic acid and aqueous potassium permanganate at conditions of 25°C and atmospheric pressure for 12 hours, no measurable reaction occurred. However, they observed 29 % double bond consumption when using the supercritical fluid medium for a 12-hour batch reaction at 25°C and a pressure of 7 MPa. Mercangöz et al. only considered aqueous solutions of potassium permanganate; however, Sam and Simmons (1972) studied the oxidation of organic compounds with potassium permanganate without the use of water. Instead, a crown ether was used as a complexing agent to bring the solid potassium permanganate into an organic solvent (benzene) so that the oxidant could react with the compound of interest. Using this approach, reactions of olefins were found to occur very rapidly with complete conversion observed in many cases.

Based upon the work by Mercangöz et al. (2004) and Sam and Simmons (1972), the goal of this study was to evaluate the effect of oxidizing oleic acid with solid potassium permanganate in supercritical carbon dioxide. Since carbon dioxide is already oxidized, it is well suited for oxidation reactions because it is not altered by the permanganate ion. The effects of the supercritical fluid on oleic acid conversion and product yield were evaluated, along with a preliminary investigation into the solubility of potassium permanganate in supercritical carbon dioxide.

Experimental Methods

Materials

The following lipids were purchased from Sigma-Aldrich: oleic acid (*cis*-9-octadecenoic acid; CAS No. 112-80-1; $\text{CH}_3(\text{CH}_2)_7\text{CH}=\text{CH}(\text{CH}_2)_7\text{COOH}$; $\approx 99\%$ purity), pelargonic acid (nonanoic acid; CAS No. 112-05-0; $\text{CH}_3(\text{CH}_2)_7\text{COOH}$; minimum 96 % purity), azelaic acid (nonanedioic acid; CAS No. 123-99-9; $\text{COOH}(\text{CH}_2)_7\text{COOH}$; $\geq 99\%$ purity), and pelargonaldehyde (nonanal; CAS No. 124-19-6; $\text{CH}_3(\text{CH}_2)_7\text{CHO}$; $\geq 95\%$ purity). Potassium permanganate (CAS No. 7722-64-7; KMnO_4 ; 99+% purity) and 1,3-dichlorobenzene ($\geq 99.0\%$ purity) were also purchased from Sigma-Aldrich. Water (demineralized), hexane (Optima grade), toluene (Optima grade), methanol (Optima grade), and sulfuric acid (technical grade) were obtained from Fisher Scientific. Carbon dioxide (99.5 % purity) was purchased from NexAir (Memphis, TN) and was further purified by being passed through a 2 μm filter (Valco Instrument Company, Inc., Houston, TX). All other chemicals were used without further purification.

Procedure

Oxidation in the Absence of Supercritical Carbon Dioxide

For the experiments at ambient pressure, 8 g of potassium permanganate were placed into a 100 mL round bottom glass reactor (Chemglass Model CG 1514-01; Vineland, NJ), which was equipped with a thermometer to monitor temperature. The reactor was placed in an oil bath and heated to the desired temperature of the reaction. Then 1 mL (0.891 g) of oleic acid was added dropwise to the reactor over a period of 10

minutes using a pipette. Adding the oleic acid slowly to the potassium permanganate minimized the effect of the exothermic reaction on the bulk temperature. After addition of the oleic acid, magnetic stirring was initiated and the reaction time was started. The reactor was capped with a solid PTFE stopper to minimize oxidation of the oleic acid with atmospheric oxygen. Experiments were conducted for 12 hours at 308.15 K (35°C) and 318.15 K (45°C).

At the end of the reaction time, the reactor was removed from the oil bath, and a solution of 2 % by weight sulfuric acid in methanol was added to the reaction mixture in five 10-mL portions, and this served to quench the reaction. The methanol reacted with potassium permanganate to form manganese dioxide. Due to the large excess of methanol compared to potassium permanganate, the volume of methanol consumed in the quenching reaction was negligible. A 1-mL aliquot was filtered over a Whatman Type GF/B Filter (Fisher Scientific) with 3 mL of 2 % by weight sulfuric acid in methanol to remove the manganese dioxide. The filtrate was collected in a 20 mL test tube. Then an additional 2 mL of the sulfuric acid in methanol solution was added to the test tube along with 1mL of toluene, and the vial was incubated overnight at 50°C to convert the products to methyl esters for analysis. This derivatization method was based upon the technique described by Christie (2003b) and is discussed in greater detail in Chapter IV.

Oxidation in Supercritical Carbon Dioxide

For the supercritical fluid experiments, 8 g of potassium permanganate were placed into a 250 mL stainless steel reaction vessel (Model R250; Thar Technologies; Pittsburgh, PA), and then the vessel was sealed with a Nitronic 60 stainless steel cap

equipped with a magnetic stirrer. The reactor was heated while carbon dioxide was fed into the reactor using a dual-piston pump (Model P-50; Thar Technologies; Pittsburgh, PA) until the required pressure was reached. Then 1 mL (0.891 g) of oleic acid was added to the reactor over a period of 10 minutes using a syringe pump (Teledyne Isco Model 100DX; Lincoln, NE). Based upon data from the literature [Zou et al., 1990; Foster et al., 1991; Nilsson et al., 1991; Maheshwari et al., 1992; Yu et al., 1992; Škerget et al., 1995], the oleic acid was completely soluble in the supercritical carbon dioxide. After adding the oleic acid, stirring at 1000 RPM was initiated, and the reaction time was started. A schematic of the experimental apparatus can be seen in Figure 4.6. Reactions were conducted at a pressure of 12.2 MPa and at temperatures of 308.15 K and 318.15 K for times ranging from 10 to 720 minutes.

At the end of the reaction period, agitation was stopped and heating was turned off. Then the reactor was depressurized by allowing the gas phase to exit through the pressure release valve shown in Figure 4.6. An Erlenmeyer flask topped with glass wool trapped products entrained in the gas phase. Then a 2 % by weight sulfuric acid in methanol solution was added to the contents of the Erlenmeyer flask and the stainless steel reactor in five 10-mL portions. Then 1-mL aliquots from the flask and the reactor were prepared for analysis as previously described.

Analysis of Reaction Products

At the end of the derivatization period, the oxidation products were extracted with hexane. Then a solution of 1,3-dichlorobenzene was added as an internal standard prior to analysis with a Varian 3600 gas chromatograph (GC) coupled to a Saturn 2000 mass

spectrometer (MS) detector (Varian; Palo Alto, CA). Prior to sample analysis, the GC-MS was calibrated in electron impact (EI) mode for methyl oleate, methyl pelargonate, and dimethyl azelate with 1,3-dichlorobenzene as an internal standard. The external standards were generated from fatty acid standards using the acid-catalyzed esterification technique previously mentioned. Chemical ionization (CI) mode with isobutane was used to determine molecular weight of unidentified species. A discussion of GC-MS operating principles along with a complete description of the EI and CI methods can be found in Chapter IV.

Solubility of Potassium Permanganate in Supercritical Carbon Dioxide

Solubility of solid potassium permanganate in supercritical carbon dioxide (SC-CO₂) was determined using the same dynamic technique as used in Chapters VII and VIII. The solubility experiments used a supercritical-fluid extractor manufactured by Thar Technologies (Model SFE-100; Pittsburgh, PA). Chapter IV provides a complete description of the experimental apparatus, along with a diagram of the experimental setup (Figure 4.4). The system was composed of a Coriolis mass-flow meter, dual-piston pump, backpressure regulator, and cyclone separator. The uncertainty of the mass flow rate measurements was 0.2 %. The uncertainties of the temperature and pressure measurements were 1 K and 0.2 MPa, respectively.

A quantity of ≈ 1 g of potassium permanganate was placed in a stainless-steel equilibrium vessel (volume of 100 mL) packed with alternating layers of 2 mm diameter borosilicate glass beads (Chemglass; Vineland, NJ) and glass wool (Fisher Scientific). The packing served to reduce channeling of the SC-CO₂ [Maxwell, 1996; Lee et al.,

1994]. The temperature of the equilibrium vessel was increased to the prescribed operating value using a heating jacket. CO₂ was pumped through a heat exchanger to raise its temperature prior to entering the equilibrium cell. Upon entering the equilibrium vessel, the CO₂ was in a supercritical state at the desired pressure, which was maintained by a backpressure regulator.

Approximately 0.6 kg of SC-CO₂ was allowed to flow over the potassium permanganate in each experiment. A Coriolis mass-flow meter was used to quantify the mass of liquid CO₂ used. The carbon dioxide was delivered by a dual-piston pump at a flow rate of 0.25 g·s⁻¹. The solute-solvent mixture flowed from the equilibrium vessel to the cyclone separator through the valve of the backpressure regulator undergoing a continuous expansion. Then the pressure was reduced resulting in a phase separation; the gaseous CO₂ exited the system while the potassium permanganate was deposited on the vessel walls. The cyclone separator was rinsed with 25 mL of demineralized water to dissolve the potassium permanganate, and the resulting solution was collected in a tared, 40 mL amber glass vial. The concentration of potassium permanganate in the 40 mL vial was evaluated with a LAMBDA 25 UV/VIS Spectrophotometer (PerkinElmer; Waltham, MA). The scanning mode of the spectrophotometer was used to determine that 510 nm was a suitable wavelength of light to use for analysis. The spectrophotometer was calibrated with standard solutions of potassium permanganate in demineralized water. Potassium permanganate solubility experiments were performed in triplicates at 308.15 K and 318.15 K and at a pressure of 10 MPa.

Results and Discussion

Oxidation of oleic acid with potassium permanganate in supercritical carbon dioxide resulted in over 95 % conversion within 12 hours at both 308.15 K and 318.15 K. Figure 10.1 shows a plot of normalized oleic acid concentration versus time. The error bars in Figure 10.1 represent standard deviations of triplicate measurements. The concentration of potassium permanganate was not measured over time. The differential method of rate analysis described by Fogler (1999) was used to determine the oleic acid oxidation rate law:

$$-r_{OA} = kC_{OA}^{\alpha} \quad (10.1)$$

where r_{OA} is the reaction rate, k is the reaction rate constant, C_{OA} is the concentration of oleic acid, and α is the reaction order. Polymath 5.1 (Polymath Software; Willimantic, CT) was used to determine the rate law parameters, which are shown in Table 10.1. The rate of the reaction showed to have second order dependence upon oleic acid concentration ($\alpha = 2$). Once the reaction rate constants were determined, the activation energy could be evaluated. The activation energy can be considered the minimum energy that reacting molecules must possess before reaction will occur [Fogler, 1999]. The reaction rate constant can be related to activation energy by the Arrhenius equation:

$$k = A \exp\left(-\frac{E}{RT}\right) \quad (10.2)$$

where k is the previously defined rate constant, A is a frequency factor, E is the activation energy, R is the gas constant, and T is absolute temperature. Since rate constants were determined for two temperatures, the activation energy can be expressed as follows:

$$E = \frac{-R \ln \left(\frac{k_1}{k_2} \right)}{\left(\frac{1}{T_1} - \frac{1}{T_2} \right)} \quad (10.3)$$

Based on the results from Table 8.2, the activation energy for this reaction was 6.75 kJ·mol⁻¹. Once the activation energy was known, Eq. (10.2) was solved for the frequency factor, which was evaluated to be $3.23 \times 10^{-4} \text{ m}^3 \cdot \text{mol}^{-1} \cdot \text{s}^{-1}$. As a comparison, the activation energy and the frequency factor for the autoxidation oleic acid (a second-order reaction) have been reported to be 134 kJ·mol⁻¹ and $2.63 \times 10^{-2} \text{ m}^3 \cdot \text{mol}^{-1} \cdot \text{s}^{-1}$, respectively [Takahashi, 2000]. Therefore, the oxidation of oleic acid with potassium permanganate in supercritical carbon dioxide requires a lower activation energy and is less sensitive to temperature [Fogler, 1999].

A comparison of the 12-hour results between ambient reactions and high-pressure reactions is shown in Figure 10.2. The error bars in Figure 10.2 indicate standard deviation derived from triplicate measurements. The conversion of oleic acid in supercritical carbon dioxide reached 95.1 % at 308.15 K and 95.6 % at 318.15 K. In the absence of supercritical carbon dioxide, the oleic acid conversion after 12 hours was only 50.8 % at 308.15 K and 51.7 % at 318.15 K. Hence, conversion of oleic acid was improved greatly by incorporating the supercritical carbon dioxide. As Figure 10.2 illustrates, target product yields were also affected by the presence of the supercritical fluid. The yields of azelaic acid and pelargonic acid were increased when supercritical carbon dioxide was used as a reaction medium. Based upon GC-MS analysis, products other than azelaic acid and pelargonic were formed during the reaction. Figure 10.3

provides a comparison of chromatograms for 12-hour reaction results at 318.15 K. Based upon peak area, the major reaction products in the supercritical reaction were dimethyl azelate and methyl pelargonate, which correspond to azelaic acid and pelargonic acid, respectively. However, in the case of the ambient pressure reaction, the major reaction products based on peak area were compounds eluting near the methyl pelargonate and dimethyl azelate. Based upon CI analysis with isobutane, these compounds were hypothesized to be derived from the aldehydes of pelargonic acid and azelaic acid. Based upon the oxidation studies discussed in Chapter III, aldehydes are logical oxidation precursors to carboxylic acids. The aldehyde precursor to azelaic acid would be 9-oxononanoic acid, while nonanal (pelargonaldehyde) would be the precursor to pelargonic acid. To aid in confirming this hypothesis, a pelargonaldehyde standard was put through the same derivatization process as a reaction sample and analyzed on the GC-MS. The resulting product (an acetal) had the same retention time, ion fragmentation pattern in EI mode, and molecular weight in CI mode as the unknown peak from the samples. Figure 10.3 also shows that products were formed that had higher molecular weights than methyl oleate, which corresponds to oleic acid. Among the products identified using the NIST Mass Spectral Search Program 2.0 were derivatives of dihydroxystearic acid and epoxystearic acid; however, these products were not quantified. Both of these compounds are precursors to other oxidation products such as aldehydes. When supercritical carbon dioxide was not used as a reaction medium, more high-molecular-weight oxidation products were detected due to the slower progress of the reaction. These compounds are known to be intermediates to the formation of carboxylic acids [Mercangöz, 2004].

Figure 10.4 shows results for the determination of potassium permanganate solubility in supercritical carbon dioxide. The error bars represent standard deviations for triplicate measurements. The solubility of potassium permanganate at 308.15 K was $(1.00 \times 10^{-4} \pm 8.93 \times 10^{-6}) \text{ kg}\cdot\text{m}^{-3}$, but an increase in temperature to 318.15 K resulted in a decrease in solubility to $(6.68 \pm 1.27) \times 10^{-5} \text{ kg}\cdot\text{m}^{-3}$. Unfortunately, no solubility data for the potassium permanganate + supercritical carbon dioxide system could be located. However, Clarke et al. (1997) found that aqueous potassium permanganate could be dispersed in SC-CO₂ at a level of $0.079 \text{ kg}\cdot\text{m}^{-3}$ at 15 MPa and 32°C using a surfactant. Based upon the work by Foster et al. (1991), the solubility of oleic acid in supercritical carbon dioxide at a pressure of 10 MPa would be $2.15 \text{ kg}\cdot\text{m}^{-3}$ at 308.15 K and $0.78 \text{ kg}\cdot\text{m}^{-3}$ at 318.15 K. Although the solubility of potassium permanganate was several orders of magnitude lower than oleic acid, it was still high enough to allow the oxidation reaction to occur.

Conclusions

The oxidation of oleic acid with potassium permanganate was performed in supercritical carbon dioxide at 12.2 MPa. Conversions of over 95 % were achieved in 12 hours at temperatures of 308.15 K and 318.15 K. Oxidation reactions in the absence of supercritical carbon dioxide only resulted in about 50 % conversion of oleic acid. Incorporation of the supercritical fluid also resulted in higher yields of azelaic acid and pelargonic acid; moreover, in the absence of supercritical carbon dioxide, greater percentages of other oxidation products such as pelargonaldehyde and dihydroxystearic acid were observed. The solubility of potassium permanganate in supercritical carbon

dioxide at 10 MPa was determined to be $(1.00 \times 10^{-4} \pm 8.93 \times 10^{-6}) \text{ kg}\cdot\text{m}^{-3}$ at 308.15 K and $(6.68 \pm 1.27) \times 10^{-5} \text{ kg}\cdot\text{m}^{-3}$ at 318.15 K. To the author's knowledge, no previous studies have evaluated the solubility of potassium permanganate in supercritical carbon dioxide. Although the potassium permanganate exhibited a low solubility in supercritical carbon dioxide, it was still able to sufficiently interact with the oleic acid.

Table 10.1: Rate law modeling results for oxidation of oleic acid with potassium permanganate at 12.2 MPa

T/K	$k/$ $\text{m}^3 \cdot \text{mol}^{-1} \cdot \text{s}^{-1}$	r^2
308.15	2.32×10^{-5}	0.999
318.15	2.52×10^{-5}	0.995

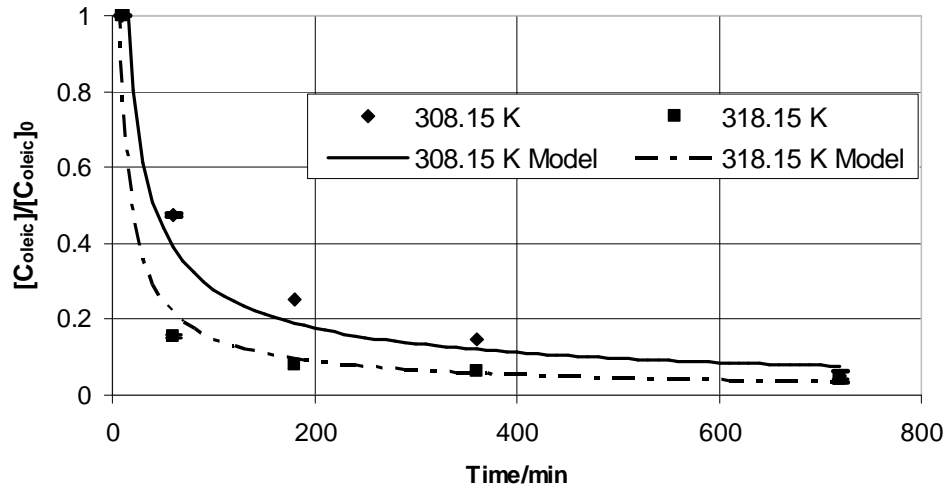


Figure 10.1: Change of normalized oleic acid concentration with time for oxidation of oleic acid with potassium permanganate at 12.2 MPa

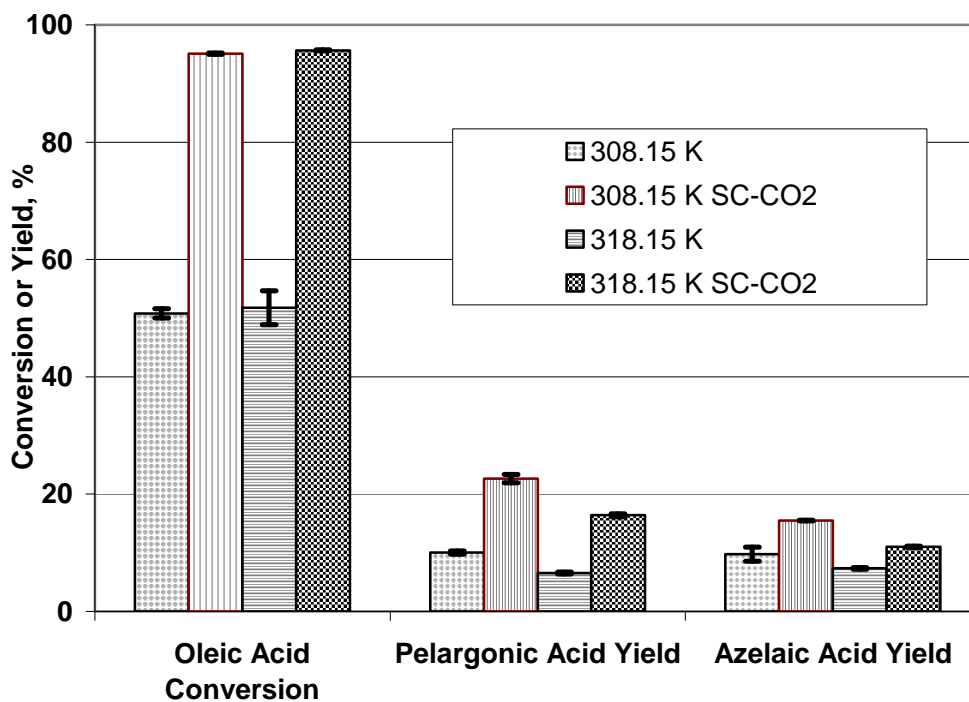


Figure 10.2: Comparison of 12-hour oleic acid oxidation reactions with potassium permanganate conducted with and without supercritical carbon dioxide

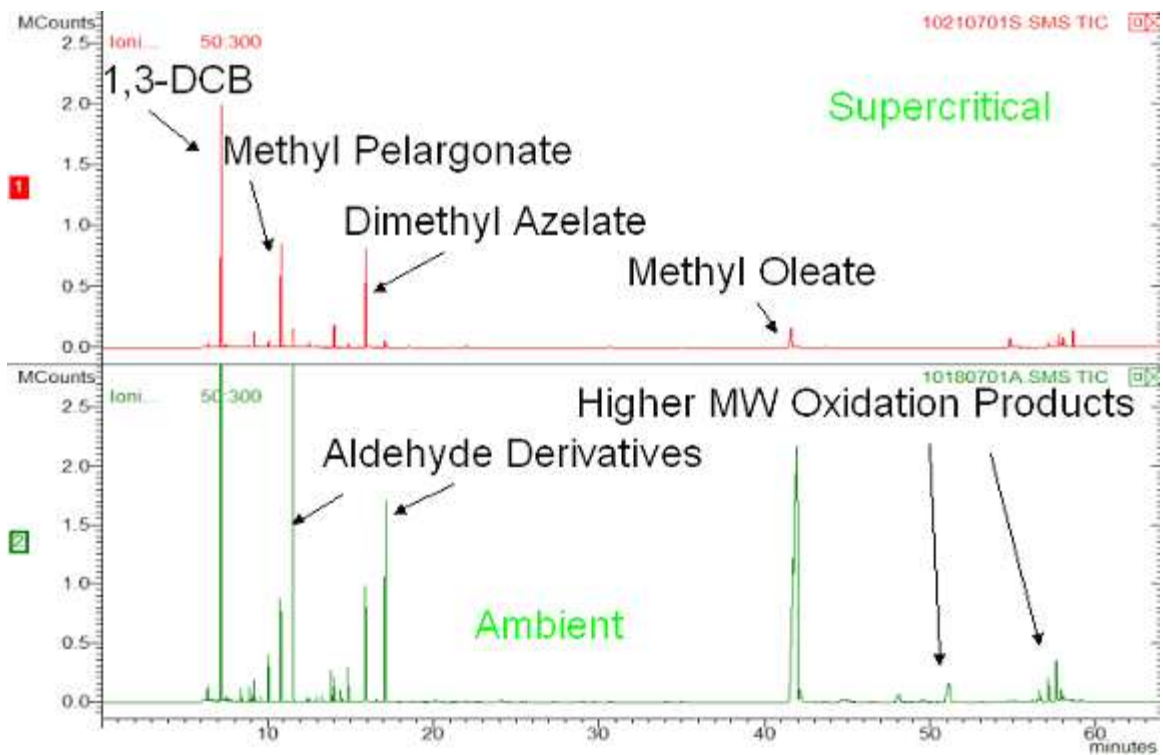


Figure 10.3: Comparison of typical chromatograms for 12-hour reactions at 318.15 K

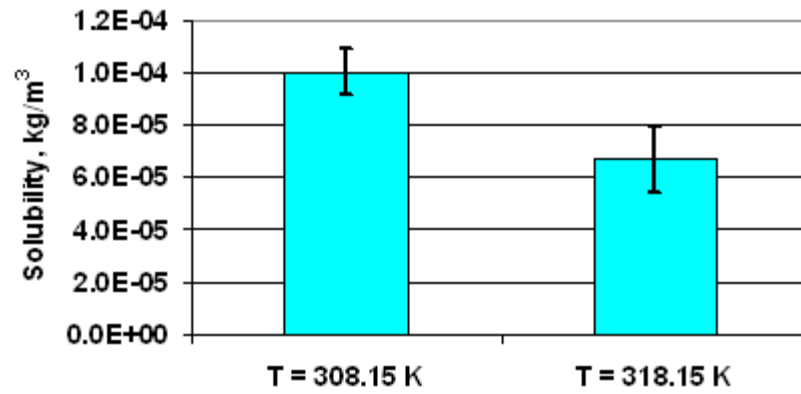


Figure 10.4: Solubility of KMnO_4 in supercritical carbon dioxide at 12.2 MPa

CHAPTER XI

ENGINEERING SIGNIFICANCE AND FUTURE WORK

The results of this research show that supercritical carbon dioxide can have a positive impact on the oxidation of oleic acid to pelargonic acid and azelaic acid. Also, the solubility studies indicate that supercritical fractionation of the reaction products is feasible. The solubility of pelargonic acid and azelaic acid differ by several orders of magnitude, resulting in facilitated separation. In previous studies on potassium permanganate oxidation, researchers focused on identifying emulsifiers or phase-transfer catalysts that would transfer the oxidant from an aqueous phase to an organic phase. To achieve significant reaction, the emulsifiers and phase-transfer catalysts have to be specifically matched to the organic phase. The results from this research show that water is not necessary, both in terms of the reaction and as a solvent for the potassium permanganate. Due to the tunable nature of supercritical carbon dioxide, it can be tailored for used with a variety of compounds. Therefore, the need for specific emulsifiers and phase-transfer catalysts can be avoided. Additionally, the use of organic solvents can be avoided, which is advantageous in terms of cost, safety, and environmental stewardship.

The solubility data generated in this study serve to fill in some of the gaps in terms of lipid + supercritical carbon dioxide solubility. As supercritical fluids are incorporated into more processes, solubility data are crucial. For example, supercritical

carbon dioxide is already being used for particle formation in the pharmaceutical industry. Therefore, the azelaic acid solubility data could be used in designing better, more efficient processes for the production of azelaic acid-based medicines.

Based upon the solubility studies, several suggestions were proposed for the use of density-based models. The first suggestion was the use of normalized or dimensionless variables. Currently, there is no consistency among solubility studies in terms of units used for variables such as density. If this modification becomes accepted among researchers, then it will become easier to compare model parameters from one study to another. The second proposal was the use of a new model that better accounts for temperature and density effects than previous models such as the equations of Chrastil, del Valle and Aguilera, and Adachi and Lu.

Unfortunately, no reaction was observed for the oleic acid oxidation with ozone in supercritical carbon dioxide; however, this was due to an experimental limitation, not a constraint on the usefulness of the supercritical fluid. As mentioned in Chapter X, the concentration of ozone in the reactor was very low and limited the reaction. High-pressure ozone generators could not be located, and ozone is not sold in gas cylinders due to its instability. However, there are several ideas for ozone generation that could be considered for future work. Koike et al. (2000) showed that silica gel would selectively adsorb ozone onto its surface over oxygen, resulting in high ozone concentrations. By increasing the temperature of the silica gel, the ozone can be desorbed and made available for reaction. Depending on the pore diameter of the silica gel, up to ≈ 0.1 g of ozone can be adsorbed per 1 g of silica gel. Another approach would be to continuously generate the ozone *in-situ* via ultraviolet (UV) light. The high pressure reactor is

equipped with sapphire windows, which could be used to transmit UV light into the reactor. Also, depending upon the wavelength of the UV light, it could directly cause oxidation of oleic acid.

If a suitable method of ozone generation could be found, then ozonolysis of oleic acid in supercritical carbon dioxide would be possible. A block flow diagram of the current oleic acid oxidation process is shown in Figure 11.1. By utilizing supercritical carbon dioxide as a reaction medium, the process would be improved in terms of the oxidation reaction and product separation, resulting in the modified process shown in Figure 11.2. In this study, high purity oleic acid was used for experimentation, but, industrially, oleic acid is only about 70 % to 75 % pure with other fatty acids such as linoleic acid and palmitic acid comprising the impurities. Therefore, the solubilities of these impurities in supercritical carbon dioxide would have to be determined either experimentally or from the literature. Also, the susceptibility of the impurities to oxidation would have to be considered. For example, linoleic acid is polyunsaturated and oxidized more readily than oleic acid, but palmitic acid is saturated and is less susceptible to oxidation than oleic acid. The future work should also consist of an economic analysis of any proposed process to evaluate its potential as a replacement to the current process.

The potassium permanganate experiments discussed in Chapter X served primarily as a proof of concept. However, future work could include studying the effect of pressure, mixing rate, mole ratio of potassium permanganate to oleic acid, and fatty acid impurities on the reaction. More experiments could also be conducted to expand the solubility data set of potassium permanganate in supercritical carbon dioxide.

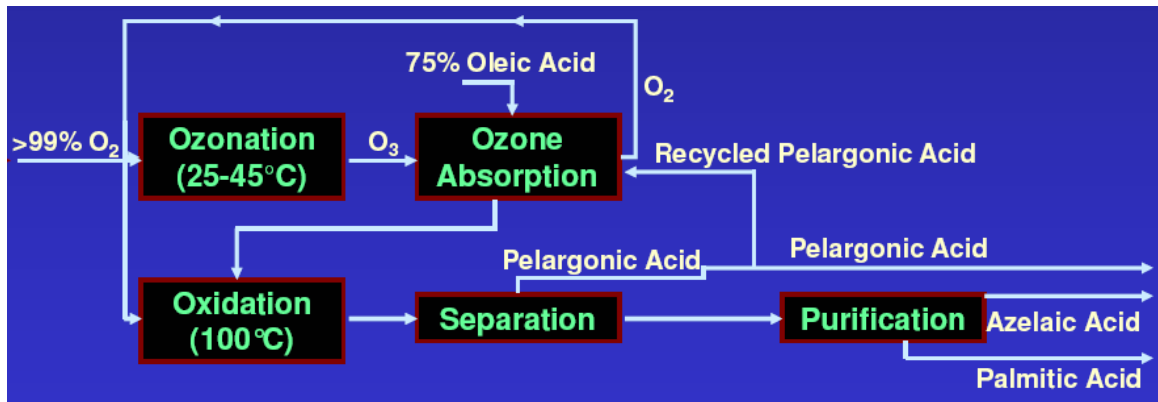


Figure 11.1: Conventional oleic acid oxidation process

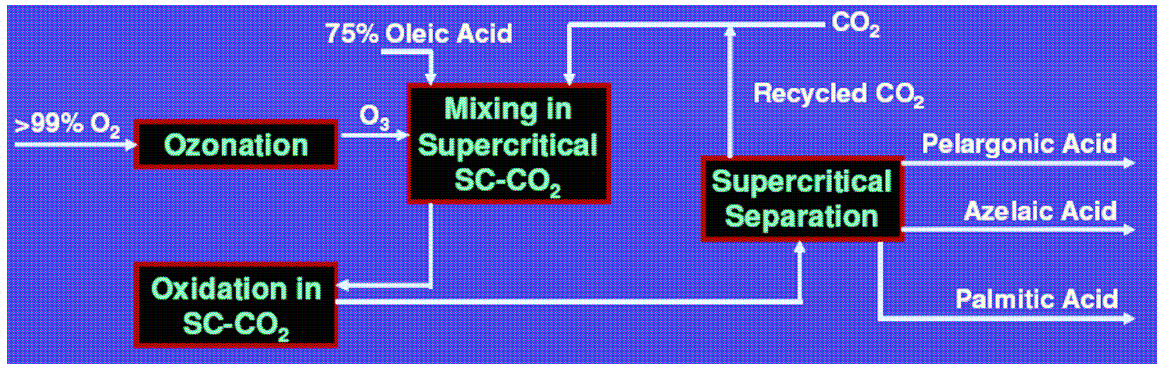


Figure 11.2: Oleic acid oxidation in supercritical carbon dioxide

CHAPTER XII

CONCLUSIONS

Based upon the results of this research, addition of supercritical carbon dioxide as a reaction medium can lead to several advantages over traditional oxidation techniques. In the case of oxidation with potassium permanganate, oleic acid conversion and target product yields were both increased in the presence of supercritical carbon dioxide. Also, the solubilities of azelaic acid and pelargonic acid differ by such a large extent that supercritical fractionation of these compounds is feasible. Therefore, incorporation of the supercritical carbon dioxide can result in an integrated reaction-separation scheme. Individual conclusions are summarized below.

- The results of the modeling study showed that semi-empirical models could be expressed in terms of dimensionless variables without loss of effectiveness. The use of a quadratic function to express the dependence of the association number on solvent density was found to not be necessary for the solids considered in the modeling study. This was also found to be true for the case of liquid-phase lipids such as oleic acid (Chapter VIII). One of the models proposed in the modeling study was a combination of the Adachi-Lu equation and the del Valle-Aguilera equation, and it provided the best fit in terms of lowest average error. Compared to other common density-based, semi-empirical models, the

new model better accounted for the dependence of solubility on density and temperature.

- The solubility of azelaic acid in supercritical carbon dioxide was determined experimentally and had a mole fraction range of $0.42 \cdot 10^{-6}$ at 333.15 K and 10.0 MPa to $10.12 \cdot 10^{-6}$ at 313.15 K and 26.7 MPa. To the author's knowledge, this is the first set of reported data for the azelaic acid + supercritical carbon dioxide system. In general, the solubility of azelaic acid increased with increasing temperature only after exceeding the crossover pressure that occurred between 17 MPa and 20 MPa. Both the semi-empirical methods (Chrastil's equation and Méndez -Teja equation) and the equation of state approach to modeling the data provided good correlations.
- The solubility of pelargonic acid in supercritical carbon dioxide was determined experimentally and varied from $0.14 \pm 0.07 \text{ kg} \cdot \text{m}^{-3}$ at 333.15 K and 10.0 MPa to $25.39 \pm 0.61 \text{ kg} \cdot \text{m}^{-3}$ at 313.15 K and 30.0 MPa. In general, the solubility of pelargonic acid increased with increasing pressure at constant temperature, and overall, the solubility was higher at 313.15 K than at 333.15 K. Since this is believed to be the first reported data of pelargonic acid solubility in SC-CO₂, the validity of the experimental approach was verified with oleic acid with good results. The solubility data were modeled with a semi-empirical equation intermediate to Chrastil's equation and the Adachi-Lu equation. To avoid dimensional inconsistency, the proposed model was expressed in

terms of normalized concentration and reduced density and temperature.

The model provided a better fit than Chrastil's equation and was comparable to the Adachi-Lu equation.

- The separation factor showed that pelargonic acid solubility in supercritical carbon dioxide was two to three orders of magnitude higher than azelaic acid under the experimental conditions considered in this work. Based upon these values of the separation factor, supercritical fluid fractionation of pelargonic acid and azelaic acid appears feasible.
- Complete conversion of oleic acid was achieved in less than 2 hours using the traditional ozonolysis technique. The two observed products were azelaic acid and pelargonic acid. Based upon a mass balance of the initial compounds versus the observed products, 97.2 % of mass was accounted for by pelargonic acid and azelaic acid. The remaining mass could be due to volatile aldehydes that were swept out of the reaction system by the exiting ozone + oxygen stream. The traditional ozonolysis reaction was zero-order with a reaction rate constant of $0.077 \text{ mol}\cdot\text{s}^{-1}\cdot\text{m}^{-3}$. Based upon the apparent order of the reaction, the ozonolysis of oleic acid was mass-transfer limited. No reaction was observed for the ozonolysis of oleic acid in supercritical carbon dioxide, which could be due in part to the lack of sufficient ozone for reaction.
- The oxidation of oleic acid with potassium permanganate was performed in supercritical carbon dioxide at 12.2 MPa for 12 hours. Conversions of over 95 % were achieved at temperatures of 308.15 K and 318.15 K.

Oxidation reactions in the absence of supercritical carbon dioxide only resulted in $\approx 50\%$ conversion of oleic acid. Incorporation of the supercritical fluid also resulted in higher yields of azelaic acid and pelargonic acid; however, in the absence of supercritical carbon dioxide, greater percentages of other oxidation products such as pelargonaldehyde and dihydroxystearic acid were observed.

- The solubility of potassium permanganate in supercritical carbon dioxide at 10 MPa was determined to be $(1.00 \times 10^{-4} \pm 8.93 \times 10^{-6}) \text{ kg}\cdot\text{m}^{-3}$ at 308.15 K and $(6.68 \pm 1.27) \times 10^{-5} \text{ kg}\cdot\text{m}^{-3}$ at 318.15 K. To the author's knowledge, no previous studies have evaluated the solubility of potassium permanganate in supercritical carbon dioxide. Although the potassium permanganate exhibited a low solubility in supercritical carbon dioxide, it was still able to sufficiently interact with the oleic acid for reaction.

REFERENCES

- Adachi, Y., Lu, B.C.Y. 1983. "Supercritical Fluid Extraction with Carbon Dioxide and Ethylene." *Fluid Phase Equilibria*, 14, 147-156.
- Agrice. 1999. "Production of Azelaic and Pelargonic Acid by Oxidative Blending." Online posting. Last Accessed 16 August 2007: http://www.ademe.fr/partenaires/agrice/Fiches_GB/card.asp?nc=9901C0003.
- Azelaic Acid. 1996. *The Merck Index, 12th Ed.*, Merck & Co., Inc., Whitehouse, NJ, 155-156.
- Baiker, A. 1999. "Supercritical Fluids in Heterogeneous Catalysis." *Chem. Rev.*, 99, 453-473.
- Bamford, C.H., Tipper, C.F.H. 1980. *Comprehensive Chemical Kinetics*, Vol. 16, Elsevier, Amsterdam, The Netherlands.
- Bartle, K.D., Clifford, A.A., Jafar, S.A., Shilstone, G.F. 1991. "Solubilities of Solids and Liquids of Low Volatility in Supercritical Carbon Dioxide." *J. Phys. Chem. Ref. Data*, 20, 713-756.
- Biermann, U., Friedt, W., Lang, S., Lühs, W., Machmüller, G., Metzger, J.O., Rüschen, Klaas, M., Schäfer, H.J., Schneider, M.P. 2000. "New Syntheses with Oils and Fats as Renewable Raw Materials for the Chemical Industry." *Angew. Chem. Int. Ed.*, 39, 2206-2224.
- Benson, T., Hernandez, R., French, T., Alley, E., Holmes, W. 2007. "Reactions of Fatty Acids in Superacid Media: Identification of Equilibrium Products." *Journal of Molecular Catalysis A: Chemical*, 274, 173-178.
- Bergstra, R. 2007. "Emerging Opportunities for Natural Oil Based Chemicals." MTN Consulting Associates. Online posting. Last Accessed 23 September 2007: <http://www.mtnconsulting.ca/Oleochem%20Final%20rjbergstra.pdf>.
- Bharath, R., Inomata, H., Arai, K., Shoji, K., Noguchi, Y. 1989. "Vapor-Liquid Equilibria for Binary Mixtures of Carbon Dioxide and Fatty Acid Ethyl Esters." *Fluid Phase Equil.*, 50, 315-327.

- Bondioli, P. 2003. "From Oilseeds to Industrial Products: Present and Near Future of Oleochemistry." *Ital. J. Agron.*, 7, 129-135.
- Boudreau, T.M., Hill, G.A. 2006. "Improved Ethanol-Water Separation Using Fatty Acids." *Process Biochemistry*, 41, 980-983.
- Brennecke, J.F. 1993. "Chapter 16: Spectroscopic Investigations of Reactions in Supercritical Fluids," in: Kiran, E. and Brennecke, J.F. (Eds.), *Supercritical Fluid Engineering Science: Fundamentals and Applications*, American Chemical Society, Washington, D.C., 201-219.
- Brimberg, U.I. 1993. "On the Kinetics of the Autoxidation of Fats. II. Monounsaturated Substrates." *JAOCs*, 70, 1063-1067.
- Brunner, G. 2004. *Supercritical Fluids as Solvents and Reaction Media*, Elsevier, Amsterdam, The Netherlands, Preface.
- Bush, G.W. 2007. "Fact Sheet: Twenty in Ten: Reducing America's Dependence on Oil." Online posting. Last Accessed 9 September 2007: <http://www.whitehouse.gov/news/releases/2007/03/20070320-2.html>.
- Caballero, A. C., Hernández, L. N., Estévez, L. A. 1992. "Calculation of Interaction Parameters for Binary Solid-SCF Equilibria Using Several EOS and Mixing Rules." *J. Supercrit. Fluids*, 5, 283-295.
- Capello, C., Fischer, U., Hungerbühler, K. 2007. "What is a Green Solvent? A Comprehensive Framework for the Environmental Assessment of Solvents." *Green Chem.*, 9, 927-934.
- CHEMCAD Component Data. 2005. *CHEMCAD 5.5.0*. Chemstations, Inc., Houston, TX.
- Chemical Market Reporter. 2001. "Cognis Expands Azelaic Acid." *Chemical Market Reporter*, 260, 3.
- ChemicalLand21. 2007. Website developed and hosted by Arokor Holdings, Inc. Online posting. Last Accessed August 2007: <http://www.chemicalland21.com>.
- Chum, H.L., Overend, R.P. 2001. "Biomass and Renewable Fuels." *Fuel Processing Technology*, 71, 187-195.
- Chrastil, J., 1982. "Solubility of Solids and Liquids in Supercritical Gases." *J. Phys. Chem.*, 86, 3016-3021.

- Christie, W.W. 2003a. "Lipids: Their Structures and Occurrence." *Lipid Analysis: Isolation, Separation, Identification and Structural Analysis of Lipids, 3rd Ed.*, The Oily Press, Bridgwater, England, 3-36.
- Christie, W.W. 2003b. "Preparation of Derivatives of Fatty Acids." *Lipid Analysis: Isolation, Separation, Identification and Structural Analysis of Lipids, 3rd Ed.*, The Oily Press, Bridgwater, England, 208.
- Christie, W.W. 2003c. "Chromatographic Analysis of Lipids: General Principles." *Lipid Analysis: Isolation, Separation, Identification and Structural Analysis of Lipids, 3rd Ed.*, The Oily Press, Bridgwater, England, 37-89.
- Clarke, M.J., Harrison, K.L., Johnston, K.P., Howdle, S.M. 1997. "Water in Supercritical Carbon Dioxide Microemulsions: Spectroscopic Investigation of a New Environment for Aqueous Inorganic Chemistry." *J. Am. Chem. Soc.*, 119, 6399-6406.
- Clifford, A.A., Bartle, K.D., Rayner, C.M. 2007. *University of Leeds*. Online posting. Last Accessed 24 November 2007: <http://www.chem.leeds.ac.uk/People/CMR/criticalpics.html>.
- Coleman, J.E., Ricciuti, C., Swern, D. 1956. "Improved Preparation of 9(10),10(9)-Keto-hydroxystearic Acids by Oxidation of Oleic Acid with Potassium Permanganate in Neutral Solution." *Journal of the American Chemical Society*, 78, 5342-5345.
- Cooper, C.D., Alley, F.C. 1994. "Overview of Particulate Control Equipment." *Air Pollution: A Design Approach, 2nd Ed.*, Waveland Press, Inc., Prospect Heights, IL, 120.
- Cygnarowicz-Provost, M. 1996. "Chapter 7: Design and Economic Analysis of Supercritical Fluid Extraction Processes," in: King, J.W., List, G.R. (Eds.), *Supercritical Fluid Technology in Oil and Lipid Chemistry*, AOCS Press, Champaign, IL, 155-179.
- del Valle, J. M., Aguilera, J. M. 1988. "An Improved Equation for Predicting the Solubility of Vegetable Oils in Supercritical CO₂." *Ind. Chem. Eng. Res.*, 27, 1551-1553.
- DeSimone, J.M. 2002. "Practical Approaches to Green Solvents." *Science*, 297, 799-803.
- Ding, Z., Lu, G.Q., Greenfield, P.F. 2000. "A Kinetic Study on Photocatalytic Oxidation of Phenol in Water by Silica-Dispersed Titania Nanoparticles." *Journal of Colloid and Interface Science*, 232, 1-9.

- Dobbs, J.M., Wong, J.M., Johnson, K.P. 1986. "Nonpolar Co-Solvents for Solubility Enhancement in Supercritical Fluid Carbon Dioxide." *J. Chem. Eng. Data*, 31, 303-308.
- Downard, K. 2004. "The Mass Spectrum." *Mass Spectrometry: A Foundation Course*, The Royal Society of Chemistry, Cambridge, UK, 10-21.
- Dufreche, S., Hernandez, R., French, T., Sparks, D., Zappi, M., Alley, E. 2007. "Extraction of Lipids from Municipal Wastewater Plant Microorganisms for Production of Biodiesel." *JAACS*, 84, 181-187.
- Encinar, J.M., Beltran, F.J., Frades, J.M. 1993. "Liquid Phase Oxidation of α -Pinene Initiated by Ozone. 1. Conversion of α -Pinene and Formation of Its Hydroperoxide." *Chem. Eng. Technol.*, 16, 68-74.
- Encinar, J.M., Beltran, F.J., Frades, J.M. 1994. "Liquid Phase Oxidation of α -Pinene Initiated by Ozone. 2. Formation of Verbenol, Verbenone and Acid Products." *Chem. Eng. Technol.*, 17, 187-194.
- Energy Information Administration (EIA). 2007a. "Crude Oil and Total Petroleum Imports Top 15 Countries." Online posting. Last Accessed 9 September 2007: http://www.eia.doe.gov/pub/oil_gas/petroleum/data_publications/company_level_imports/current/import.html.
- Energy Information Administration (EIA). 2007b. "Petroleum Products." Online posting. Last Accessed 9 September 2007: <http://www.eia.doe.gov/neic/infosheets/petroleumproducts.html>.
- Energy Information Administration (EIA). 2007c. "Alternatives to Traditional Transportation Fuels 2005 (Part II – User and Fuel Data)." Online posting. Last Accessed 8 December 2007: http://www.eia.doe.gov/cneaf/alternate/page/atftables/afvtransfuel_II.html#consumption.
- Fogler, H.S. 1999. *Elements of Chemical Reaction Engineering*, 3rd Ed., Prentice Hall, Upper Saddle River, NJ.
- Foglia, T.A., Barr, P.A., Malloy, A.J. 1977. "Oxidation of Alkenes with Use of Phase Transfer Catalysts." *JAACS*, 54, 858A-861A.
- Foster, N.R. Yun, S.L.J., Ting, S.S.T. 1991. "Solubility of Oleic Acid in Supercritical Carbon Dioxide." *The Journal of Supercritical Fluids*, 4, 127-130.

- Frankel, E.N., Neff, W.E., Rohwedder, W.K., Khambay, B.P., Garwood, R.F., Weedon, B.C. 1977. "Analysis of Autoxidized Fats by Gas Chromatography-Mass Spectrometry: I. Methyl Oleate." *Lipids*, 12, 901-907.
- García-González, J., Molina, M.J., Rodríguez, F., Mirada, F. 2002. "Solubilities of Hydroquinone and *p*-Quinone in Supercritical Carbon Dioxide." *Fluid Phase Equilibria*, 200, 31-39.
- Gardeler, H., Gmehling, J. 2004. "Chapter 1.1: Experimental Determination of Phase Equilibria and Comprehensive Examination of the Predictive Capabilities of Group Contribution Equations of State with a View to the Synthesis of Supercritical Extraction Processes." in: Brunner, G. (Ed.), *Supercritical Fluids as Solvents and Reaction Media*, Elsevier, Amsterdam, The Netherlands, 3-38.
- Garrett, D., Rowland, J. 2004. "Azelaic Acid Production Facility Design." Plant Design Project, *Mississippi State University*.
- Garti, N., Avni, E. 1981. "Permanganate Oxidation of Oleic Acid Using Emulsion Technology." *JAACS*, 58, 840-841.
- Ghiasvand, A.R., Hosseini, M., Sharghi, H., Yamini, Y., Shamsipur, M. 1999. "Solubilities of Some Hydroxyxanthone Derivatives in Supercritical Carbon Dioxide." *J. Chem. Eng. Data*, 44, 1135-1138.
- Goebel, C.G., Brown, A.C., Oehischlaeger, H.F., Rolfer, R.P. 1957. "Method of Making Azelaic Acid." U.S. Patent 2,813,113.
- Graham, D.M. 1997. "Use of Ozone for Food Processing." *Food Technology*, 51, 72-75.
- Gross, J.H. 2004. "Mass Spectrum." *Mass Spectrometry*, Springer, Heidelberg, Germany, 4-6.
- Güçlü-Üstündağ, Ö., Temelli, F. 2000. "Correlating the Solubility Behavior of Fatty Acids, Mono-, Di-, and Triglycerides, and Fatty Acid Esters in Supercritical Carbon Dioxide." *Ind. Eng. Chem. Res.*, 39, 4756-4766.
- Haas, M.J. 2005. "Improving the Economics of Biodiesel Production Through the Use of Low Value Lipids as Feedstock: Vegetable Oil Soapstock." *Fuel Processing Technology*, 86, 1087-1096.
- Hammam, H. 1992. "Solubilities of Pure Lipids in Supercritical Carbon Dioxide." *The Journal of Supercritical Fluids*, 5, 101-106.

- Hargis, L.G. 1988a. "Gas Chromatography." *Analytical Chemistry: Principles and Techniques*, Prentice Hall, Upper Saddle River, NJ, 507-525.
- Hargis, L.G. 1988b. "Principles and Instruments of Spectrophotometry." *Analytical Chemistry: Principles and Techniques*, Prentice Hall, Upper Saddle River, NJ, 377-406.
- Harrison, A.G. 1992. "Chemical Ionization Reagent Ion Systems." *Chemical Ionization Mass Spectrometry, 2nd Ed.*, CRC Press. Boca Raton, FL, 71-112.
- Harvey, A.H. 1990. "Supercritical Solubility of Solids from Near-Critical Dilute-Mixture Theory." *J. Phys. Chem.*, 94, 8403.
- Hearn, J.D., Smith, G.D. 2004. "Kinetics and Product Studies for Ozonolysis Reactions of Organic Particles Using Aerosol CIMS." *J. Phys. Chem. A*, 108, 10019-10029.
- Hill, K. 2000. "Fats and Oils as Oleochemical Raw Materials." *Pure Appl. Chem.*, 72, 1255-1264.
- Hoffman, V. 2003. "Biodiesel Fuel." North Dakota State University. Online posting. Last Accessed 20 November 2007: <http://www.ag.ndsu.edu/pubs/ageng/machine/ae1240w.htm>.
- Huang, Z., Kawi, S., Chiew, Y.C. 2004. "Solubility of Cholesterol and Its Esters in Supercritical Carbon Dioxide With and Without Cosolvents." *J. Supercrit. Fluids*, 30, 25-39.
- Hung, H., Katrib, Y., Martin, S.T. 2005. "Products and Mechanisms of the Reaction of Oleic Acid with Ozone and Nitrate Radical." *J. Phys. Chem. A*, 109, 4517-4530.
- INFORSE-Europe. 2007. "Vision 2050 for the EU 25." The International Network for Sustainable Energy. Online posting. Last Accessed 20 November 2007: <http://www.inforse.org/europe/VisionEU25.htm>.
- Inomata, H., Kondo, T., Hirohama, S., Arai, K., Suzuki, Y., Konno, M. 1989. "Vapor-Liquid Equilibria for Binary Mixtures of Carbon Dioxide and Fatty Acid Methyl Esters." *Fluid Phase Equil.*, 46, 41-52.
- Johnston, K.P., Ziger, D.H., Eckert, C.A. 1982. "Solubilities of Hydrocarbon Solids in Supercritical Fluids. The Augmented van der Waals Treatment." *Ind. Eng. Chem. Fundam.*, 21, 191-197.
- Jordan, T.E. 1954. *Vapor Pressure of Organic Compounds*, Interscience Publishers, Inc., New York.

- Kadesch, S.G. 1979. "Fat-Based Dibasic Acids." *JAOCS*, 56, 845A-849A.
- Katrib, Y., Martin, S.T., Hung, H.M., Rudich, Y., Zhang, H., Slowik, J.G., Davidovits, P., Jayne, J.T., Worsnop, D.R. 2004. "Products and Mechanisms of Ozone Reactions with Oleic Acid for Aerosol Particles Having Core-Shell Morphologies." *J. Phys. Chem. A*, 108, 6686-6695.
- Koike, K., Fukuda, T., Ichimura, S., Kurokawa, A. 2000. "High-Concentration Ozone Generator for Oxidation of Silicon Operating at Atmospheric Pressure." *Review of Scientific Instruments*, 71, 4182-4187.
- Kroha, H. 2004. "Industrial Biotechnology Provides Opportunities for Commercial Production of New Long-Chain Dibasic Acids." *Inform*, 15, 568-571.
- Kruse, A., Schmieder, H. 1998. "Supercritical Oxidation in Water and Carbon Dioxide." *Environmental Progress*, 17, 234-239.
- Lee, H., Kim, C.; Kim, S., Choi, C. 1994. "Solid Solubilities of Methoxyphenylacetic Acid Isomer Compounds in Supercritical Carbon Dioxide." *J. Chem. Eng. Data*, 39, 163-165.
- Logan, R.L. 1979. "Tall Oil Fatty Acids." *JAOCS*, 56, 777A-779A.
- Leitner, W. 2000. "Green Chemistry: Designed to Dissolve." *Nature*, 405, 129-130.
- Macsai, M.S., Mannis, M.J., Huntley, A.C. 1996. "Acne Rosacea. In Eye and Skin Disease: Part X. Acneiform Diseases." *Dermatology Online Journal*, 1, no. 2, Chapter 41. Online posting. Last Accessed 22 November 2007: <http://dermatology.cdlib.org/DOJvol1num2/review/rosacea.html>
- Maheshwari, P., Nikolov, Z.L., White, T.M., Hartel; R. 1992. "Solubility of Fatty Acids in Supercritical Carbon Dioxide." *JAOCS*, 69, 1069-1076.
- March, R.E. 1997. "An Introduction to Quadrupole Ion Mass Spectrometry." *Journal of Mass Spectrometry*, 32, 351-369.
- Maxwell, R. J. 1996. "Solubility Measurements of Lipid Constituents in Supercritical Fluids." *Supercritical Fluid Technology in Oil and Lipid Chemistry*; AOCS Press, Champaign, IL, 20-34.
- Méndez-Santiago, J., Teja, A. 1999. "The Solubility of Solids in Supercritical Fluids." *Fluid Phase Equilib.*, 158-160, 501-510.

- Mercangöz, M., Küsefoğlu, S., Akman, U., Hortaçsu, Ö. 2004. "Polymerization of Solybean Oil via Permanganate Oxidation with Sub/Supercritical CO₂." *Chemical Engineering and Processing*, 43, 1015-1027.
- Metzger, J.O., Bornscheuer, U. 2006. "Lipids as Renewable Resources: Current State of Chemical and Biotechnological Conversion and Diversification." *Appl Microbial Biotechnol*, 71, 13-22.
- Moise, T., Rudich, Y. 2002. "Reactive Uptake of Ozone by Aerosol-Associated Unsaturated Fatty Acids: Kinetics, Mechanism, and Products." *J. Phys. Chem. A*, 106, 6469-6476.
- Mountain High Water. 2007. "About Ozone." Mountain High Water, LLC. Online posting. Last Accessed 20 November 2007: http://mtnhighwater.com/new_page_1.htm.
- Musie, G., Wei, M., Subramanian, B., Busch, D.H. 2001. "Catalytic Oxidations in Carbon Dioxide-Based Reaction Media, Including Novel CO₂-Expanded Phases." *Coordination Chemistry Reviews*, 219-221, 789-820.
- National Biodiesel Board (NBB). 2007. "Estimated US Biodiesel Sales." Online posting. Last Accessed 30 September 2007: http://www.biodiesel.org/pdf_files/fuelfactsheets/Biodiesel_Sales_Graph.pdf.
- National Renewable Energy Laboratory (NREL). 2007. "Biomass Research." Online posting. Last Accessed 9 September 2007: <http://www.nrel.gov/biomass/biorefinery.html>.
- Neaves, D.E. 2007. "Evaluation of Fatty Acid Fraction Derived from Tall Oil as a Feedstock for Biodiesel Production." Masters Thesis, *Mississippi State University*.
- Nilsson, W.B. Gauglitz, E.J. Hudson, J.K. 1991. "Solubilities of Methyl Oleate, Oleic Acid, Oleyl Glycerols, and Oleyl Glycerol Mixtures in Supercritical Carbon Dioxide." *JAOCs*, 68, 87-91.
- NIST Thermophysical Properties of Fluid System. 2007. National Institute of Standards and Technology, Available on line: <http://webbook.nist.gov/chemistry/fluid>. Accessed: October 2007.
- Noureddini, H., Rempe, M.L. 1996. "Pelargonic Acid in Enhanced Oil Recovery." *JAOCs*, 73, 939-941.
- Noureddini, H., Kanabur, M. 1999. "Liquid-Phase Catalytic Oxidation of Unsaturated Fatty Acids." *JAOCs*, 76, 305-312.

- Pages-Xatart-Pares, X., Bonnet, C., Morin, O. 1999. "Synthesis of New Derivatives from Vegetable Oil Methyl Esters via Epoxidation and Oxirane Opening." In: Knothe, G., Derksen, J.T.P. (eds.): *Recent Developments in the Synthesis of Fatty Acid Derivatives*, AOCS Press, Champaign, IL, 141-156.
- Pang, T.H., Minghua, Y., Knopf, F.C., Dooley, K.M. 1991. "Catalytic Oxidation of Model Waste Aromatic Hydrocarbons in a Dense Fluid." *Chem. Eng. Comm.*, 110, 85-97.
- Pelargonic Acid. 1996. *The Merck Index, 12th Ed.*, Merck & Co., Inc., Whitehouse, NJ, 1214.
- Peng, D., Robinson, D.B. 1976. "A New Two-Constant Equation of State." *Ind. Eng. Chem., Fundam.*, 15, 59-64.
- PerkinElmer. 2004. "Technical Specifications for the LAMBDA 25/35/45 UV/Vis Spectrophotometers." Online posting. Last Accessed 15 November 2007: http://las.perkinelmer.com/content/relatedmaterials/specificationsheets/spc_LAMBDA253545.pdf
- Pernyeszi, T., Dékány, I. 2001. "Photooxidation of Oleic Acid, Toluene, Asphaltene, and Crude Oil in Titanium Dioxide Aqueous Suspensions." *Recent Advances in Enhanced Oil and Gas Recovery*, 3, 233-244.
- Prausnitz, J.M., Lichtenthaler, R.N., and Azevedo, E.G. 1999. "Chapter 5: Fugacities in Gas Mixtures." *Molecular Thermodynamics of Fluid Phase Equilibria, 3rd Ed.*, Prentice Hall, Inc., Upper Saddle River, NJ, 123-211.
- Punrattanasin, W., Spada, C. 1997. "Environmental Sampling & Monitoring Primer: Gas Chromatography." Online posting. Last Accessed 15 November 2007: <http://www.cee.vt.edu/ewr/environmental/teach/smprimer/gc/gc.html>.
- Ramsay, M.E., Hsu, J.T., Novak, R.A., Reightler, W.J. 1991. "Processing Rice Bran by Supercritical Fluid Extraction." *Food Technology*, 45, 98-104.
- Rayner, C.M., Oakes, R.S. 2005. "Chapter 4: Supercritical Carbon Dioxide," in: Mikami, K. (Ed.), *Green Reaction Media in Organic Synthesis*, John Wiley & Sons, Inc., Hoboken, NJ, 125-182.
- Rayner, C.M. 2007. "Solvent Properties of Supercritical Fluids." *University of Leeds*. Online posting. Last Accessed 24 November 2007: <http://www.chem.leeds.ac.uk/People/CMR/props.html>

- Reid, R.C., Prausnitz, J.M., Poling, B.E. 1987. "Chapter 2: Pure Component Constants." *The Properties of Gases and Liquids*, 4th Ed., McGraw-Hill, Inc., New York, NY, 11-28.
- Reynolds, J.C., Last, D.J., McGillen, M., Nijs, A., Horn, A.B., Percival, C., Carpenter, L.J., Lewis, A.C. 2006. "Structural Analysis of Oligomeric Molecules Formed from the Reaction Products of Oleic Acid Ozonolysis." *Environ. Sci. Technol.*, 40, 6674-6681.
- Rheonik, Inc. 2006. "The World's Largest Range of Mass Flowmeters." Online posting. Last Accessed 13 November 2007:
http://www.rheonik.com/media.php/388/910/rheonik_brochure_en_us%20_v1.pdf
- Ribeiro da Silva, M.A.V., Monte, M.J.S., Ribeiro, J.R. 1999. "Vapour Pressures and the Enthalpies and Entropies of Sublimation of Five Dicarboxylic Acids." *J. Chem. Thermodynamics*, 31, 1093-1107.
- Rood, D. 1991. "Gas Chromatographs." *A Practical Guide to the Care, Maintenance, and Troubleshooting of Capillary Gas Chromatographic Systems*, Hüthig Buch Verlag, Heidelberg, Germany, 2-3.
- Růžická, K., Fulem, M., Růžická, V. 2005. "Recommended Vapor Pressure of Solid Naphthalene." *J. Chem. Eng. Data*, 50, 1956-1970.
- Sam, D.J., Simmons, H.F. 1972. "Crown Polyether Chemistry. Potassium Permanganate Oxidations in Benzene." *Journal of the American Chemical Society*, 94, 4024-4025.
- Santacesaria, E., Sorrentino, A., Rainone, F., Di Serio, M., Speranza, F. 2000. *Ind. Eng. Chem. Res.*, 39, 2766-2771.
- Santacesaria, E., Ambrosio, M., Sorrentino, A., Tesser, R., Di Serio, R. 2003. "Double Bond Oxidative Cleavage of Monoenic Fatty Chains." *Catalysis Today*, 79-80, 59-65.
- Sauceau, M., Letourneau, J.J., Richon, D., Farges, J. 2003. "Enhanced Density-Based Models for Solid Compound Solubilities in Supercritical Carbon Dioxide with Cosolvents." *Fluid Phase Equilibria*, 208, 99-113.
- Scott, R.P.W. 2007. "Detectors for Use with Capillary Columns." *Capillary Chromatography*. Online posting by the *Journal of Chromatographic Science*. Last Accessed 14 November 2007:
<http://www.chromatography-online.org/Capillary/Detectors/rs18.html>.

- Škerget, M., Knez, Ž., Habulin, M. 1995. "Solubility of B-Carotene and Oleic Acid in Dense CO₂ and Data Correlation by a Density Based Model." *Fluid Phase Equilibria*, 109, 131-138
- Škerget, M., Novak-Pintarič, Z., Knez, Ž., Kravanja, Z. 2002. "Estimation of Solid Solubilities in Supercritical Carbon Dioxide: Peng-Robinson Adjustable Binary Parameters in the Near Critical Region." *Fluid Phase Equilibria*, 203, 111-132.
- Sparks, D., Hernandez, R., Zappi, M., Blackwell, D., Fleming, T. 2006. "Extraction of Rice Bran Oil Using Supercritical Carbon Dioxide and Propane." *JAOCS*, 83, 885-891.
- Sparks, D. L., Estévez, L.A., Meyer, N., Hernandez R. 2007a. "Solubility of Azelaic Acid in Supercritical Carbon Dioxide." Proceedings of the Iberoamerican Conference on Supercritical Fluids, PROSCIBA 2007, Foz do Iguaçu, Brazil. April 10-13, 2007. Paper SC-185.
- Sparks, D. L., Hernandez, R., Estévez, L.A. 2007b. "Evaluation of Density-Based Models for the Solubility of Solids in Supercritical Carbon Dioxide and Formulation of a New Model." *Chemical Engineering Science* (Under Review).
- Sparks, D. L., Hernandez, R., Estévez, L.A., Meyer, N., French, T. 2007c. "Solubility of Azelaic Acid in Supercritical Carbon Dioxide." *J. Chem. Eng. Data*, 52, 1246-1249.
- Sparks, D. L., Hernandez, R., Estévez, L.A., Barlow, K., French, T. 2007d. "Solubility of Nonanoic (Pelargonic) Acid in Supercritical Carbon Dioxide." *J. Chem. Eng. Data* (Under Review).
- Sovova, H., Stateva, R.P. 2001. "Biologically Active Substances Treated with Supercritical Fluids." *Bulgarian Chemical Communications*, 33, 247-258.
- Starks, C.M. 1971. "Phase-Transfer Catalysis. I. Heterogeneous Reactions Involving Anion Transfer by Quaternary Ammonium and Phosphonium Salts." *Journal of the American Chemical Society*, 93, 195-199.
- Suslow, T.V. 2004. "Ozone Applications for Postharvest Disinfection of Edible Horticultural Crops." University of California Division of Agricultural and Natural Resources Publication 8133.
- Suslow, T. 1998. "Basics of Ozone Applications for Postharvest Treatment of Fruits and Vegetables." *Perishables Handling Quarterly Issue No. 94*, 9-11.
- Takahashi, A., Kitakawa, N., Yonemoto, T. 2000. "Kinetic Analysis for Oxidation of Oleic Acid." *Journal of Chemical Engineering of Japan*, 33, 481-488.

- Thornberry, T., Abbatt, J.P.D. 2004. "Heterogeneous Reaction of Ozone with Liquid Unsaturated Fatty Acids: Detailed Kinetics and Gas-Phase Product Studies." *Phys. Chem. Chem. Phys.*, 6, 84-93.
- Toro-Vasquez, J.F., Castillo-M, A.A., Hernandez-C, R. 1993. "A Multiple-Variable Approach to Study Corn Oil Oxidation." *JAOCS*, 70, 261-267.
- Tsekhanskaya, Y.V., Iomtev, M.B., Mushkina, E.V. 1964. "Solubility of Naphthalene in Ethylene and Carbon Dioxide Under Pressure." *Russian Journal of Physical Chemistry*, 38, 1173-1176.
- United States International Trade Commission (USITC). 2005. "Potassium Permanganate from China." Publication 3778 (Investigation No. 731-TA-125). Online posting. Last Accessed 15 October 2007: http://hotdocs.usitc.gov/docs/pubs/701_731/pub3778.pdf.
- Valderrama, J.O. 2003. "The State of Cubic Equations of State." *Ind. Eng. Chem. Res.*, 42, 1603-1618.
- Vannozzi, G.P. 2006. "The Perspectives of Use of High Oleic Sunflower for Oleochemistry and Energy Raws." *HELIA*, 29, 1-24.
- Wikipedia. 2007a. "Fatty Acid." Online posting. Last Accessed 22 October 2007: http://en.wikipedia.org/wiki/Fatty_acid.
- Wikipedia. 2007b. "Potassium Permanganate." Online posting. Last Accessed 15 October 2007: http://en.wikipedia.org/wiki/Potassium_permanganate.
- Williams, J.R., Clifford, A.A. 2000. *Supercritical Fluid Methods and Protocols*, Humana Press, Totowa, NJ.
- Wits, J.J. 1989, "Diester Compressor Lubricants in Petroleum and Chemical Plant Service." *The Journal of Synthetic Lubrication*, 5, 319-326.
- Wong, J.M., Johnston, K.P. 1986. "Solubilization of Biomolecules in Carbon Dioxide Based on Supercritical Fluids." *Biotechnology Progress*, 2, 29-39.
- Yu, Z., Rizvi, S.S.H. 1992. "Phase Equilibria of Oleic Acid, Methyl Oleate, and Anhydrous Milk Fat in Supercritical Carbon Dioxide." *The Journal of Supercritical Fluids*, 5, 114-122.
- Yu, Z., Singh, B., Rizvi, S.S.H. Zollweg, J.A. 1994. "Solubilities of Fatty Acids, Fatty Acid Esters, Triglycerides, and Fats and Oils in Supercritical Carbon Dioxide." *J. Supercrit. Fluids*, 7, 51-59.

- Zappi, M., Hernandez, R., Sparks, D., Horne, J., Brough, M., Arora, S., and Motsenbocker, D. 2003. "A Review of the Engineering Aspects of the Biodiesel Industry." A Report for the Mississippi Biomass Council in Jackson, MS (MSU E-TECH Laboratory Report ET-03-003).
- Ziemann, P.J. 2005. Aerosol Products, Mechanisms, and Kinetics of Heterogeneous Reactions of Ozone with Oleic Acid in Pure and Mixed Particles." *Faraday Discuss.*, 130, 1-22.
- Zimmermann, F., Meux, E., Mieloszynski, J.L., Lecuire, J.M., Oget, N. 2005. "Ruthenium Catalyzed Oxidation without CCl₄ of Oleic Acid, Other Monoenic Fatty Acids and Alkenes." *Tetrahedron Letters*, 46, 3201-3203.
- Zosel, K. 1978. "Separation with Supercritical Gases: Practical Applications." *Angew. Chem., Int. Ed. Engl.*, 17, 702-709.
- Zou, M., Yu, Z.R., Kashulines, P., Rizvi, S.S.H. 1990. "Fluid-Liquid Phase Equilibria of Fatty Acid Methyl Esters in Supercritical Carbon Dioxide." *The Journal of Supercritical Fluids*, 3, 23-28.

APPENDIX A

COMPLETE SOLUBILITY REFERENCE DATA USED IN CHAPTER VI

Table A.1: Solubility of naphthalene in supercritical carbon dioxide at 308.15 K

P/MPa	$\rho_1/\text{kg}\cdot\text{m}^{-3}$	$\rho_{r,1}$	$10^4 y_2$	$c_2/\text{kg}\cdot\text{m}^{-3}$
6.08	162.64	0.35	2.4	0.11
7.60	288.33	0.62	7.5	0.63
7.70	307.42	0.66	8.7	0.78
7.80	332.07	0.71	10.7	1.04
7.90	366.82	0.78	13.7	1.47
7.95	390.96	0.84	30.1	3.44
8.06	459.55	0.98	47.6	6.40
8.11	494.66	1.06	61.1	8.86
8.71	637.92	1.36	81	15.17
9.22	676.5	1.45	92	18.29
10.64	733.94	1.57	110	23.77
11.15	747.7	1.60	117	25.78
12.16	770.28	1.65	125	28.40
13.17	788.58	1.69	132	30.72
14.19	804.08	1.72	139	33.01
15.20	817.58	1.75	146	35.28
16.21	829.58	1.77	151	37.04
19.25	859.41	1.84	163	41.47
22.29	883.24	1.89	174	45.55
24.32	896.93	1.92	177	47.07
29.38	925.97	1.98	184	50.55
33.44	945.45	2.02	187	52.47

Table A.2: Solubility of naphthalene in supercritical carbon dioxide at 318.15 K

P/MPa	$\rho_l/\text{kg}\cdot\text{m}^{-3}$	$\rho_{r,l}$	$10^4 y_2$	$c_2/\text{kg}\cdot\text{m}^{-3}$
6.28	152.26	0.33	4.7	0.21
7.30	198.05	0.42	4.8	0.28
7.80	227.62	0.49	6.7	0.44
8.21	256.59	0.55	7.8	0.58
8.56	287.75	0.62	11	0.92
8.82	314.7	0.67	13	1.19
9.22	368.81	0.79	21	2.26
9.58	427.64	0.91	43	5.38
9.78	462.71	0.99	51	6.91
9.93	487.48	1.04	61	8.71
10.13	517.26	1.11	69	10.47
10.64	574.17	1.23	97	16.38
10.94	599.05	1.28	113	19.94
11.96	655.85	1.40	142	27.51
12.67	682.94	1.46	154	31.11
14.19	724.79	1.55	183	39.35
15.50	751.38	1.61	197	43.98
20.27	815.48	1.74	245	59.65
27.86	877.12	1.88	285	74.94
31.41	898.41	1.92	294	79.26

Table A.3: Solubility of naphthalene in supercritical carbon dioxide at 328.15 K

P/MPa	$\rho_l/\text{kg}\cdot\text{m}^{-3}$	$\rho_{r,l}$	$10^4 y_2$	$c_2/\text{kg}\cdot\text{m}^{-3}$
7.70	190.53	0.41	11	0.61
9.22	269.11	0.58	24	1.89
9.42	282.41	0.60	20	1.65
9.93	319.48	0.68	24	2.24
10.23	344.5	0.74	30	3.02
10.64	380.78	0.81	42	4.68
11.15	428.8	0.92	61	7.66
11.45	457.27	0.98	77	10.33
11.65	475.45	1.02	92	12.86
11.96	501.02	1.07	108	15.93
12.26	524.26	1.12	127	19.64
12.56	545.14	1.17	142	22.87
13.17	580.6	1.24	181	31.17
14.29	629.48	1.35	234	43.93
15.20	659.48	1.41	264	52.08
16.21	686.28	1.47	300	61.82
17.23	708.42	1.52	324	69.09
18.24	727.27	1.56	356	78.19
19.76	751.18	1.61	399	90.92
23.30	794.17	1.70	459	111.27
25.33	813.65	1.74	485	120.79
32.42	866.04	1.85	550	146.80

Table A.4: Solubility of fluorene in supercritical carbon dioxide at 308.15 K

P/MPa	$\rho_f/\text{kg}\cdot\text{m}^{-3}$	$\rho_{r,1}$	$10^4 y_2$	$c_2/\text{kg}\cdot\text{m}^{-3}$
8.37	589.91	1.26	4.15	0.93
10.43	727.58	1.56	11.80	3.25
13.88	799.65	1.71	15.30	4.63
20.77	871.89	1.86	22.60	7.46
34.56	950.40	2.03	24.30	8.74
41.45	977.58	2.09	27.20	10.07

Table A.5: Solubility of fluorene in supercritical carbon dioxide at 323.15 K

P/MPa	$\rho_l/\text{kg}\cdot\text{m}^{-3}$	$\rho_{r,1}$	$10^4 y_2$	$c_2/\text{kg}\cdot\text{m}^{-3}$
6.99	171.60	0.37	0.11	0.01
8.37	240.69	0.51	0.36	0.03
10.43	436.96	0.93	4.28	0.71
13.88	668.38	1.43	15.40	3.89
17.33	746.48	1.60	23.90	6.75
20.77	793.35	1.70	30.80	9.26
27.67	854.72	1.83	38.70	12.54
34.56	896.92	1.92	40.80	13.88
41.45	929.64	1.99	43.60	15.38

Table A.6: Solubility of fluorene in supercritical carbon dioxide at 343.15 K

P/MPa	$\rho_1/\text{kg}\cdot\text{m}^{-3}$	$\rho_{r,1}$	$10^4 y_2$	$c_2/\text{kg}\cdot\text{m}^{-3}$
8.37	185.80	0.40	0.69	0.05
10.43	266.74	0.57	1.92	0.19
13.88	450.26	0.96	9.85	1.68
17.33	593.06	1.27	25.40	5.70
20.77	673.94	1.44	40.50	10.35
34.56	823.10	1.76	76.70	24.03
41.45	864.57	1.85	87.40	28.79
48.34	897.50	1.92	91.80	31.41

Table A.7: Solubility of hydroquinone in supercritical carbon dioxide at 333 K

P/MPa	$\rho_1/\text{kg}\cdot\text{m}^{-3}$	$\rho_{r,1}$	$10^5 y_2$	$c_2/\text{kg}\cdot\text{m}^{-3}$
10	291	0.62	0.70	0.01
12.5	475	1.02	1.20	0.01
15	607	1.30	2.12	0.03
17.5	679	1.45	2.81	0.05
20	725	1.55	2.90	0.05
22.5	760	1.63	2.89	0.05
25	788	1.69	3.13	0.06
27.5	811	1.73	3.08	0.06
30	831	1.78	3.24	0.07
32.5	848	1.81	3.35	0.07
35	864	1.85	3.38	0.07

Table A.8: Solubility of hydroquinone in supercritical carbon dioxide at 348 K

P/MPa	$\rho_1/\text{kg}\cdot\text{m}^{-3}$	$\rho_{r,1}$	$10^5 y_2$	$c_2/\text{kg}\cdot\text{m}^{-3}$
10	234	0.50	0.90	0.01
12.5	343	0.73	1.00	0.01
15	466	1.00	2.00	0.02
17.5	562	1.20	2.43	0.03
20	628	1.34	3.12	0.05
22.5	676	1.45	3.13	0.05
25	713	1.52	3.52	0.06
27.5	743	1.59	3.67	0.07
30	768	1.64	4.04	0.08
32.5	789	1.69	4.10	0.08
35	809	1.73	4.24	0.09

Table A.9: Solubility of hydroquinone in supercritical carbon dioxide at 363 K

P/MPa	$\rho_1/\text{kg}\cdot\text{m}^{-3}$	$\rho_{r,1}$	$10^5 y_2$	$c_2/\text{kg}\cdot\text{m}^{-3}$
10	203	0.43	1.00	0.01
12.5	282	0.60	1.20	0.01
15	373	0.80	1.59	0.01
17.5	461	0.99	2.15	0.02
20	535	1.14	2.83	0.04
22.5	592	1.27	3.19	0.05
25	637	1.36	4.10	0.07
27.5	674	1.44	4.40	0.07
30	704	1.51	4.95	0.09
32.5	730	1.56	5.15	0.09
35	753	1.61	5.59	0.11

Table A.10: Solubility of anthracene in supercritical carbon dioxide at 303.15 K

P/MPa	$\rho_1/\text{kg}\cdot\text{m}^{-3}$	$\rho_{r,1}$	$10^4 y_2$	$c_2/\text{kg}\cdot\text{m}^{-3}$
10.43	780.95	1.67	0.29	0.09
13.88	834.36	1.78	0.52	0.17
27.67	936.66	2.00	0.69	0.26
41.45	993.33	2.12	0.80	0.32

Table A.11: Solubility of anthracene in supercritical carbon dioxide at 323.15 K

P/MPa	$\rho_1/\text{kg}\cdot\text{m}^{-3}$	$\rho_{r,1}$	$10^4 y_2$	$c_2/\text{kg}\cdot\text{m}^{-3}$
9.06	289.85	0.62	0.04	0.00
10.44	438.19	0.94	0.04	0.01
11.81	572.12	1.22	0.16	0.04
13.88	668.38	1.43	0.50	0.13
17.33	746.48	1.60	0.89	0.27
20.77	793.35	1.70	1.09	0.35
27.67	854.72	1.83	1.40	0.48
34.56	896.92	1.92	1.54	0.56
38.01	914.19	1.96	1.61	0.60
41.45	929.64	1.99	1.72	0.65

Table A.12: Solubility of anthracene in supercritical carbon dioxide at 343.15 K

P/MPa	$\rho_l/\text{kg}\cdot\text{m}^{-3}$	$\rho_{r,1}$	$10^4 y_2$	$c_2/\text{kg}\cdot\text{m}^{-3}$
11.81	335.54	0.72	0.14	0.02
12.92	397.24	0.85	0.22	0.04
13.88	450.26	0.96	0.36	0.07
15.26	517.48	1.11	0.63	0.13
17.33	593.06	1.27	0.71	0.17
20.77	673.94	1.44	1.68	0.46
27.67	766.31	1.64	2.48	0.77
34.56	823.1	1.76	3.09	1.03
41.45	864.57	1.85	3.49	1.22

Table A.13: Solubility of cholesterol in supercritical carbon dioxide at 308.15 K

P/MPa	$\rho_1/\text{kg}\cdot\text{m}^{-3}$	$\rho_{r,1}$	$10^5 y_2$	$c_2/\text{kg}\cdot\text{m}^{-3}$
12.36	774.19	1.66	1.39	0.09
15.39	819.95	1.75	2.61	0.19
18.27	850.59	1.82	3.07	0.23
20.3	868.16	1.86	4.15	0.32
25.36	903.44	1.93	5.19	0.41
25.76	905.86	1.94	5.25	0.42
27.89	918.04	1.96	5.55	0.45

Table A.14: Solubility of cholesterol in supercritical carbon dioxide at 313.15 K

P/MPa	$\rho_1/\text{kg}\cdot\text{m}^{-3}$	$\rho_{r,1}$	$10^5 y_2$	$c_2/\text{kg}\cdot\text{m}^{-3}$
10.09	635.16	1.36	7.08	0.40
12.27	725.24	1.55	8.69	0.55
15.2	783.33	1.68	9.74	0.67
18.45	824.39	1.76	12.6	0.91
20.35	843.04	1.80	15.4	1.14
25.27	881.32	1.88	19.2	1.49
27.6	896.14	1.92	25	1.97

Table A.15: Solubility of cholesterol in supercritical carbon dioxide at 333.15 K

P/MPa	$\rho_1/\text{kg}\cdot\text{m}^{-3}$	$\rho_{r,1}$	$10^5 y_2$	$c_2/\text{kg}\cdot\text{m}^{-3}$
10.1	296.13	0.63	2.91	0.08
12.15	445.81	0.95	5.97	0.23
15.15	609.61	1.30	9	0.48
18.22	691.77	1.48	13.6	0.83
20.34	729.01	1.56	20	1.28
25.36	790.14	1.69	32.4	2.25
27.33	808.3	1.73	38	2.70

APPENDIX B

COMPLETE SOLID SOLUBILITY MODELING RESULTS

Table B.1: Chrastil equation modeling results

Comp.	T/K	Normal (Eq. 5.1)				Dimensionless (Eq. 5.14)			
		k	α	β/K	AVERR %	k	α	β	AVERR %
Naph.	308.15				12.86				12.58
	318.15	3.871	-0.919	-6.65E+03	12.11	3.869	16.621	-21.736	12.25
	328.15				5.76				5.83
Fluor.	308.15				8.92				9.02
	323.15	4.035	-10.661	-4.56E+03	7.5	4.040	8.047	-15.052	7.45
	343.15				5.06				5.05
Hydroq.	333				6.79				6.79
	348	2.613	-12.487	-2.59E+03	5.45	2.613	-2.569	-8.502	5.45
	363				6.97				6.97
Anthrac.	303.15				10.92				10.83
	323.15	4.352	-14.028	-5.21E+03	9.31	4.352	6.579	-17.124	9.35
	343.15				8.55				8.54
Chol.	308.15				118.27				114.34
	313.15	6.503	-19.108	-7.81E+03	39.43	6.754	15.254	-26.391	40.41
	333.15				13.40				13.57
Chol.	313.15				14.79				14.78
	333.15	6.786	-27.437	-5.67E+03	13.18	6.776	8.103	-18.602	13.17

Table B.2: del Valle-Aguilera (Eq. 5.3) modeling results

Comp.	T/K	k	α	β/K	γ/K^2	AVERR %
Naph.	308.15	3.888	1.05E+02	-7.40E+04	1.07E+07	11.51
	318.15					8.16
	328.15					5.48
Fluor.	308.15	4.028	-1.389	-1.06E+04	9.95E+05	8.78
	323.15					7.28
	343.15					5.07
Hydroq.	333	2.617	3.860	-1.40E+04	1.98E+06	6.58
	348					5.30
	363					7.00
Anthrac.	303.15	4.36	-1.693	-1.34E+04	1.34E+06	8.65
	323.15					9.03
	343.15					8.51
Chol.	308.15	6.818	-9.95E+02	6.20E+05	-1.01E+08	8.58
	313.15					14.84
	333.15					13.20
Chol.	313.15	6.786	-23.717	-8.07E+03	3.88E+05	14.79
	333.15					13.18

Table B.3: del Valle-Aguilera (Eq. 5.15) dimensionless modeling results

Comp.	T/K	k	α	β	γ	AVERR %
Naph.	308.15	3.870	1.23E+02	-2.44E+02	1.16E+02	11.31
	318.15					7.83
	328.15					5.66
Fluor.	308.15	4.037	17.179	-34.769	10.625	8.76
	323.15					7.31
	343.15					5.05
	333					6.6
Hydroq.	348	2.617	11.976	-41.78	19.008	5.28
	363					6.99
	303.15					8.65
Anthrac.	323.15	4.36	19.008	-43.982	14.48	9.04
	343.15					8.51
	308.15					8.62
Chol.	313.15	6.809	-9.60E+02	2.04E+03	-1.09E+03	14.82
	333.15					13.2
	313.15					14.78
Chol.	333.15	6.776	7.53	-17.385	-0.646	13.17

Table B.4: Adachi-Lu (Eq. 5.5) modeling results

Comp.	T/K	e_0	$e_1/m^3 \cdot kg^{-1}$	$e_2/m^6 \cdot kg^{-2}$	α	β/K	AVERR %
Naph.	308.15	0.246	2.08E-03	-1.04E-06	15.916	-6.40E+03	10.93
	318.15						10.49
	328.15						2.79
Fluor.	308.15	0.289	2.21E-03	-1.08E-06	6.779	-4.40E+03	8.40
	323.15						5.52
	343.15						2.10
Hydroq.	333	-1.216	2.11E-03	-1.05E-06	5.906	-2.43E+03	4.76
	348						5.79
	363						4.43
Anthrac.	303.15	9.562	-1.25E-03	2.45E-07	-43.732	-5.02E+03	11.70
	323.15						7.49
	343.15						7.97
Chol.	308.15	-	1.02E-02	-3.96E-06	1.18E+02	-7.86E+03	114.05
	313.15						40.01
	333.15						10.58
Chol.	313.15	-2.798	1.60E-03	2.90E-08	29.239	-6.10E+03	13.57
	333.15						6.43

Table B.5: Adachi-Lu dimensionless (Eq. 5.16) modeling results

Comp.	T/K	e_0	e_1	e_2	α	β	AVERR %
Naph.	308.15	2.817	2.268	-0.879	15.719	-20.893	10.49
	318.15						10.63
	328.15						2.96
Fluor.	308.15	2.978	2.499	-0.927	7.306	-14.478	8.40
	323.15						5.47
	343.15						2.11
Hydroq.	333	0.920	2.863	-1.058	-3.074	-7.997	4.8
	348						5.84
	363						4.34
Anthrac.	303.15	7.026	-1.297	0.085	5.646	-16.477	11.87
	323.15						7.55
	343.15						7.73
Chol.	308.15	-8.172	15.07	-4.045	15.205	-25.752	114.04
	313.15						39.95
	333.15						10.35
Chol.	313.15	-0.739	3.542	-0.212	10.489	-20.001	13.55
	333.15						6.4

Table B.6: Modeling results for Eq. (6.5)

Comp.	T/K	e_0	$e_1/m^3 \cdot kg^{-1}$	α	β/K	AVERR %
Naph.	308.15	6.503	-5.02E-04	-16.376	-6.47E+03	11.77
	318.15					10.66
	328.15					4.01
Fluor.	308.15	8.228	-7.21E-04	-35.139	-4.44E+03	8
	323.15					6.20
	343.15					3.37
Hydroq.	333	3.419	-1.66E-04	-17.207	-2.51E+03	6.00
	348					6.72
	363					8.39
Anthrac.	303.15	7.814	-5.98E-04	-34.535	-5.01E+03	11.93
	323.15					7.55
	343.15					7.73
Chol.	308.15	3.801	5.01E-04	-2.637	-8.17E+03	114.26
	313.15					40.56
	333.15					12.23
Chol.	313.15	-2.937	1.66E-03	29.932	-6.09+03	13.57
	333.15					6.45

Table B.7: Modeling results for Eq. (6.6)

Comp.	T/K	e_0	$e_1/\text{m}^3\cdot\text{kg}^{-1}$	α	β/K	AVERR %
Naph.	308.15	5.2	-0.651	15.933	-21.114	10.93
	318.15					10.7
	328.15					3.98
Fluor.	308.15	6.18	-0.893	7.486	-14.752	8.13
	323.15					5.93
	343.15					3.01
Hydroq.	333	3.183	-0.308	-2.837	-8.229	5.92
	348					6.75
	363					8.36
Anthrac.	303.15	6.708	-0.976	5.636	-16.455	11.99
	323.15					7.57
	343.15					7.66
Chol.	308.15	5.529	0.491	15.692	-26.647	114.34
	313.15					40.49
	333.15					12.84
Chol.	313.15	-0.223	2.86	10.577	-20.082	13.51
	333.15					6.33

Table B.8: Modeling results for Eq. (6.8)

Comp.	T/K	e_0	e_1	α	β	γ	AVERR %
Naph.	308.15	5.152	-0.628	1.18E+02	-2.36E+02	1.12E+02	9.50
	318.15						5.44
	328.15						3.76
Fluor.	308.15	6.365	-0.971	23.48	-49.409	18.716	7.29
	323.15						5.39
	343.15						2.97
Hydroq.	333	3.274	-0.353	15.224	-49.596	23.647	5.61
	348						6.84
	363						8.6
Anthrac.	303.15	6.795	-1.007	19.362	-46.161	16.027	10.3
	323.15						6.94
	343.15						7.69
Chol.	308.15	-0.214	2.856	-9.76E+02	2.08E+03	-1.11E+03	6.16
	313.15						13.51
	333.15						6.33
Chol.	313.15	-0.223	2.86	12.668	-24.524	2.357	13.51
	333.15						6.33

Table B.9: Modeling results for Eq. (6.9)

Comp.	T/K	e_0	e_1	e_2	α	β	γ	AVERR %
Naph.	308.15							9.03
	318.15	2.538	2.595	-0.974	1.18E+02	-2.36E+02	1.13E+02	5.59
	328.15							2.63
Fluor.	308.15							7.97
	323.15	2.128	3.495	-1.215	25.517	-53.834	21.228	4.12
	343.15							1.93
Hydroq.	333							4.30
	348	0.668	3.306	-1.222	19.937	-60.740	30.166	5.61
	363							4.13
Anthrac.	303.15							10.41
	323.15	6.28	-0.507	-0.129	19.587	-46.623	16.287	6.95
	343.15							7.57
Chol.	308.15							6.11
	313.15	-0.784	3.604	-0.232	-9.74E+02	2.07E+03	-1.11E+03	13.56
	333.15							6.4
Chol.	313.15							13.55
	333.15	-0.739	3.542	-0.212	12.618	-24.525	2.400	6.4

Table B.10: Méndez-Teja modeling results

Comp.	T/K	Normal (Eq. 5.6)			Dimensionless (Eq. 5.18)		
		A/K	B/K·m ³ ·kg ⁻¹	AVERR %	A*	B*	AVERR %
Naph.	308.15			47.30			43.35
	318.15	9.65E+02	2.341	16.87	3.86	3.197	18.4
	328.15			27.32			25.15
Fluor.	308.15			10.41			11.21
	323.15	1.04E+03	3.047	14	4.569	4.059	6.85
	343.15			12.45			4.63
Hydroq.	333			75.37			72.9
	348	9.64E+02	1.886	42.00	2.913	3.105	38.65
	363			25.44			29.19
Anthrac.	303.15			33.54			33.86
	323.15	1.31E+03	2.882	12.66	4.33	4.417	13
	343.15			13.25			12.76
Chol.	308.15			210.82			193.55
	313.15	3.72E+03	0.818	57.04	12.237	1.221	58.82
	333.15			95.49			96.79
Chol.	313.15			52.21			52.74
	333.15	3.33E+03	1.533	79.82	10.92	2.38	79.53

Table B.11: Modified Méndez-Teja modeling results

Comp.	T/K	Normal (Eq. 5.8)				Dimensionless (Eq. 5.19)			
		A'/K	B'/K·m ³ ·kg ⁻¹	C'	AVERR %	A''	B''	C''	AVERR %
Naph.	308.15				21.49				12.63
	318.15	-9.04E+03	2.175	22.263	14.67	-34.751	3.586	24.621	10.5
	328.15				12.42				3.59
Fluor.	308.15				15.93				6.54
	323.15	-9.46E+03	2.746	19.661	10.82	-28.789	4.019	15.9	4.65
	343.15				6.65				3.81
Hydroq.	333				6.55				6.56
	348	-5.04E+03	1.780	3.818	4.98	-16.566	2.737	1.818	4.98
	363				10.13				10.12
Anthrac.	303.15				15.29				15.18
	323.15	-1.02E+04	2.963	18.196	8.15	-33.653	4.561	16.19	8.2
	343.15				9.64				9.67
Chol.	308.15				188.89				188.63
	313.15	-1.02E+04	3.154	18.274	29.00	-33.537	4.759	16.315	28.85
	333.15				23.68				22.36
Chol.	313.15				17.12				17.96
	333.15	-1.02E+04	3.223	18.302	14.33	-33.499	4.825	16.354	15.18

Table B.12: Bartle modeling results

Comp.	T/K	Normal (Eq. 5.11)			Dimensionless (Eq. 5.20)		
		A	C/m ³ .kg ⁻¹	AVERR %	A	C	AVERR %
Naph.	308.15			88.93			88.93
	318.15	-0.417	5.11E-03	35.4	-0.417	2.389	35.4
	328.15			83.81			83.81
Fluor.	308.15			129.79			129.79
	323.15	-2.682	6.54E-03	22.51	-2.681	3.056	22.51
	343.15			96.72			96.72
Hydroq.	333			42.43			43.43
	348	-5.791	3.83E-03	17.95	-5.676	1.581	21.68
	363			49.78			49.15
Anthrac.	303.15			199.3			199.17
	323.15	-5.542	5.06E-03	45.83	-5.435	2.234	48.18
	343.15			100.15			99.75
Chol.	308.15			223.26			213.73
	313.15	-4.927	2.97E-03	53.76	-4.646	0.992	58.4
	333.15			90.52			90.4
Chol.	313.15			50.21			56.45
	333.15	-5.404	6.03E-03	72.97	-4.925	2.148	71.54

Table B.13: Modified Bartle modeling results

Comp.	T/K	Normal (Eq. 5.13)				Dimensionless (Eq. 5.21)			
		<i>a</i>	<i>b</i> /K	<i>C</i> /m ³ ·kg ⁻¹	AVERR %	<i>a</i>	<i>b</i>	<i>C</i>	AVERR %
Naph.	308.15				12.71				12.72
	318.15	26.410	-8.67E+03	7.19E-03	10.19	26.413	-28.5	3.364	10.19
	328.15				3.18				3.17
Fluor.	308.15				11.82				11.81
	323.15	17.049	-6.48E+03	7.79E-03	4.93	17.048	-21.300	3.641	4.93
	343.15				4.25				4.25
Hydroq.	333				4.86				4.21
	348	5.325	-3.93E+03	5.14E-03	5.3	5.323	-12.918	2.387	4.94
	363				6.75				7.42
Anthrac.	303.15				19.05				19.06
	323.15	15.657	-7.16E+03	8.30E-03	6.69	15.661	-23.54	3.88	6.71
	343.15				7.76				7.76
Chol.	308.15				111.46				111.01
	313.15	24.952	-1.04E+04	1.14E-02	41.31	24.979	-34.081	5.326	41.41
	333.15				13.33				13.34
Chol.	313.15				19.44				19.46
	333.15	14.265	-6.67E+03	9.91E-03	14.66	14.236	-21.932	4.672	14.66

Table B.14: Overall modeling results for Chrastil-type equations

Equation	OAVERR %						
	Naph.	Fluor.	Hydroq.	Anthrac.	Chol.	Chol. (308.15 K Excluded)	Combined Average
5.1	9.08	6.51	6.49	9.31	37.05	13.91	13.73
5.14	9.08	6.51	6.49	9.32	37.14	13.90	13.74
5.5	6.94	4.29	5.02	8.43	36.18	9.92	11.79
5.16	6.9	4.27	5.01	8.29	36.1	9.9	11.75
6.5	7.66	5.01	7.32	8.3	36.87	9.93	12.51
6.6	7.41	4.77	7.30	8.26	36.99	9.85	12.43
5.3	7.72	6.44	6.41	9.07	15.29	13.91	9.81
5.15	7.7	6.43	6.40	9.07	15.28	13.90	9.8
6.8	5.74	4.44	7.38	7.98	10.79	9.85	7.7
6.9	5.12	3.71	4.72	7.90	10.85	9.9	7.03

Table B.15: Overall modeling results for non-Chrastil-type equations

Equation	OAVERR %						Combined Average
	Naph.	Fluor.	Hydroq.	Anthrac.	Chol.	Chol. (308.15 K Excluded)	
6	32.18	13.49	48.46	15.39	99.11	70.74	46.56
18	29.86	6.45	47.41	15.22	99.23	70.7	44.81
8	15.55	9.50	7.88	10.03	45.90	15.57	17.41
19	7.72	4.61	7.88	10.05	45.33	16.42	15.34
11	83.71	96.33	40.16	99.95	95.77	65.41	80.22
20	83.71	96.33	40.71	100	96.17	66.45	80.56
13	7.53	5.91	5.87	8.77	37.22	16.79	14.94
21	7.53	5.91	5.97	8.77	37.23	16.81	15.11

APPENDIX C
PHYSICAL PROPERTIES OF AZELAIC ACID AND CARBON DIOXIDE USED
FOR EQUATION OF STATE CALCULATIONS

Table C.1: Physical properties of carbon dioxide^a

$T_c/^\circ\text{C}$	P_c/MPa	ω	$MW/\text{g}\cdot\text{mol}^{-1}$
31.05	7.38152	0.231	44.01

^a CHEMCAD (2005)

Table C.2: Physical properties of azelaic acid

$T_c/^\circ\text{C}$	P_c/MPa	ω	$MW/\text{g}\cdot\text{mol}^{-1}$	$10^4 P^{sub}/\text{Pa}$ at 313.15 K	$10^4 P^{sub}/\text{Pa}$ at 333.15 K	$T_B/^\circ\text{C}$	$\rho/\text{kg}\cdot\text{m}^{-3}$
537.85 ^a	2.56 ^a	1.087 ^b	188.224 ^a	0.1297 ^c	4.735 ^c	360.21 ^a	1029.1 ^d

^a CHEMCAD (2005)

^b Calculated value based on T_B , T_c , and P_c

^c Estimated from Ribeiro et al. (1999)

^d Azelaic Acid (1996)

APPENDIX D
EXPERIMENTAL AND LITERATURE VALUES OF OLEIC ACID SOLUBILITY IN
SUPERCRITICAL CARBON DIOXIDE

Table D.1: Solubility of oleic acid in supercritical carbon dioxide

T/K	P/MPa	$\rho_l^a/$ $kg \cdot m^{-3}$	$c_2/$ $kg \cdot m^{-3}$	c_2 STDEV/ $kg \cdot m^{-3}$	c_2^*	c_2^* STDEV	Reference
323.15	12.4	607.85	1.04	-	0.0017	-	Nilsson et al., 1991
	13.7	662.45	2.59	-	0.0039	-	
	15.1	702.19	4.10	-	0.0058	-	
	17.2	744.31	7.37	-	0.0099	-	
	20.6	791.41	11.97	-	0.0151	-	
323.15	16.5	731.85	2.9	-	0.0040	-	Škerget et al., 1995
	17.35	746.82	3.3	-	0.0044	-	
	19.08	772.53	3.1	-	0.0040	-	
	20.88	794.60	5.8	-	0.0073	-	
	23.95	825.18	7.9	-	0.0096	-	
	25.1	835.02	8.4	-	0.0101	-	
	25.65	839.48	8.3	-	0.0099	-	
26.22	843.96	8.7	-	0.0103	-		
323.15	13.8	665.78	2.00	0.53	0.0030	0.0008	Maheshwari et al., 1992
	20.7	792.56	11.89	0.79	0.0150	0.0010	
	27.6	854.22	19.65	1.37	0.0230	0.0016	
323.15	15.0	699.75	1.97	0.26	0.0028	0.0004	Experimental
	20.0	784.29	8.75	0.46	0.0112	0.0006	
	25.0	834.19	13.15	1.88	0.0158	0.0023	

^a NIST (2007)